FUNCTIONALIZED ELECTROSPUN NANOFIBERS FOR SAMPLE PREPARATION AND ANALYTE DETECTION IN MICROFLUIDIC BIOANALYTICAL SYSTEMS

A Dissertation

Presented to the Faculty of the Graduate School

of Cornell University

in Partial Fulfillment of the Requirements for the Degree of

Doctor of Philosophy

By

Lauren Elizabeth Matlock-Colangelo

May 2015

FUNCTIONALIZED ELECTROSPUN NANOFIBERS FOR SAMPLE PREPARATION AND ANALYTE DETECTION IN MICROFLUIDIC BIOANALYTICAL SYSTEMS

Lauren Matlock-Colangelo, Ph.D.

Cornell University 2015

Microfluidic biosensors which incorporate both sample preparation and analyte detection, also referred to as lab-on-a-chip (LOC) devices, are a promising means of providing low cost, rapid, and portable analyte detection in point-of-care, rural, and developing world applications[1–3]. However, despite numerous reports of LOC devices capable of detecting a range of clinical analytes[1–3], there are several key challenges that face the development of true LOC devices. First, due to the small size of these miniaturized systems, it is often necessary to significantly concentrate the sample volume to the nL-µL range [4]. Additionally, samples must be purified to remove particulates and impurities that may impede analyte detection. Finally, fluid flow in microfluidic devices is generally laminar, which limits the amount of fluid mixing that occurs within the channels[5–7]. Because rapid fluid mixing is typically required to facilitate chemical reactions and ensure access of analytes to functional surfaces within the microchannels, micromixers need to be incorporated into the design of a LOC device. This research aims to address the need for both better sample preparation and fluid mixing within microfluidic assays through the use of functionalized electrospun nanofibers.

Electrospinning is a fiber formation process in which electrical forces are used to form ultrathin fibers from viscous polymer spinning solutions[8]. The nonwoven fiber mats produced during electrospinning are characterized by extremely large surface-area-to-volume ratios and high porosities. Additionally, electrospun nanofibers can easily be functionalized either through

the inclusion of nanoscale materials into the polymer spinning dope, or through post-spinning modifications. In this work, positively and negatively charged poly(vinyl alcohol) (PVA) nanofibers were created through the addition of hexadimethrine bromide (polybrene) and poly(methyl vinyl ether-alt-maleic anhydride) (poly(MVE/MA), respectively, into a 10% w/v PVA spinning solution. Additionally, larger diameter polystyrene (PS) microfibers with a range of morphologies were spun using 12.5, 15, and 17% w/v PS spinning solutions. Previously, gold microelectrodes patterned onto poly(methyl methacrylate) (PMMA) were used to incorporate the nanofibers into microfluidic channels[9,10]. However, in this work, fibers were bonded into microchannels without the use of a gold electrode, resulting in simple, inexpensive device fabrication. Both PVA and PS fibers were spun onto metal collector plates and manually transferred to pieces of PMMA that had undergone UV-Ozone treatment. In order to produce nanofiber mats with uniform fiber distributions along their height, thin nanofiber mats were stacked together to create multilayered mats [11,12].

Positively charged PVA mats were shown to successfully bind and concentrate *E. coli* cells, while negatively charged PVA mats repelled the cells and were used to minimize nonspecific retention within the channels. The 3D morphology of the PVA nanofiber mats was optimized to eliminate nonspecific mechanical retention of the *E. coli* while also providing sufficient surface area for *E. coli* capture. Finally, anti-*E. coli* antibodies were immobilized on negatively charged PVA fibers to allow for successful specific capture of the analyte.

Fluid mixing within Y-shaped microchannels was enhanced through the incorporation of both PVA nanofibers and PS microfibers, though the PVA fibers produced the most significant mixing. We assume that mixing within the PVA nanofiber mats is caused by the inhomogeneity of pore size and pore distribution within the mats rather than by the individual nanofibers.

Statistical analysis of mixing within the nanofiber mats indicates that mixing is dependent on the height of the nanofiber mat (i.e. the number of layers) but is independent of the length of the nanofiber mat. As expected, the amount of mixing observed increased with decreasing fluid flow rate. The results of this study can be used to provide both enhanced sample preparation and fluid mixing with microfluidic biosensors. In addition, further functionalization of the nanofiber surfaces can be used to allow for detection of a wide range of analytes.

BIOGRAPHICAL SKETCH

Lauren was born in Denver, Colorado to Richard and Judith Matlock. She holds Bachelor of Science and Master of Science degrees from the Cornell Department of Biological and Environmental Engineering. Her research interests include lab-on-a-chip devices, fiber science, and nanotechnology.

This work is dedicated to my wonderful husband, Nick, who is a constant source of love and support

ACKNOWLEDGEMENTS

I would like to express my gratitude to my research advisor, Dr. Antje Baeumner, for her support and guidance. Additionally, I would like to thank my collaborative advisor, Dr. Margaret Frey, for her encouragement and for introducing me to electrospinning. I would also like to acknowledge Dr. Brian Kirby, whose excellent teaching helped inform and guide my microfluidics research.

I would like to express my appreciation to Nicholas Colangelo for his constant support and knowledge of statistics.

I am grateful for the guidance of Dr. Edouard Azzam, Dr. Sonia De Toledo, and Dr. Roger Howell. Thank you for allowing me to work alongside your labs and for teaching me about radiobiology.

Special thanks to Dr. Thomas Hirsch and Dr. Axel Duerkop, along with my colleagues at the University of Regensburg.

I would like to acknowledge my colleagues at Cornell and in the Azzam and Howell Labs. Thank you for brainstorming sessions, encouragement, and lunchtime conversation.

Finally, I would like to thank the Lester B. Knight Foundation at Cornell and the NSF IGERT program run through the Cornell Center for Materials Research for financially supporting my graduate education. Additionally, I would like to thank the funding sources that made my research possible, including the NSF CBET-0852900 and the Cornell Agricultural Experiment Station federal funding project 356: “Novel Nanofiber Biosensor for Food Safety”.

TABLE OF CONTENTS

LIST OF FIGURES

CHAPTER 1

CHAPTER 2

CHAPTER 3

APPENDIX A: SUPPLEMENTARY INFORMATION

LIST OF TABLES

CHAPTER 1

CHAPTER 2

CHAPTER 3

LIST OF ABBREVIATIONS

BSA	Bovine serum albumin
CFU	Colony forming units
CNF	Cornell NanoScale Science and Technology Facility
CS	Chondroitin Sulfate
DCM	Dichloromethane
DI	Deionized
DMEM	Dulbecco's Modified Eagle Medium
DMF	Dimethylformamide
ECM	Extracellular Matrix
E. coli	*Escherichia coli*
EDC	1-ethyl-3-(3-dimethylaminopropyl) carbodiimide hydrochloride
FITC	Fluorescein isothiocyanate
HIV	Human Immunodeficiency Virus
hMSCs	Human Mesenchymal stem cells
HRP	Horseradish peroxidase
K_m	Michaelis Constant
LB	Luria Broth
LFAs	Lateral Flow Assays
LOC	Lab-on-a-chip
MIPs	Molecularly imprinted polymers
PAN	Polyacrylonitrile
PANI	Polyaniline
PBS	Phosphate buffered saline
PCL	Poly(ε-caprolactone)
PDLGA	Poly(D,L-lactide-*co*-glycolide)

PDMS	Polydimethylsiloxane
PEG	Pol(ethylene glycol)
PEI	Polyethyleneimine
PEO	Poly(ethylene oxide)
PEUU	Poly(ester urethane) urea
PLGA	Poly(lactic-*co*-glycolic acid)
PLLA	Poly(L-lactic acid)
Polybrene	Hexadimethrine bromide
Poly(MVE/MA)	Poly(methyl vinyl ether-alt-maleic anhydride)
PMMA	Poly(methyl methacrylate)
PMPPh	Poly[bis(*p*-methylphenoxy)phosphazene]
Poly(AN-*co*-MMA)	Poly(acrylonitrile-*co*-methyl methacrylate)
PPL	Propranolol
PS	Polystyrene
PSA	Poly(styrene-*co*-maleic anhydride)
PTFE	Polytetrafluoroethylene
PVA	Poly(vinyl alcohol)
PVP	Polyvinylpyrrolidone
S. aureus	*Staphylococcus aureus*
SEM	Scanning electron microscope
SPE	Solid phase extraction
SRB	Sulforhodamine B
Sulfo-NHS	N-hydroxysulfosuccinimide
TBA	Thrombin-binding aptamer
TEM	Transmission electron microscope
TFE	Tetrafluoroethylene
THF	Tetrahydrofuran
μTAS	microTotal Analysis System

UVO	Ultraviolet Ozone
V_{max}	Maximum Velocity

CHAPTER 1

Biologically-Inspired Nanofibers for Use in Translational Bioanalytical Systems

Abstract

Electrospun nanofiber mats are characterized by large surface-area-to-volume ratios, high porosities, and a diverse range of chemical functionalities. Although electrospun nanofibers have been used successfully to increase the immobilization efficiency of biorecognition elements and improve the sensitivity of biosensors, the full potential of nanofiber-based biosensing has not yet been realized. Therefore, this review presents novel electrospun nanofiber chemistries developed in fields such as tissue engineering and drug delivery that have direct application within the field of biosensing. Specifically, this review focuses on fibers that directly encapsulate biological additives that serve as immobilization matrices for biological species, and that are used to create biomimetic scaffolds. Biosensors that incorporate these nanofibers are presented, along with potential future biosensing applications such as the development of cell culture and *in vivo* sensors.

Introduction

Bioanalytical systems rely on the specific and sensitive binding of a biorecognition molecule with its analyte, such as glucose oxidase with glucose, an antibody with its antigen, and a DNA oligonucleotide with its complementary sequence. Together with the choice of biorecognition molecule and signal transduction principle, the sensor surface is the characteristic that has the most dramatic influence on sensor performance. Providing a hindrance-free and recognition-site-concentrated surface is critical and is generally accomplished through the immobilization of the biorecognition molecule on a planar surface. One-dimensional, nanoscale

materials can be used to improve the performance of these devices by dramatically increasing the surface area available for detection [13–16]. Because the sensitivity of a sensor is related to the number of detection sites available, it is beneficial to provide an increase in functionalized surface area without increasing the sample volume needed [17]. Nanoscale materials have inherently large surface-area-to-volume ratios and provide a marked improvement over conventional materials such as polymer films and fibrous membranes, which have limited surface areas and low loading capacities [18]. Additionally, nanoscale materials can be made with a wide range of surface chemistries and mechanical properties, making them ideally suited for use in biosensing devices [14,15,19].

Nanofibers [16,20,21], nanowires [15,22,23], nanotubes [13,15], and nanoparticles [13,23] have been successfully incorporated into sensing devices, improving their sensitivity and efficiency. Of these materials, electrospun nanofibers stand out for their porous, nonwoven structure. The high porosity and surface area of electrospun nanofiber mats provide excellent loading capacities for immobilization of biological molecules and allow for an improved mass-transfer rate for a substrate to functionalized sites within the mat [24]. Nanofiber mats are durable, easy-to-handle, reusable, and appropriate for use within microfluidic devices [10,18]. In addition, electrospun nanofibers are easy to fabricate and functionalize [8,19]. Of the different fiber formation processes that can be used to produce nanofibers, electrospinning is arguably the best-suited method for the mass production of continuous fibers with uniform diameters [19]. In addition to straight-forward fabrication, electrospinning allows for the creation of fibers from materials that could not be used easily in other fiber-formation processes [25]. For example, proteins cannot be incorporated easily into fibrous forms because of their complex three-dimensional structure and strong inter/intra molecular forces [25]. However, several have reported on electrospun nanofibers made from

proteins, such as bovine serum albumin (BSA) and casein, which are electrospun by coupling the proteins with a second, more easily spun polymer [21,25,26].

Scope and Structure of Review

Although some significant papers have demonstrated highly successful integration of biologically functionalized nanofibers into sensing platforms [16], the field is in its infancy and we must learn from other disciplines, such as tissue engineering, to expand the types of materials available for use in biosensors [27,28]. Recently, there have been many exciting advances in the types of nanofibers that can be produced by electrospinning and translational studies are needed to bring these findings to full bear in bioanalytical systems. Therefore, this review begins with a discussion of novel nanofiber chemistries, focusing on fibers created by incorporating biological additives into spinning dopes [20,21,24,25], fibers used as immobilization matrices for biological species [29–31], and fiber scaffolds used to duplicate the structure of biological materials [27,32,33]. Then, we present potential applications of these novel nanofiber types in biosensing. Specifically, we discuss the creation of more sensitive and efficient biosensors, biomimetic biosensors for use in cell culture analysis, and biocompatible and reagentless *in vivo* biosensors.

Electrospinning

Nanofibers can be fabricated by a variety of methods, such as interfacial polymerization, catalytic synthesis, and self-assembly [16,34]. However, these methods each have their limitations. On the one hand, they can have slow production rates, expensive fabrication, restricted ranges of usable materials, and few possible nanofiber morphologies [34]. On the other hand, electrospinning is a relatively simple, high-throughput process in which electrical forces are used to form nanofibers with uniform diameters and long lengths from a viscous polymer solution [8,16,34].

Unlike many other fiber formation methods, electrospinning can be used to create fibers made from an extremely wide range of materials, including biological polymers [35,36], globular proteins [21,26], and conductive materials [37]. Furthermore, several types of fiber morphologies can be made by electrospinning, including beaded, ribbon-shaped, and core-shell fibers [34].

A typical electrospinning apparatus is composed of a spinneret (typically a syringe), a spinning dope, a high voltage source, and a grounded collector plate (Figure 1.1) [8]. Often, a syringe pump is used to slowly push the spinning solution out of the spinneret. The high voltage source is connected to the tip of the spinneret and confers a constant charge to the spinning solution, causing the solution to form what is referred to as the Taylor cone at the tip of the spinneret [8,16]. The spinning dope will accelerate out of the tip of the Taylor cone once the electrostatic attraction between the grounded collector plate and the charged solution overcomes the surface tension at end of the syringe tip [38]. As the polymer jet travels from the spinneret to the collector plate, it undergoes whipping and the solvent in the jet evaporates, leaving behind a solid polymer fiber that collects as a non-woven mat on the grounded collector plate. These nanofiber mats are characterized by extremely large surface-area-to-volume ratios, high porosities, and small pore sizes [39].

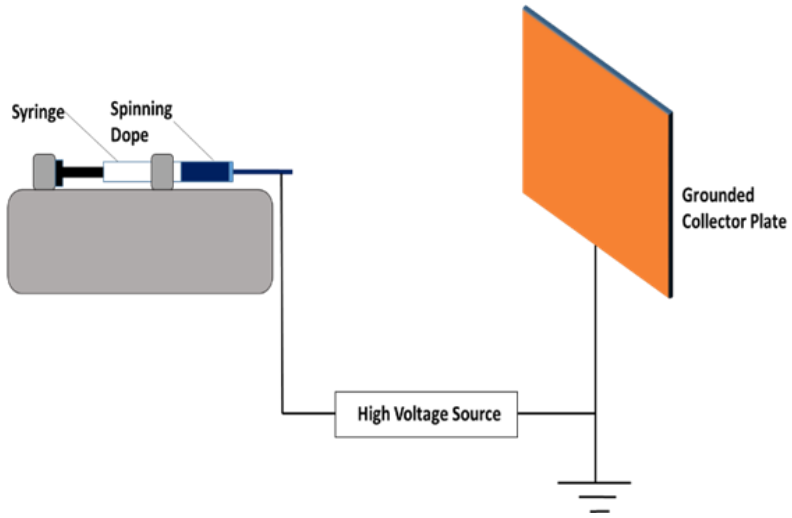

Figure 1.1 A typical spinning apparatus consisting of a syringe pump, spinneret, high voltage power source, and grounded collector plate

Electrospun nanofibers can easily be functionalized, either through post-spinning chemical modifications or by directly incorporating nanoscale materials into the spinning dope. Nanofiber mats can be modified using standard chemical coupling strategies to immobilize biological species such as enzymes [29] and antibodies [32]. Often, the immobilization efficiency on nanofiber mats is dramatically improved when compared to conventional materials [24]. The process of incorporating biological species into a spinning dope is a more elegant functionalization of the nanoscale material as no post-processing is required. However, it is also a more complex procedure given that spinning conditions have to be tailored toward conditions acceptable for the biomolecule to be immobilized. Examples of successful biomolecule incorporation include nanofibers containing biotin [18,40], antibodies [20], and enzymes [25]. These biological materials retain their native function, and can have increased stability due to their immobilization within the mats [24].

Creation of Biofunctional Nanofibers

Many biological species have been incorporated successfully within electrospun nanofiber mats. These materials can be directly spun into fibers, coupled with secondary polymers that enhance their spinnability, or they can be immobilized on nanofibers post-spinning. Regardless of the fabrication method used, the high surface area of electrospun nanofiber mats results in an increase in the number of immobilization sites available when compared to conventional materials.

Globular Proteins

Globular proteins are difficult to process into fibrous forms because the proteins do not have the same viscoelastic properties as classic polymers due to the proteins' strong inter- and intra-molecular forces [25,41,42]. To overcome these limitations, globular proteins can be co-electrospun with another polymer which serves to reduce the inter- and intra- molecular bonding of the proteins and results in successful production of nanofibers [21,25,26,43]. However, it is also possible to spin the proteins without the use of a second polymer [41,42]. Currently, globular protein-based nanofibers are primarily utilized within tissue engineering scaffolds, however they can also be easily functionalized to produce biocompatible, stable fibers for use in cell culture analysis or *in vivo* sensing (Table 1.1) [21]. In addition, functionalized casein- or BSA-based nanofibers could be utilized to prevent non-specific binding on fiber surfaces, eliminating or reducing the need for additional blocking steps within biosensing systems.

Table 1.1 Electrospinning of globular proteins

Biological Additive	Spinning Method	Co-Polymer(s) Spun	Demonstrated Application	Citation	Additional Potential Bioanalytical Use
BSA	Secondary polymer support	-PEG -FitcBSA -PCL	Tissue engineering scaffold	Zhang et al. (2006)	- integrated sensing moieties - release of cofactors for catalytic biosensors
BSA	Secondary polymer support	-Polycaprolactone	Tissue engineering scaffold	Valmikinathan et al. (2009)	-release of cofactors for catalytic biosensors
BSA	Spinning	NA	NA	Dror et al. (2008)	-biostabilization for biorecognition elements
Casein	Secondary polymer support	-PEO -PVA	Enzyme immobilization	Xie et al. (2003)	- Catalytic biosensors
Hemoglobin and Myoglobin	Spinning	NA	Oxygen delivery wound-healing scaffold	Barnes et. Al (2006).	-High sensitivity electrochemical biosensors
Hemoglobin	Spinning	NA	H_2O_2 and nitrite biosensor	Ding et al. (2010)	-High sensitivity electrochemical biosensors

BSA is conventionally used as a blocking agent, enzyme stabilizer and tissue culture nutrient [21,26]. Generally, it has proven difficult to spin without the use of a second polymer such as poly(ethylene oxide) (PEO) [21] or poly(ethylene glycol) (PEG) [26]. Kowalczyk et al. produced a simple pH sensor from electrospun BSA fibers stained with fluorescein isothiocyanate (FITC) for use in cell culture analysis [21]. A water-resistant PEO core was used to increase the stability and spinnability of the fibers. Directly after spinning, the PEO/BSA fibers were water soluble, but after aging for two weeks at ambient conditions they were rendered insoluble and retained their structure in solution [21]. FITC was coupled to the fiber surfaces by immersing the mats in a 0.02wt% FITC solution for 24 hours at room temperature. The biocompatibility of the resulting fiber and simplicity of its pH response make it a desirable candidate for use as an intracellular

pH monitor. Zhang et al. report a slightly more complex approach in which coaxial electrospinning was used for the production of BSA nanofibers [26]. Here, water-soluble PEG, FITC-conjugated BSA (fitcBSA) and biodegradable poly(ε-caprolactone) (PCL) were coaxially spun to create a biologically mimetic tissue engineering scaffold capable of sustained release of fitcBSA. The fiber composition was controlled to prevent an initial burst release of fitcBSA. Similarly, a polycaprolactone and BSA nanofiber has been developed for use in peripheral nerve tissue engineering scaffolds [43]. Nerve growth factor was successfully encapsulated within the fibers, resulting in a nanofiber mat that mimicked the structure of the extracellular matrix while also providing an increased surface area for release of nerve growth factor. The nanofibers had a reduced initial burst release of nerve growth factor and an improved loading efficiency when compared to other hydrophobic polymers. The nerve growth factor was consistently released for 28 days and was capable of inducing neutrite outgrowth from PC12 cells grown on the scaffold [43].

Dror et al. were able to spin BSA fibers without the use of a second polymer support by manipulating the BSA's existing disulfide bonds to allow for the formation of a structure rich in inter- and intra-molecular disulfide covalent bonds [41]. A high concentration of trifluoroethanol was used to disrupt the tertiary structure of the BSA to get an open helical structure with many hydrophobic protein segments exposed to the solvent. β-mercaptoethanol was used to open the intramolecular disulfide bridges of the BSA, producing a marked improvement in the rheological properties and spinnability of the solution. The resulting BSA fibers had uniform morphologies, high tensile strength and high degrees of crystallinity, making them well-suited for applications in tissue engineering or sensing [41].

Hemoglobin and myoglobin are redox proteins used within electrochemical biosensors [44,45]. Generally, the proteins are immobilized within a matrix, such as a polyacrylamide film [46], or immobilized onto the surface of nanoparticles and nanotubes before they can be used within a biosensor [45,47]. Recently, however, the feasibility of spinning both myoglobin and hemoglobin nanofibers has been established, allowing for the creation of protein-based biosensors that do not require complicated immobilization procedures [42,44]. Myoglobin and hemoglobin have both been successfully spun into ribbon-like nanofibers without the use of a second polymer [42]. The proteins were solubilized in 2,2,2-Trifluoreoethanol prior to spinning. Nanofibers were spun with hemoglobin concentrations between 100-250 mg/mL and a myoglobin concentration of 250 mg/mL. The fibers were cross-linked to improve stability through vapor fixation with a 50% w/w glutaraldehyde solution. Although the mats were stable when handled gently, they lacked the mechanical strength to withstand harsh conditions. However, both fiber mats were deemed sturdy enough for use as a potential biocompatible wound dressing [42]. Hemoglobin has also been electrospun to produce a biosensor for the detection of hydrogen peroxide and nitrite [44]. The hemoglobin was spun onto a glassy carbon electrode surface to create an electrochemical sensor. The hemoglobin retained its activity after spinning and required no immobilization matrix to adhere to the glassy carbon electrode, making it an attractive alternative to conventional immobilization. The fibers were spun from 175 mg/mL hemoglobin in 2,2,2-trifluoreoethanol solution and were cross-linked in glutaraldehyde vapor after spinning to render them insoluble. An amperometric sensor created from the fibers showed limits of detection of 0.61 μM for H_2O_2 and 0.47 μM for nitrite [44].

Casein is typically used as a blocking agent to prevent non-specific binding within biosensors. As with BSA, casein can be difficult to spin without the support of a second polymer

and has been successfully spun through incorporation in a PEO and poly(vinyl alcohol) (PVA) spinning dope [25]. Furthermore, lipase enzyme was added to the spinning solution to create a functionalized nanofiber. Lipase immobilized within the casein fibers demonstrated a higher catalytic activity towards the hydrolysis of olive oil than lipase immobilized on planar materials [25]. The resulting fiber could be used to lower the nonspecific binding within a sensing device and to simultaneously permit enhanced enzyme-based detection of analytes.

Enzymes

Enzymes are used as catalytic biorecognition molecules in bioanalytical sensors. Maintaining an enzyme's tertiary structure during immobilization/spinning is necessary to maintain its catalytic activity. Several groups have reported the successful integration of enzymes into electrospun nanofiber mats, either by adding the enzymes to a polymer spinning dope or through post-spinning immobilization on the mats (Table 1.2). The enzyme-based nanofibers have several advantages over conventional enzyme immobilization strategies, including increased immobilization efficiency due to the large surface area of the nanofibers, improved mass-transfer for the substrates to the enzyme reactive sites, improved long-term enzyme stability, higher enzyme activities than enzymes immobilized in films, and simpler immobilization procedures [24].

Table 1.2 Immobilization of enzymes within nanofiber mats

Biological Additive	Immobilization Method	Additional Polymer(s) Spun	Results	Citation	Potential Bioanalytical Use
Lipase	Co-spinning with casein and secondary polymer	-PEO -PVA	Increased enzyme activity	Xie et al. (2003)	-Prevention of non-specific binding
Lipase	Adsorption on coaxial spun fibers	-PMPPh -PAN	Increased enzyme stability	Wang et al. (2012)	-Long-term storage - continuous/ long-term measurement sensors
β-galactosidase	Covalently attached via carbonyl groups of spacer arms	-Poly(AN-co-MMA)	Better activity Better temperature stability	El-Assar et al. (2013)	- Sensors for use at extreme temperatures
Glucose Oxidase	Post-spinning	-Chitosan -PVA	Sensor with improved stability in neutral and alkaline conditions	Wu et al. (2013)	- Sensors modified for use under extreme pH conditions

Enzymes can be spun successfully into nanofiber mats by incorporating them into polymer spinning dopes [24,25,48]. As previously discussed, lipase has been co-spun into casein nanofibers by using PEO and PVA to improve the spinnability of the proteins [25]. The immobilized lipase had greater ability to hydrolyze olive oil than did lipase immobilized in films. Herricks et al. successfully spun α-chymotrypsin by incorporating it into poly(styrene-*co*-maleic anhydride) (PSA) dissolved in dioctyl sulfosuccinate-toluene solution [24]. The nanofibers were stabilized using glutaraldehyde, resulting in fibers that were stable in solution. Alpha-chymotrypsin immobilization within the fibers resulted in greater enzyme stability compared to immobilization in conventional materials such as bulk films. Additionally, there was an increased mass-transfer rate for the substrates to the enzyme reactive sizes due to the morphology of the nanofiber mats.

The stable α-chymotrypsin fibers were almost five times as active as glutaraldehyde treated α-chymotrypsin films [24]. A water-soluble polyvinylpyrrolidone (PVP) nanofiber has been created to facilitate storage of horseradish peroxidase (HRP) within microfluidic biosensors [48]. The HRP was spun directly into the fibers, resulting in better enzyme activity after long-term storage in ambient conditions and easier integration of HRP into microfluidic sensors. The immobilized HRP retained 80% of its native activity after spinning, and retained 40% activity after storage for 280 days at ambient conditions. The spinning of HRP into the fibers eliminated the need for lyophilization of the enzymes and is an attractive option for the immobilization of other biological recognition elements in point-of-care sensors [20,48].

Enzymes are also immobilized on nanofibers through post-spinning chemical coupling [29,49]. The shared goal among the reports is to increase the surface area of available enzyme and allow for better mass transfer of substrate to enzyme active sites. Wang et al. report coaxial-electrospun fibers with a poly[bis(*p*-methylphenoxy)phosphazene] (PMPPh) sheath and polyacrylonitrile (PAN) core [49]. The PAN was used to facilitate better fiber formation of the PMPPh. The resulting fibers were able to immobilize lipase via adsorption. The core/sheath fiber had better adsorption capacity (20.4 $\pm$ 2.7 mg/g) and increased enzyme activity (63.7%) than lipase immobilized on a PAN membrane. The organic side groups of the phosphosphazene allowed for easy nucleophilic substitute and creation of a wide range of side-groups that can be used to immobilize different biological recognition elements. In contrast to this adsorptive approach, β-galactosidase has also been immobilized onto nanofiber mats via covalent bonding in an effort to improve enzyme stability [29]. Poly(acrylonitrile-*co*-methyl methacrylate) [poly(AN-*co*-MMA)] fibers were spun and modified with a polyethyleneimine (PEI) spacer arm that was used to covalently attach the β-galactosidase to the carbonyl groups on the fibers. Glutaraldehyde

was used as a coupling agent. After immobilization, the enzyme stability was improved (V_{max}=8.8 µmol/min, K_m=236.7 mM), particularly at higher temperatures.

An amperometric cholesterol biosensor was created by immobilizing cholesterol oxidase onto electrospun polyaniline and polystyrene nanofibers [30]. Polyaniline is a conductive material, allowing the cholesterol oxidase-modified fibers to be used as a working electrode. Polystyrene was used to enhance the spinnability of the polyaniline. The finished biosensor consisted of a nanofiber mat immersed in a beaker, with an Ag/AgCl reference electrode and platinum wire counter electrode. A glucose biosensor was also created through immobilization of glucose oxidase on a composite electrospun fiber composed of Prussian blue, chitosan, and PVA [31]. Prussian blue is often used in amperometric glucose sensors due to its high biocompatibility and enhanced electron transport. However, in its native form it is not stable in neutral or alkaline solutions. Spinning the Prussian blue directly into the fibers resulted in improved stability in neutral and weakly alkaline solutions. The resulting sensor had a limit of detection of 3.61×10^{-7} M.

Antibodies

There are few reports of the successful spinning of antibodies into polymer-based nanofibers [20] which may be a result of the high costs of antibodies, limiting extensive spinning studies. However, the large surface areas of nanofiber mats have been utilized, primarily as scaffolds in tissue engineering, to immobilize antibodies after spinning [32].

Jin et al. report a capillary flow microfluidic *Escherichia coli* biosensor that utilized water-soluble nanofibers for the storage of HRP-tagged antibodies [20]. The HRP-tagged antibodies were incorporated into nanofibers composed of 15wt% PVP and 5wt% sucrose

dissolved in DI water. The spinning process dehydrated the antibodies and allowed them to be stored long-term in ambient conditions without losing functionality. These fibers were incorporated within microfluidic channels, and they dissolved upon contact with solution, releasing the antibodies. The three-dimensional structure of the nanofiber mats resulted in a uniform distribution of antibodies within the microfluidic channels. A limit of detection of 10^6 CFU/mL of *E. coli* O157 was reported, which demonstrated that the biofunctionality of the antibodies was retained after spinning and storage.

Electrospun PCL nanofibers have been used to create a matrix for the growth of endothelial cells [32]. Anti-CD31 antibodies were immobilized on the scaffolds through adhesive proteins called hydrophobins, resulting in an increase in the attachment and retention of endothelial cells. The fibers were made of 10% w/v PCL dissolved in dichloromethane (DCM) and dimethylformamide (DMF). Antibody immobilization did not require a crosslinking agent and took place using a self-assembled HFBI film on the electrospun fibers. After the class II hydrophobin (HFBI) film was deposited on the fibers, the fibers were functionalized by incubation in 10µg/mL of primary antibody solution overnight at 4°C. Hou et al. created a microfluidic chip for the detection, isolation, and analysis of circulating melanoma cells through the immobilization of anti-CD146 antibodies on Poly(lactic-*co*-glycolic acid) (PLGA) nanofibers [50]. Carboxylic acid groups on the PLGA fibers were activated using *N*-hydroxysuccinimide and used to covalently conjugate streptavidin to the fiber surfaces, which could then immobilize the anti-CD146 antibodies. Senecal et al. report the development of carboxylated and aminated nanofibers for the covalent immobilization of antibodies [51]. Carboxylated fibers were created by spinning polyvinyl chloride that was 1.8% carboxylated. Aminated functional membranes were

made by spinning water-soluble polyamine and water insoluble polyurethane. Antibodies could then be immobilized using conventional crosslinking chemistries.

Molecularly Imprinted Polymers

Molecularly imprinted polymers (MIPs) have been utilized to create synthetic, stable biological recognition elements for a variety of analytes. Several groups have investigated incorporating MIPS directly within electrospun nanofibers to make sensitive diagnostic devices and separation membranes [52–54].

Propranolol (PPL) MIPs were created from methyl methacrylate monomers, a PPL template, and a divinylbenzene cross-linker and then spun into 40% w/v Eudragit-RS100 nanofiber mats [55]. The resulting membranes were able to selectively bind PPL and did not bind other beta blockers such as atenolol, metaprolol, and timolol. Sueyoshi et al. incorporated a MIP into electrospun chiral separation membranes [56]. The membranes were composed of polysulfone with aldehyde (PSf-CHO-05 or PSf-CHO-10) and *N*-*α*-benzyloxycarbonyl-d-glutamic acid (Z-d-Glu) or *N*-*α*-benzyloxycarbonyl-l-glutamic acid (Z-l-Glu) serving as print molecules. A chiral selector composed from polysulfones was created for optical resolution [57]. The membranes were able to purify target molecules from a solution containing both by-products of the target molecule, solvents and contaminants. Nanofiber membranes prepared from polymeric materials had adsorption selectivity with mixtures of racemic Glu. The fluxes for the nanofiber membranes were increased two to three orders of magnitude when compared to traditional membranes [57].

Nucleic Acids

Aptamers are synthetic single-stranded nucleic acid sequences that can be used as biorecognition elements within biosensors due to their high affinity and specificity for target molecules [58]. Typically, aptamers are used in protein purification systems by immobilizing the aptamers within monolithic capillary chromatography columns [59] or on magnetic or agarose beads within short-column systems [60,61]. Additionally, they have been incorporated in biosensors as an alternative to antibodies due to their relatively easy synthesis and high stability [62]. Recently, several groups have utilized the large surface areas of electrospun nanofiber mats to allow for the development of sensitive biosensors and protein purification scaffolds [61,63,64]. Lee et al. report the creation of a sandwich assay for the detection of thrombin by immobilizing two thrombin-binding aptamers, TBA29 and TBA15, on the surfaces of electrospun polystyrene-PSMA (PS-PSMA) nanofibers [63]. The aptamers were immobilized on the nanofibers in a post-spinning process by coating fibers with a solution of streptavidin and utilizing biotin-labeled TBA29 as the capture aptamer. Fluorescent detection of bound thrombin was achieved by using quantum dot or fluorescein dye-labelled TBA15. The resulting biosensor had a 25,000-fold higher sensitivity than a similar microwell plate assay, with a limit of detection of 10 pM with quantum dot detection. TBA29 immobilized on PS-PSMA nanofibers has also been used for purification of thrombin from solution [61]. An 85% recovery yield of proteins was reported with the nanofiber-based purification system, which was both stable and reusable. The purification membrane was used repeatedly over a period of seven months and exhibited only a 10% reduction in recovery yield [61].

The traditional use of nucleic acids in hybridization with complementary DNA or RNA sequences has also been demonstrated. Specifically, a nucleic acid-based electrochemical biosensor for the detection of the *p53* tumor suppressor gene has been developed through

electrospinning carboxylated multi-walled carbon nanotubes within a nylon 6 spinning dope [64]. Electropolymerization was used to deposit pyrrole on the nanofiber surfaces, creating a composite nanofiber surface suited for immobilization of ssDNA and detection of the wild-type *p53* sequence. The resulting sensor had a limit of detection of 50 Fm [64].

Biotin

Biotin is frequently utilized within sensors because of its rapid and specific binding with streptavidin [17]. Generally, streptavidin is immobilized on the surface of a substrate and is then coated with a biotinylated biorecognition element to facilitate capture of target analytes [17]. Nonwoven biotin-based fiber mats for use in biosensing platforms have been created by dispensing biotin in a PLA/chloroform/acetone spinning dope [17,40]. X-ray photoelectron spectroscopy revealed that there was a higher biotin concentration at the surface of the fibers than would be expected from uniform biotin distribution. A colorimetric assay demonstrated that the biotin retained its function and was able bind to streptavidin. Biotinylated nanofibers spun on copper-backed laminate were able to be incorporated within a lateral flow biosensor for the capture of *E. coli* DNA [17]. Biotinylated poly(ethylene glycol)-b-poly(L-lactide)-b-poly(L-lysine) has been spun with poly(L-lactide-co-glycolide) into nanofibers to facilitate immobilization of proteins on nanofiber surfaces [65]. The biotinylated nanofibers were successfully used to immobilize HRP-labelled streptavidin and rabbit anti-goat IgG.

Biotin has also been immobilized on nanofiber surfaces post-spinning to allow for enhanced sensitivity within a biosensing platform [18]. Wang et al. electrospun poly(ethylene-*co*-glycidyl methacrylate) and cellulose acetate butyrate nanofibers that could be easily aminated and then biotinylated [18]. HRP-labeled streptavidin could be immobilized on the fiber surfaces.

The fibers were shown to be reusable, with 15% of relative activity retained after 10 repeated uses.

Pharmaceuticals

Several groups have developed biocompatible electrospun nanofibers encapsulating pharmaceuticals for localized drug delivery *in vivo* [66,67]. Utilizing drug-delivery scaffolds can improve delivery of pharmaceuticals to different tissue types, allow for a lower dose than would be required for systemic drug delivery, and localize treatment only to affected areas [66,68].

Antimicrobials and antibiotics can be incorporated within nanofiber mats to create dressings that deliver necessary pharmaceuticals directly to a wound [66]. The goal is to decrease the bacterial load in a wound simultaneously allow efficient drug delivery to tissues (such as granulating tissues) that do not receive sufficient antibiotics from systemic administration [66]. The nanofiber mats can also be used to prevent post-surgical adhesions [68]. PLGA has been utilized to create biodegradable nanofibers for antibiotic delivery *in vivo* [66]. PLGA is a frequently used polymer that is fully biocompatible and can be tailored to maintain different degradation properties. It has been approved by the U.S. Food and Drug Administration for use in numerous drug-delivery applications. Within the body, PLGA is degraded by hydrolysis and is metabolized by the citric acid cycle [66]. The antibiotic cefazolin has been successfully spun within PLGA to create biodegradable wound dressings. This was done by dissolving both in a DMF and tetrahydrofuran (THF) solvent system [66]. Cefazolin loading of 10% or 30% produced uniform fibers with good morphology. PLGA nanofibers have also been created for the sustained release of Mefoxin, a hydrophobic antibiotic [68]. A 5wt% drug loading percentage in the scaffold was investigated, which corresponds to one-twentieth of the daily systemic Mefoxin dose typically given after surgery. PLGA was used to control the degradation of the scaffolds, while PLA was

utilized to create a mechanically strong scaffold. Finally, amphiphilic poly(ethylene glycol)-b-poly(lactic acid) (PEG-b-PLA) was also incorporated within the spinning dope to encapsulate the antibiotic. The final fibers were composed of PLGA:PLA:PEG-b-PLA in an 80:5:15 ratio. Drug release was sustained for one week and was effective in inhibiting *S. aureus* bacterial growth in agar and liquid environments. Hong et al. created biodegradable poly(ester urethane) urea (PEUU) and PLGA nanofibers encapsulating tetracycline hydrochlorine through two-stream electrospinning [69]. The PEUU provided increased elasticity to the scaffold, and the PLGA allowed for controlled drug release. The nanofibers were capable of sustaining drug release for one week *in vivo* and reduced abscess formation in rat abdominal surgery models [69,70]. Zeng et al. created a poly(L-lactic acid) (PLLA) nanofiber containing rifampin, a tuberculosis drug, and paclitaxel, a chemotherapy drug [67]. The spinning dope was composed of 3.9 wt% PLLA dissolved in a 2:1 (v/v) chloroform and acetone solution. Pharmaceuticals were placed directly into the spinning dope. The encapsulated pharmaceuticals were steadily released from the nanofibers through the action of proteinase K, with no burst release observed during the initial 7 hours of use [67].

Mimicking the Physical Structure of Biological Materials

Biocompatible functionalized nanofibers are being investigated for use in cell culture of *in vivo* as tissue engineering scaffolds [71,72]. In these cases, the nanofiber mats are utilized for their chemical functionality as well as their unique three-dimensional structures, which closely mimic the structure of the extracellular matrix [72,73]. Electrospun nanofiber mats are ideal for use as tissue engineering scaffolds due to their high porosity and very large surface areas, which make it easier to promote cell infiltration into the scaffolds [74,75]. Additionally, the mechanical properties of electrospun nanofibers can be tailored to mimic the properties of native materials.

Although the materials presented here are not currently utilized in biosensors, their unique structures and functionalities make them ideal for use in sensors that monitor cell cultures or *in vivo* phenomenon and should be investigated for that purpose.

PCL is a biodegradable polymer commonly used in the creation of nanofiber-based tissue engineering scaffolds because it is non-toxic, inexpensive, and has slow degradation in cell culture and *in vivo* [71,72,75]. Xu and coworkers created a nanofiber scaffold capable of mimicking the structure of the extracellular matrix from a poly(L-lactide-co-ε-caprolactone) [P(LLA-CL)] copolymer [72,73]. The fibers had diameters between 400 and 800 nm, corresponding to the dimensions of the native extracellular matrix (ECM). When tested, the mechanical properties of the nanofiber mats were similar to those of a human coronary artery. The fibers were tested as a matrix for human smooth muscles cells as well as endothelial cells. Both cell types were seeded for seven days on the nanofiber mats and were capable of attaching and proliferating on the scaffolds. They retained their phenotypic shapes during growth and created a three-dimensional cellular network within the fibers. Choi et al. have investigated the use of electrospun nanofibers made of PCL and collagen to create an implantable muscle tissue [71]. The nanofiber mats were used to seed human skeletal muscle cells and their adhesion, proliferation and organization were studied. Nanofibers that were unidirectional resulted in better muscle cell alignment and myotube formation, whereas randomly oriented nanofibers did not. Mesenchymal stem cells have also been cultured on PCL scaffolds to culture bone tissue [75]. The stem cells were seeded on non-woven PCL scaffolds created from a 10wt% PCL dissolved in chloroform spinning solution. After spinning, the mats were desiccated for several days, sterilized in a 70% ethanol solution, and then soaked in a collagen solution to allow for better cell attachment to the finished membrane. Histological studies of the nanofiber mats demonstrated that there was successful

formation of extracellular matrix after one week and cells had migrated into the interior of the nanofiber mats. After four weeks, the extracellular matrix had an increased density and significant calcification was observed. In addition, collagen type I was detected in the inner and outer portions of the nanofiber scaffolds after four weeks.

Poly(D,L-lactide-*co*-glycolide) (PDLGA) is another material frequently used as a scaffold in tissue engineering [76]. Typically, three-dimensional PDLGA scaffolds can be created using a variety of methods, including molding/particulate leaching [76] or gas-forming and controlled-precipitation [77]. Recently, there have been reports of electrospun PDLGA fiber mats used to create biocompatible scaffolds for *in vivo* use [78,79]. Xin et al. examined whether human Mesenchymal stem cells (hMSCs) grown on PDLGA nanofiber scaffolds could differentiate into chondrocytes and osteocytes [79]. Fibers were created by dissolving PDLGA beads (85:15 PLA:PGA) in tetrahydrofuran (THF) and DMF. The PDLGA fibers were pre-wetted and sterilized with ethylene oxide prior to seeding of hMSCs. The scaffolds seeded with cells were cultured in a supplemented Dulbecco's Modified Eagle Medium (DMEM) solution. Proliferation of the cells was observed, as indicated by an increase in DNA contents of the hMSCs after 14 days of culturing. There was evidence that the PDLGA nanofibers were able to support the differentiation of hMSCs into osteoblasts and chondrocytes.

Natural polymers such as collagen and elastin have also been utilized to create highly biocompatible nanofiber mat scaffolds [74]. As previously discussed, nanofiber mats from PCL are sometimes soaked in collagen solutions prior to use in order to facilitate cell adhesion [75]. Incorporating collagen or elastin directly in the spinning dope simplifies the fabrication process and results in a nanofiber mat that has enhanced cell adhesion properties. In particular, collagen and elastin nanofibers have been shown to promote infiltration of cells into the scaffold mats and

are able to supply cells with oxygen and nutrients [74]. However, when these materials are spun without the support of a synthetic polymer, mats show dimensional instability, resulting in early dissolution of fibers in culture as well as shrinkage of the mats [74]. Lee et al. created blood vessel scaffolds from electrospun nanofibers consisting of biodegradable polymers such as collagen and elastin [74]. Fibers created from a 45 wt% collagen, 15wt% elastin, and 40wt% synthetic polymer [PDLGA, poly(L-lactide), poly(ε-caprolactone), and poly(D,L-lactide-*co*-ε-caprolactone)] were able to mimic the collagen and elastin composition of blood vessels. The scaffolds utilized randomly oriented fibers and proved non-toxic and stable in *in vitro* cultures. Furthermore, the mechanical properties of the mats were able to simulate the structure of nanotube blood vessels, and were simultaneously easy to fabricate.

Heterogeneous nanofiber mats have also been developed to more closely mimic the structure of biological tissues. Xie et al. utilized PCL dissolved in dichloromethane and N,N-dimethyformamide at a ratio of 4:1 v/v at 10 % w/v concentration to create nanofiber scaffolds with gradations in the fiber organization [33]. Two nanofiber types, one composed of PCL and the other PCL and coumarin 6 dye, were spun from different syringes. The resulting composite fiber mat had a chemical gradient from spinning the second mat of coumarin fibers directly on top of the PCL fibers, resulting in the deposition of random fibers on uniaxial aligned fibers. Ionescu et al. have reported the creation of chemically heterogeneous cell culture scaffolds through co-spinning PEO fibers encapsulating PLGA microspheres and mechanically strong PCL nanofibers [80]. The PEO fibers served as a sacrificial membrane and degraded upon contact with solution, leaving behind a stable PCL fiber matrix interspersed with a high concentration of PLGA microspheres. Both BSA and chondroitin sulfate (CS) were encapsulated in the PLGA microspheres, resulting in nanofiber scaffolds capable of sustaining a dual-release profile for 35

days [80]. The authors hypothesize that more complex chemical gradients, such as growth factor cascades, could be simulated through controlled encapsulation of different biomolecules within the PLGA microspheres [80].

Possible Applications: The Future of Functionalized Nanofibers in Bioanalytical Systems

Electrospun nanofibers are frequently utilized in many biological fields, including tissue engineering [78], drug delivery [70], and to a very limited degree, biosensing [31,44]. In biosensing, functionalized nanofibers have primarily been used to increase the number of binding sites available, resulting in better immobilization efficiencies and detection sensitivities [16]. However, the full potential of these nanoscale materials to significantly enhance the performance of bioanalytical devices has yet to be realized. We predict that utilizing the many exciting surface chemistries and structures offered by electrospun nanofibers within both simple lateral flow assays and complex lab-on-a-chip systems could revolutionize the way biosensing is done today. For example, the functionalized nanofibers presented in this review could be used to create highly sophisticated integrated sensing systems, particularly for cell culture and *in vivo* sensing applications (Table 1.3).

Table 1.3 Nanofibers used within other fields that have direct applications within biosensing

Polymer	Biological Additive	Functionalization Method	Results	Citation	Potential Bioanalytical Use
PCL	Anti-CD31 antibodies	Post-spinning immobilization using adhesive proteins (hydrophobins)	Increased attachment and retention of endothelial cells	Zhang et al. (2011)	Enhanced biorecognition element immobilization
	Collagen	Co-electrospinning	Muscle cell culture and myotube formation	Choi et al. (2008)	Biocompatible fibers for *in vivo* or cell culture sensors
	Coumarin (dye)	Incorporation in spinning dope	Heterogeneous nanofiber mats	Xie et al. (2012)	Bioanalysis of effects of chemical gradients on cell cultures
PLGA	Anti-CD146 antibodies	Post-spinning covalent conjugation of streptavidin on fiber surfaces	Isolation of circulating melanoma cells	Hou et al. (2013)	Generation of generic immobilization surfaces
	Cefazolin (antibiotic)	Incorporation in spinning dope	Drug-eluting wound dressing	Katti et al. (2004)	Sensor to test toxicity of drugs within cell cultures
PVP	Anti-*E. coli* antibodies	Incorporation in spinning dope	Improved antibody storage in ambient conditions	Jin et al. (2013)	Stable storage of reagents and biorecognition elements in sensors

Our research group's experience with the integration of nanofibers within bioanalytical platforms demonstrates their general applicability for sensing and sample preparation in lateral flow and microfluidic devices [10,17,81]. Specifically, we have integrated charged PVA nanofibers into microfluidic channels to serve as bioseparators. The fibers spun from a PVA-polybrene spinning dope have successfully been used to capture and release liposomes by controlling the pH of the solution within a microfluidic channel (Figure 1.2) [10]. We have also developed *de novo* nanofiber mats as membrane materials in lateral flow assays (Figure 1.2) [17,40,81]. These nanofiber

mats can be used for antibody immobilization, development of standard sandwich assays using antibodies and DNA oligonucleotides as biorecognition elements, and prevention of any non-specific binding by incorporation of polystyrene$_{8K}$-*block*-poly(ethylene-*ran*-butylene)$_{25K}$-*block*-polyisoprene$_{10K}$-Brij76 (KB) into PLA-PEG nanofibers [81].

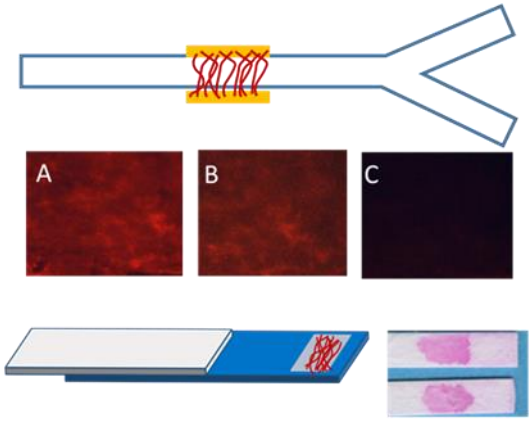

Figure 1.2 Top: (a) Microfluidic channels containing PVA –polybrene nanofibers were filled with fluorescent liposomes at pH 7. **(b)** Liposomes remained on the nanofiber mats after 20 minutes of washing with a pH 7 buffer solution. **(c)** Bound liposomes were then eluted from the mats using a pH 9 washing step[10]. **Bottom:** Nanofibers functionalized with anti-*E. coli* antibodies were incorporated into lateral flow assays for the detection of *E. coli* 0157[81].

On the basis of on our experience and considering the superior performance of nanofibers in tissue engineering and drug-delivery applications, we provide below several concrete examples and predictions of how electrospun nanofibers published and used in other disciplines could be integrated into biosensor platforms and improve specific sensing capabilities.

Improving Sensor Performance

There are many advantages to nanofiber-based sensing platforms other than an increased surface area and detection sensitivity. Several groups have demonstrated that immobilization of

biological molecules directly within fiber spinning dopes can result in better long-term stability in ambient and harsh conditions [20,31,48]. This is crucial for the development of biosensors for use in point-of-care settings, where refrigeration may not be available. Particularly useful is the notion of encapsulating reagents and biorecognition elements directly within water-soluble fibers for long-term storage in microfluidic sensors [20,48]. Furthermore, enhanced stability of enzymes within electrospun nanofibers allows for the development of sensors that can function over a wider range of temperatures and pH values [24,48].

Biosensors that utilize BSA or casein-based nanofibers could be used to significantly reduce nonspecific binding [21,25]. Because nanoscale materials have been incorporated within globular protein-based nanofibers, it would be possible to create a sensing platform that allows for specific detection of an analyte through incorporation of an antibody or enzyme within the nanofiber, with simultaneous prevention of nonspecific binding by utilizing a BSA or casein nanofiber base. This would eliminate or reduce the need for additional blocking steps within the device, resulting in more streamlined biosensors. Furthermore, it would also avoid the negative side effect of blocking binding sites, which occurs in bulk blocking procedures.

Multiplexed detection is also possible through the incorporation of more than one type of functionalized nanofiber within a biosensor. Heterogeneous nanofiber mats have been created through the co-spinning of two different polymer spinning dopes, and the same technology could easily be applied for the creation of biosensing platforms [33]. Additionally, the principle of coaxial spinning can be utilized to incorporate two functional materials within the same nanofiber, with one material concentrated at the core and one at the shell of the fiber. This has already been successfully demonstrated in the development of tissue engineering scaffolds that utilize a biodegradable shell to control the release of proteins from the core of the fiber [26]. However, it

could be used easily to create a biodegradable fiber that releases two functional molecules over time to facilitate multiplexed detection. Finally, the microsphere-encapsulating nanofibers reported by Ionescu et al. could be used to release multiple biorecognition elements into a sample matrix, allowing for the detection of many target analytes [80].

Cell culture Sensors

Biosensors have been incorporated within cell culture platforms to assess the response of different cell types to pharmaceuticals, nanoparticles, and growth conditions [82,83]. In general, three-dimensional cell culture scaffolds better replicate *in vivo* cellular conditions when compared to two-dimensional cultures composed of monolayers [82,84]. As described above, due to their highly porous three-dimensional structure, nanofiber scaffolds can support cell growth, morphogenesis, cell metabolism and cell-to-cell communication. Additionally, because electrospun nanofibers can incorporate a variety of functional additives, there is the potential for the development of nanofiber scaffolds that couple cell culture with direct monitoring of cell response to stimuli. For example, the highly biocompatible BSA nanofibers produced by Valmikinathan et al. can be functionalized with FITC to produce a non-invasive pH sensor for use within cell culture platforms [43]. Additionally, enzymes could be incorporated within nanofiber scaffolds to allow for real-time analysis of cell metabolism and toxicity.

One of the main applications of cell culture biosensors is testing the toxicity of pharmaceuticals on different cell types [83,84]. As discussed, nanofibers capable of eluting pharmaceuticals have been developed and could be incorporated directly within cell cultures to facilitate analysis. The release of pharmaceuticals into cell culture could be regulated by controlling the specific composition of nanofibers used. In addition, the large surface area and three-dimensional structure of the nanofiber mats could help ensure that there is a uniform

distribution of the drug within the cell culture, eliminating inconsistencies in cellular dosing and response.

Another application of cell culture biosensors is monitoring the metabolism of different cell types [85]. Integrating nanofibers containing glucose oxidase directly within cell culture scaffolds could facilitate real-time monitoring of cellular metabolism [31]. Additionally, incorporation of conductive nanofibers that have been rendered biocompatible through coating or co-spinning with biocompatible polymers could facilitate electrochemical detection [37].

In vivo Sensors

In vivo biosensors have the potential for allowing continuous, real time monitoring of a patient. For example, because of the feasibility of developing them, subcutaneous continuous glucose sensors have been investigated as a desirable alternative to conventional glucose monitoring [86,87]. However, the development of *in vivo* sensors is complicated by their many requirements. Generally, *in vivo* sensors need to be reagentless, stable in hostile environments, and biocompatible [86–88]. Most importantly, the sensor must have a very limited effect on surrounding tissues to ensure that it is not rejected and that sensor results are not altered by a nearby inflammatory response. Several approaches have been investigated in the creation of *in vivo* sensors, including batch sampling of biological fluids, indwelling catheters, microdialysis and subcutaneous implants [86]. Electrospun nanofibers, functionalized directly with the necessary enzymes and sensing elements, could address the need for reagentless detection and simultaneously increase the biocompatibility of the implant. Furthermore, biodegradable fibers that elute antibiotics or antimicrobial agents could be used to reduce inflammation and reaction around implant surfaces.

Conclusion

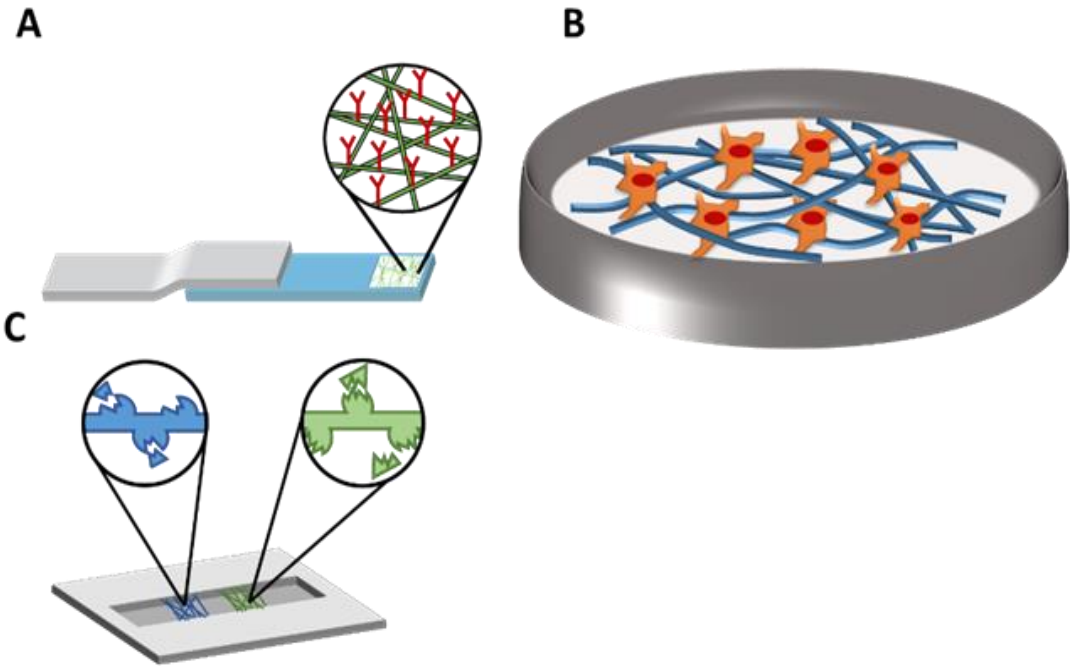

Figure 1.3 Future applications of functionalized nanofibers in biosensing **(a)** Antibody-functionalized nanofibers incorporated into lateral flow assays to increase limit of detection, improve device stability in ambient conditions, and simplify immobilization. **(b)** Cell culture sensor created from biocompatible, drug eluting nanofibers. **(c)** Multiplexed sensing facilitated by spinning multiple types of nanofibers in microfluidic devices.

Electrospun nanofibers are a versatile material with high surface-area-to-volume ratios, large porosity, and a wide range of available surface chemistries [8,38]. They have been used with great success in tissue engineering [28,72,77] and drug delivery platforms [66,67], and are increasingly being utilized in sensing platforms [20,21,31]. Generally, nanofiber-based biosensors have improved sensitivity due to the increased immobilization efficiency of biorecognition elements [16]. However, nanofibers offer much more than immense surface areas, as demonstrated by the many useful surface chemistries described in this review. Consequently, it is time to translate knowledge of nanofiber composition and fabrication generated from other disciplines into novel,

improved bioanalytical systems (Figure 1.3). In particular, electrospun nanofibers can be used to immobilize biorecognition molecules, create nonspecific binding-resistant surfaces, increase stability of biological molecules, and provide orientation of biorecognition elements. Nanofibers should therefore be utilized within bioanalytical systems to enhance sample preparation (filtration, separation, and concentration), binding events, and signal transduction. Miniaturized bioanalytical systems can particularly benefit from the use of electrospun nanofibers to enable further development of portable devices that require smaller reagent and sample volumes than traditional devices, making them more accessible for use in point-of-care settings [13,16]

CHAPTER 2

Electrospun Nanofibers as Effective Micromixers in Microfluidic Channels

Abstract

Electrospun polystyrene (PS) microfibers and poly(vinyl alcohol) (PVA) nanofibers with different morphologies were incorporated into Y-shaped poly(methyl methacrylate) (PMMA) microchannels. The effect of fiber shape, diameter, mat length, and mat height on fluid mixing within the microchannels was investigated. The most mixing was observed in mats containing PVA nanofibers, which had the smallest diameters of the fibers investigated. A 5 mm long PVA nanofiber mat resulted in 71% mixing at the outlet of the channel, which compares favorably to other passive mixers published. Unmodified control channels produced only 29% mixing. The significant inhomogeneity in pore size and distribution within the PVA mats is assumed to be the cause of this increase in diffusive mixing. Several morphologies of PS microfibers also produced significant mixing, with a maximum of 51% mixing observed in the 15% w/v PS microfibers. Interestingly, mixing was shown to increase with increasing diameter for microfibers of 0.84μm to 2.7 μm in diameter. Within all of the fiber mats, fluid mixing increased with nanofiber mat height, which correlates with the vertical space occupied within the microfluidic channel. Doubling of the height of the nanofiber mat corresponded to an average increase in fluid mixing of 14% for the PVA nanofibers and 8% for the PS microfibers. As expected, mixing decreased with increasing flow rate as the characteristic diffusive mixing length is proportional to the fluid velocity[89]. Overall, the amount of mixing observed was independent of the length of the nanofiber mat used (which ranged from 3-10mm). Therefore, we assume that most mixing occurs as the fluid enters and exits the nanofiber mats. The reproducible and significant mixing produced by the fiber mats, along with their ease of fabrication, make nanofiber-based mixing a promising and reliable tool for passive microfluidic mixing.

Introduction

Microfluidic biosensors that incorporate both sample preparation and analyte detection are referred to as microTotal Analysis systems (μTAS). They have many advantages over conventional biosensors. In particular, miniaturized devices allow for the use of smaller reagent and sample volumes while also providing shorter assay times and high-throughput detection[90]. Further, μTAS are often more portable and less expensive to manufacture and run than their larger counterparts, allowing for their use in point-of-care, developing world, or rural healthcare facilities [91] and in on-site environmental monitoring[92].

However, microfluidic channels generally feature low Reynold's number fluid flow, resulting in laminar flow patterns and limited fluid mixing [5–7]. Achieving rapid and reliable fluid mixing is essential for facilitating (bio)chemical reactions and allowing for adequate access of analytes to functional surfaces within microfluidic sensors [5]. In general, mixing within microfluidic channels can be improved through increasing the contact surface and lowering the diffusion path between fluids [5,93].

Many micromixers have been proposed and developed to address this need for fluid mixing in miniaturized devices[94–96]. These mixers can either be integrated directly within the microfluidic channel or function as a separate component that interfaces with the microfluidic device. Mixers are classified either as passive or active mixers[5,6]. Passive mixers utilize diffusion and chaotic advection to achieve mixing [6,7]. Active mixers, on the other hand, apply an external energy field to enhance mixing within the channel[6]. In general, active mixers produce reliable, complete mixing but are more complicated and expensive than passive mixers due to the need to integrate the external force field[5]. Therefore, passive mixers are often much simpler than active

mixers and can be easier to fabricate and utilize. Several common passive mixers include T-type, Y-type, split and recombine, chaotic, multi-laminating and jet colliding mixers[6]. In each of these mixers, the flow pattern is manipulated by different channel geometries or by incorporating microstructures within the channel. Most mixers are fabricated using photolithography or micromachining, which require access to a cleanroom and/or expensive machinery[92].

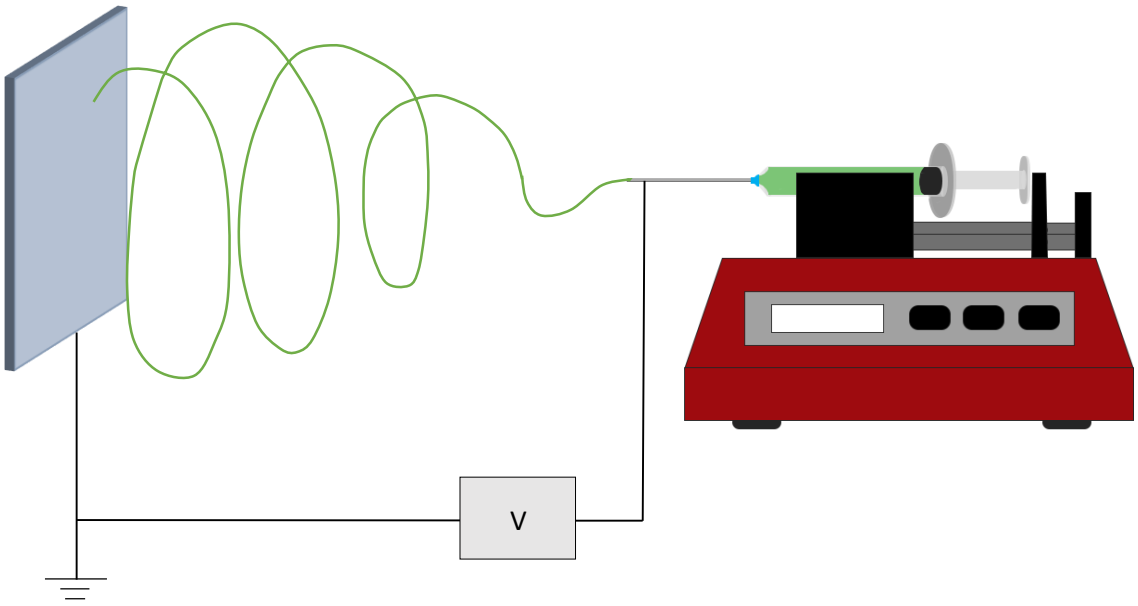

Figure 2.1 A typical electrospinning apparatus consisting of a syringe filled with a polymer spinning dope, a high voltage power source, a grounded collector plate, and a syringe pump.

Electrospinning is a well-understood and relatively simple fiber fabrication process in which an electric field is applied to a polymer spinning dope to generate nano- and microscale fibers[97]. A typical electrospinning apparatus consists of a high voltage power source, a syringe pump, a spinneret (typically a syringe) filled with a polymer spinning dope, and a grounded collector plate (Figure 2.1)[16,97]. During electrospinning, the viscous polymer solution is slowly pumped out of the spinneret, which is placed across from the grounded collector plate. When voltage is applied to the spinning solution, it forms a Taylor cone at the tip of the spinnerett[16]. Once the electrostatic attraction between the charged polymer solution and the grounded

collector plate overcomes the surface tension at the tip of the spinneret, fibers will accelerate from the tip of the Taylor cone and collect on the grounded collector plate[16]. The nonwoven nanofiber mats produced by electrospinning are characterized by extremely high surface-area-to-volume ratios, high porosities, and small pore sizes[39]. Electrospun nanofibers have been used in a variety of fields, including the development of high performance fabrics[98], fuel cells[99], tissue culture scaffolds[28], and biosensors [16,17,100]. Electrospun nanofibers can be fabricated from a variety of materials, including biocompatible polymers, and are easily functionalized through the incorporation of nanoscale materials into the polymer spinning dope[16]. Previously, we have demonstrated that electrospun poly(vinyl alcohol) (PVA) nanofibers can be used for sample preparation and analyte concentration within microfluidic systems[10]. However, due to their complex nonwoven three-dimensional structure, it is hypothesized that electrospun nanofiber mats can also be used to enhance fluid mixing within microfluidic channels through manipulation of the flow patterns within the mats. Two different polymers, PVA and PS, were used to produce fibers with different diameters and morphologies to determine their effect on mixing within PMMA microfluidic channels.

Materials and Methods

Electrospinning

The PS fibers were spun using a Spraybase vertical electrospinning system (Profector Life Sciences, Ireland), while the PVA nanofibers were spun using a homemade horizontal electrospinning system as previously described[9,10]. Positively charged PVA fibers were produced by adding hexadimethrine bromide (polybrene) (Sigma Aldrich) into the PVA spinning dope. The PVA used had a molecular weight of 78,000 and is 99.7% hydrolyzed (Polysciences Inc.,

PA) [9]. A 10% w/v PVA spinning dope was first created by dissolving PVA in deionized (DI) water at 95° C for four hours. Then, polybrene was dissolved in DI water at room temperature for 10 minutes, and was added to the PVA solution to make a final spinning dope with a 90/10 w/w PVA/polybrene ratio. The nonionic surfactant Triton X-100 was added to the spinning dope to improve spinnability, and the resulting solution was mixed for two minutes using a vortex at its highest speed. The spinning dope was then loaded into a 5 mL BD plastic syringe with an 18 gauge needle, which was placed horizontally into a syringe pump. The syringe pump was set to 0.01 mL/min. A high voltage power source was connected to the spinning needle and set to 15 kV (Gamma High Voltage Research Inc., FL). A piece of copper wrapped in aluminum foil was used as a grounded collector plate and was placed 15 cm from the syringe tip. After spinning, the aluminum foil was removed from the copper plate and was cut into strips using a razor blade. The nanofiber mats were then peeled off the foil strips using tweezers and were placed on pieces of poly(methyl methacrylate) (PMMA) that had undergone treatment in an UV-ozone (UVO) oven for 15 minutes (Jelite, CA). The UVO oven contained a low pressure mercury vapor grid lamp, which had an output of 28,000 mWatts/cm^2 at 254 nm. During UVO treatment, oxygen was flowed through the oven at 0.5 L/min. The PVA fibers were initially spun as 20, 30, and 40 µm thick mats, however the nanofiber distribution varied along the heights of the mats, producing inconsistent mixing within the channels. Therefore, nanofiber mats of approximately 10 µm height were spun and stacked to create thicker nanofiber mats with more uniform nanofiber distributions. The mats were cut into 3mm, 5mm, and 10 mm long strips for the studies examining the effect of nanofiber mat length on mixing.

The PS microfibers were spun using a solvent solution composed of 50/50 v/v THF/DMF. Polystyrene with a molecular weight of 280,000 (Sigma Aldrich) was dissolved in

the solvent solution at room temperature for 24 hours on a stir plate with medium setting. Different fiber morphologies were produced by using three different PS concentrations in the spinning solutions: 12.5%, 15%, and 17.5% w/v.

The PS spinning solution was loaded into a 5 mL glass syringe (BD) and was spun using a Spraybase vertical electrospinning system with an 18 gauge needle. The fibers were spun using a 20 cm vertical distance, 10.6 kV applied voltage, a 0.01 mL/min flow rate, and a circular metal collector plate. The fibers were then manually transferred to PMMA squares that had been treated in the UVO oven for 4 minutes at an oxygen flow rate of 0.5 L/min and lamp power of 28,000 mWatts/cm^2 (Jelite). The fiber mats were cut into 10 mm long strips using a scalpel and unwanted fibers on the PMMA surfaces were removed using a strip of adhesive tape. The mats were incorporated onto the PMMA chips in one-layer or two-layer configurations.

Analysis of Nanofiber Morphology

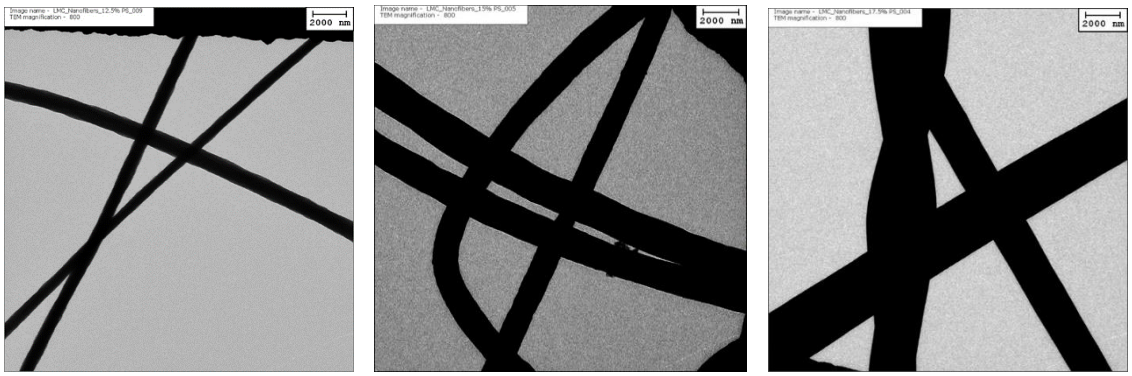

Figure 2.2 TEM image of **(a)** 12.5% w/v **(b)** 15% w/v and **(c)** 17.5% w/v PS nanofibers. Fibers were spun onto carbon-coated grids for 15 seconds. Micrographs were taken using a type CM 12 Philips TEM at 120 keV

The thickness of PVA nanofiber mats was assessed using a Leica SP2 confocal microscope to measure the thickness of the mats prior to incorporation into the microfluidic

channels [10]. The polybrene/PVA nanofibers produced in our lab have previously been demonstrated to have an average diameter between 450-550 nm [9].

Micrographs of the three different types of PS microfibers were taken using a Transmission Electron Microscope (TEM) (type CM 12 from Philips, Hamburg, Germany) at 120 keV and magnifications ranging from 800 to 3000-fold. In order to facilitate TEM analysis, the fibers were spun directly onto carbon-coated copper grids for 15 seconds. The diameter of the cylindrical portion of the different nanofiber types was measured in six points per fiber type and averaged. The 12.5% w/v PS fibers had a 0.84 $\pm$ 0.14 μm diameter, 15% w/v PS fibers had a 1.5 $\pm$ 0.2 μm diameter, and 17.5% w/v PS fibers had a 2.7 $\pm$ 0.5 μm diameter (Figure 2.2). Additionally, the 12.5% w/v PS fibers had a heavily beaded morphology (Figure 2.3), the 15% w/v fibers had sporadic beading, and the 17.5% w/v had large cylindrical diameters with no beads (Figure 2.2). The beads were not considered when measuring the microfiber diameters.

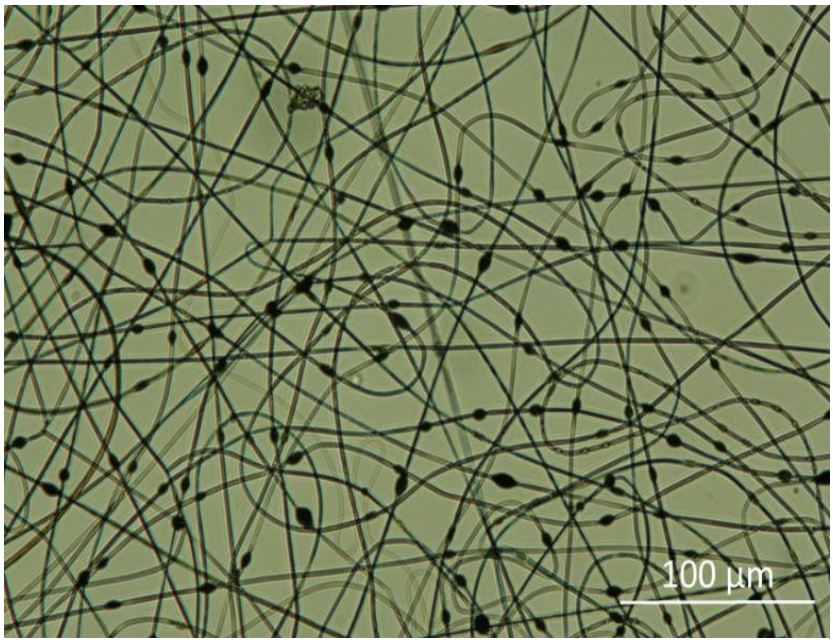

Figure 2.3 Morphology of 12.5% w/v PS nanofibers. Fibers were spun onto a metal collector plate and manually transferred to a UVO-treated piece of PMMA. Image taken with a Nikon Digital Eclipse C1 confocal microscope in brightfield setting.

Hot Embossing and Bonding of Channels

Y-shaped microfluidic channels were stamped into PMMA using hot embossing with a copper template[9]. The copper template was fabricated at the Cornell Nanoscale Facility (CNF) using KMPR 1050 photoresist (Micro-Chem Corp., MA) and copper electroplating to produce raised copper channels on a smooth copper plate[101]. The channels used in this study were 31 µm deep, 1 mm wide, and 29 mm long. The channels used with the PVA nanofibers were embossed using a Carver Laboratory Hot Press at 130 ^{o}C and 10,000 lbs (44,482 N) of force. The channels used with the PS nanofibers were embossed using a Specac Hot Press at 100 ^{o}C and 0.1 ton of force for 5 minutes. The inlet and outlet holes were drilled at each end of the channel with a 0.8 mm steel drill bit.

UVO-assisted thermal bonding was used to create the completed microfluidic devices[10]. First, the pieces of PMMA that had been embossed with the microfluidic channels were UVO treated using an oxygen flow rate of 0.5 L/min and lamp power of 28,000 mWatts/cm^2. The PMMA used with the PS microfibers was treated for 4 minutes, while the PMMA used with the PVA nanofibers was treated for 15 minutes. Then, the pieces of PMMA with the fiber mats were UVO treated for 4 minutes. The two pieces of PMMA were sandwiched together so that the fibers faced the microchannels. The sandwich assembly was placed between two blank pieces of copper and pressed on the hot press. PS fibers were bonded into channels at 80 ^{o}C and 0.1 ton force, while PVA nanofibers were bonded into channels at 100 ^{o}C and 10,000 lbs (44,482 N) of force. The different UVO treatment times, temperatures and applied forces were necessary due to differences between the two hot presses used. Polyvinyl chloride tubing (Tygon) with a 0.508 mm external diameter was glued into the inlet and outlet holes with Quicktite instant adhesive gel (Loctite).

Fluid mixing

Each Y-shaped microfluidic channel was filled with water in one inlet and a 0.03M sulforhodamine B (SRB) in water solution in the other inlet (Figure 2.4). Because channels filled with nanofiber mats are prone to form air bubbles at low flow rates, each channel was initially filled with fluid at 20 µL/min for 5 minutes to remove air bubbles from the nanofiber mats and ensure that they didn't impact the mixing observed. Then, the flow rate was dropped to 5 µL/min and a steady flow profile was allowed to develop for 5 minutes before a fluorescent microscopy image was taken of the channel (Leica). This was repeated for flow rates between 4 µL/min and 1 µL/min. Lower flow rates were not used as pulsatile flow was observed at rates below 1 µL/min.

Several fluid mixing experiments were recorded using a Nikon Eclipse 90i confocal microscope to confirm that the observed mixing was consistent along the height (z direction) of the channel (Fig A.1 in Appendix A). The fluid mixing experiments were conducted on the stage of the confocal microscope. During fluid flow, the confocal was used to perform a z-scan of the channels in order to examine the fluid flow profile along the z direction of the channel. Images of the channels were taken at 1 µm intervals in the z direction.

Data Analysis

Image J was used to measure the pixel intensity of each pixel in a column along the 1 mm width of the channel (Figure 2.4). Then, the mixing index of each column of pixels was determined using the following formula[102,103]:

$$mixing\ index = \sqrt{\frac{1}{N}\sum\left(\frac{I_K - I_O}{I_O}\right)^2}$$

I_K = intensity of pixel K

I_O= average intensity of all pixels in a column

N= number of pixels in a column

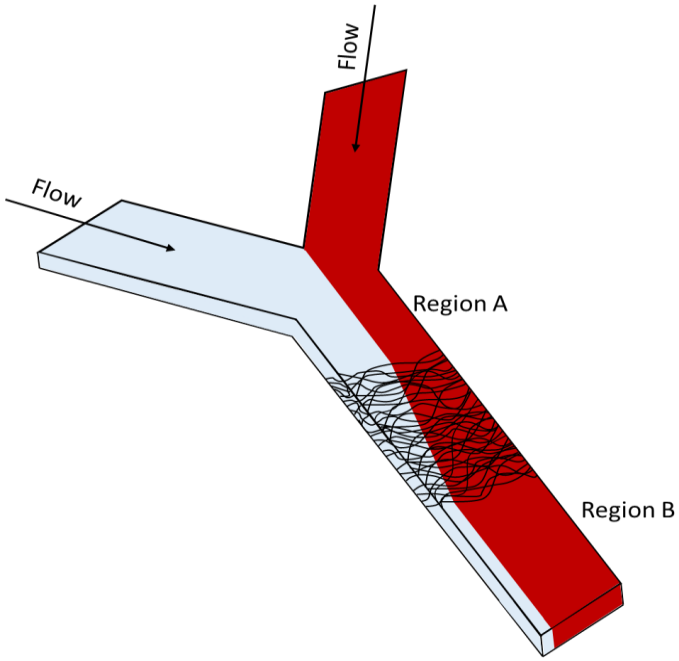

Figure 2.4 Fluid mixing experimental setup. One inlet was used to fill the channel with DI water, the other filled the channel with SRB in water. Nanofiber mats with different lengths and thicknesses were placed in the center of the channel to encourage fluid mixing.

The average mixing index at the inlet of each channel was determined by averaging the mixing index of each column in a 50 pixel wide section of the channel before the nanofiber mats where a steady flow profile existed (region A in Figure 2.4). The average mixing index of the

channel after the nanofiber mat was determined by averaging the mixing index of each column in a 50 pixel wide section of the channel near the outlet of the channel where again a steady flow profile existed (region B in Figure 2.4). Each set of parameters was tested using between 3 and 5 different channels to determine reproducibility of the results.

Statistics

Average Mixing Index data for all the channels were compiled in Microsoft Excel. A MATLAB code was written to perform multiple linear regression analysis on the data and determine the statistical significance of mixing within channels containing the nanofiber mats (as compared to mats containing no nanofibers) (Appendix B). Multiple comparisons were made using the Holm test, which controls for the accumulation of error that occurs when multiple t tests are performed [104]. The Holm test sequentially compares the p values of multiple comparisons (from smallest p value to largest p value), with each comparison getting progressively less conservative to account for the number of comparisons that have already been done[105]. The roles of nanofiber mat length, nanofiber mat height (i.e. number of fiber layers), and flow rate on observed fluid mixing was analyzed for the PVA nanofibers. The influence of nanofiber mat morphology (diameter and number of fiber layers) and flow rate on observed fluid mixing was determined for the PS nanofibers. Each condition was run in at least triplicate and the mixing values used by the MATLAB code were the average of 50 pixel lengths. Significance was set as $p < 0.05$.

Results and Discussion

Microfluidic analytical systems depend on efficient fluid mixing to ensure that the desired reactions can take place under optimal conditions. This work examines a possible mixing

effect caused by nanofiber mats that have been integrated as a functional component within a microfluidic biosensor. Many passive micromixers reported in literature utilize obstacles to split inlet streams into narrow flow streams, thus increasing the interfacial areas of the fluids, shortening diffusion pathways, and decreasing mixing time [106,107]. The obstacles used within these studies all have diameters on the order of 10 or 100 μm, making them substantially larger than the fibers used in this study[5,6,93,107]. Indeed, the individual fibers themselves are likely too small to serve as obstacles that redirect the flow pattern within the channels. However, it was postulated that the dense, porous structure of the fiber mats would lead to enhanced mixing of solutions flowing through the mats. In order to investigate which type of fibrous media was most capable of causing increased mixing within microfluidic channels, both electrospun nanofibers (PVA) and electrospun microfibers (PS) were incorporated into the microchannels. Parameters investigated were fiber mat density, mat thickness (these two are closely related in the electrospinning process[10]), mat length, fiber diameter, fiber shape, and flow rate.

Thick Nanofiber Mats

Initially, PVA nanofiber mats that were 20 μm, 30 μm, or 40 μm thick were incorporated into the microfluidic channels (31 μm deep) to determine if thicker nanofiber mats produced better mixing by increasing the volume of the channel occupied by nanofibers. Each nanofiber thickness was tested as a 3 mm, a 5 mm, and a 10 mm wide strip of fibers (Figure A.2 in Appendix A). While mixing was observed in many of the channels tested, there was significant variability in the flow profiles produced from the same nanofiber mat morphology (Figure A.2 in Appendix A). Confocal microscopy of the nanofiber mats demonstrated that the nanofiber distribution along the thickness of the mats was not uniform. The mats were most dense at the bottom of the mat and frequently had a sparse nanofiber distribution in the top of the mat (Figure

A.2 in Appendix A). However, while the fiber distribution between nanofiber mats with the same thickness also varied significantly along their depths, the first ~10 μm showed a consistent morphology both within a single nanofiber mat and between different mats spun.

Several groups have previously demonstrated that electrospun nanofibers are not evenly collected on the grounded collector plate due to the shape of the electric field that exists between the charged spinneret and the collector plate [11,12,108]. During electrospinning, the thickness uniformity of the nanofiber mats has been shown to decrease with longer spinning times, with short spinning times yielding the most uniform nanofiber mats[11]. Therefore, it was determined that the variations seen in the flow profiles in the thick nanofiber mats were caused by these non-uniformities.

Layered PVA Nanofiber Mats

In order to address the need for nanofiber filters with uniform morphologies, Podgórski et al. (2006) and Zhang et al. (2010) created multi-layered nanofiber mats by stacking thin nanofiber mats[11,108]. These multi-layered filters demonstrated both more uniform fiber distribution and improved filtration performance. Therefore, to improve the reproducibility of our mats, we spun ~10 μm thick nanofiber mats and stacked them to obtain thicker nanofiber mats with more uniform fiber distributions. This layered approach was used with varying fiber mat length (3mm, 5mm, 10mm) and thickness (one layer or two layer) (Figure 2.5).

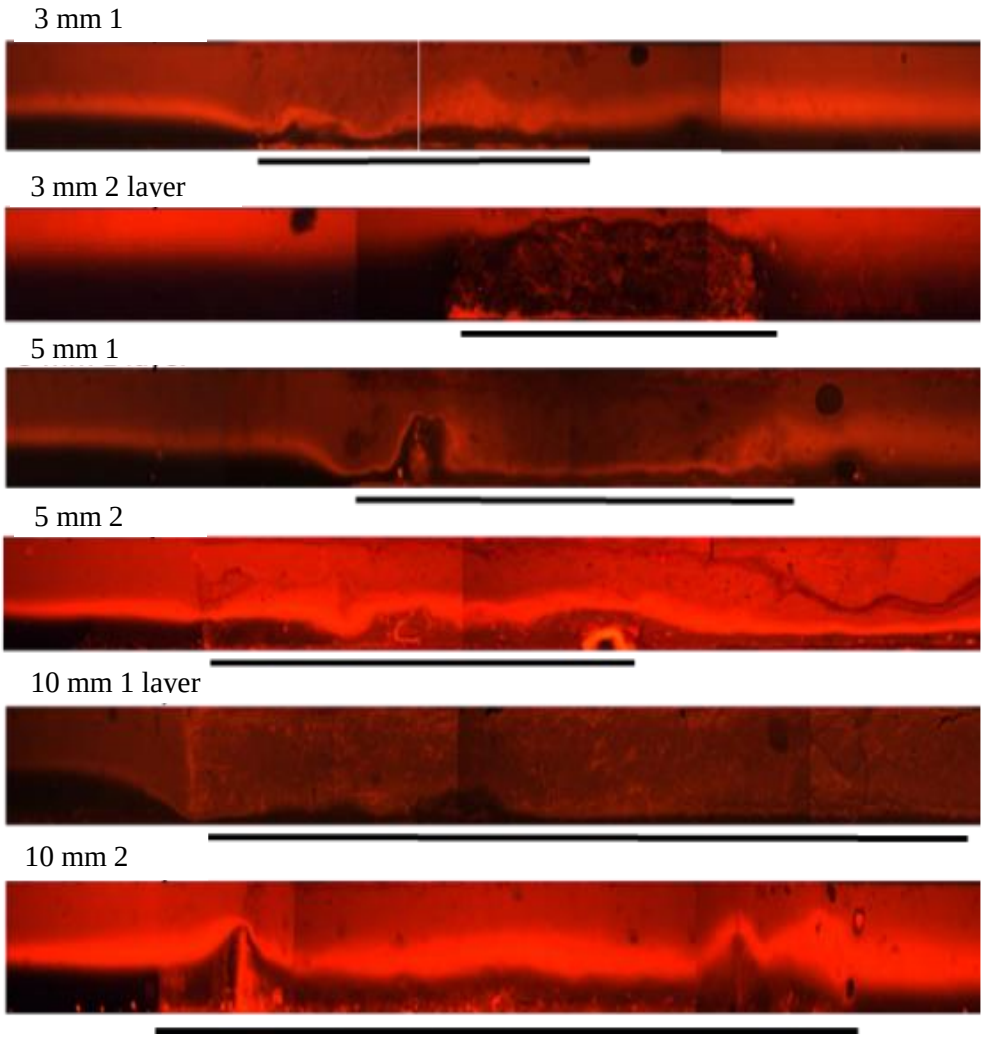

Figure 2.5 Example channels showing mixing produced by each set of nanofiber mat morphologies at a flow rate of 1 µL/min. Black lines indicate the location of nanofiber mats. Leica fluorescent microscope, 5x objective.

For data analysis, as described above, image J was used to measure the pixel intensity of each pixel in a vertical column along the 1 mm width of the channel. In the unmixed regions before the nanofiber mats, the pixel intensities along a column had a binary profile, indicating that the channel was divided into two different flows that were not mixed (Figure 2.6). The half of the channel filled with water was indicated by a pixel intensity of ~10, the half of the SRB-filled channel resulted in an intensity of ~50. A peak was observed at the interface of the two solutions. As the SRB concentration chosen exhibited a slight quenching effect, its diluted form at the interface therefore results in a higher fluorescence signal. This two-phase system enters the nanofiber mats. Mixing occurring within the nanofiber mat will result in a decline of the signal difference observed between the two halves of the channel. For quantification, the pixel intensity distribution is also measured after the solution exits the nanofiber mat. As can be seen in Figure 2.6, the profile becomes more uniform, with the pixel intensity increasing rapidly and plateauing where the solution in the channel is mixed (Figure 2.6). Furthermore, it can be

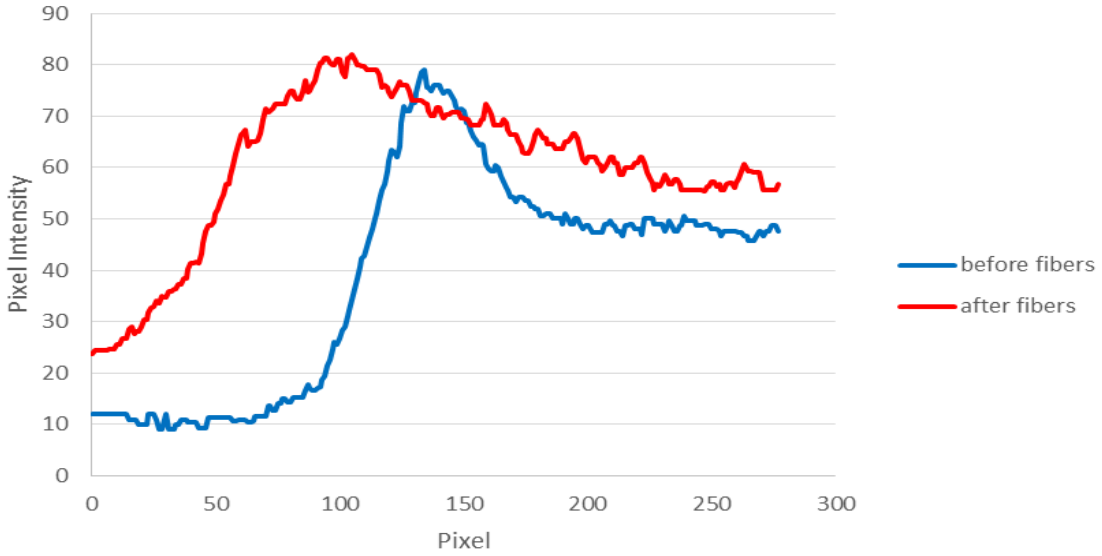

Figure 2.6 Pixel intensities of a region before the nanofiber mat and after the nanofiber mat for a 5mm, two-layer mat with flow rate of 1µL/min. Pixel intensity values shown represent the average value of 50 vertical columns across the 1 mm width of the channel.

observed that a pure buffer solution is no longer present as the minimum pixel intensity within the channel increased significantly to ~25. The highest pixel intensity is reached more quickly in the region after the nanofibers and is more consistent, as the SRB dye has spread to a larger portion of the channel and has mixed into a more uniform profile.

The average mixing index at the inlet and outlet of each type of channel was calculated using image J (Table 2.1). The change in outlet mixing index between the control channels (no nanofibers) and the nanofiber channels was calculated to determine whether the channels containing nanofiber mats exhibited more fluid mixing than empty control channels (Table 2.1). Based on their outlet mixing indexes, the nanofiber mats studied produced the most mixing in the two-layer mat configuration (Table 2.1). As the one-layer mat will only occupy approximately a third of the total height of the microchannel, the fluid can partly pass above the nanofiber mat without having to flow directly through the mat. On the other hand, the two-layer mat will likely fill most of the channel height, forcing the fluid to pass through the nanofiber mats. Additionally, the outlet mixing index values for the two-layer nanofiber mats had lower standard deviations than the one-layer mats or the control channels, indicating that the mixing observed in the two-layer mat morphology is more reproducible.

It was also observed that for the two-layer mat morphologies, the average mixing index at the inlet of the channels was markedly lower than the inlet mixing index of the channels containing no nanofibers. We assume that this is caused by back pressure produced by the mats. In turn, this pressure would slow the fluid velocity at the inlet of the channel, allowing for more diffusive mixing before the fluid even enters the nanofiber mat and enhancing the overall desired mixing of the two solutions.

Table 2.1 Average mixing index in channels containing different PVA nanofiber mats. Each mixing index was calculated for channels with a flow rate of 1 µL/min. Values shown are calculated as the average mixing index of at least three channels.

Morphology	Mixing Index (Inlet)	Stdev	Mixing Index (Outlet)	Stdev	Difference from Control Outlet Mixing Index	Stdev
No fibers	0.8	0.17	0.71	0.12	-	-
3 mm 1 layer	0.56	0.2	0.41	0.13	0.30	0.17
3 mm 2 layer	0.53	0.07	0.36	0.09	0.35	0.15
5 mm 1 layer	0.64	0.08	0.45	0.11	0.26	0.16
5 mm 2 layer	0.45	0.08	0.29	0.09	0.42	0.15
10 mm 1 layer	0.74	0.22	0.52	0.07	0.19	0.14
10 mm 2 layer	0.57	0.21	0.32	0.06	0.39	0.13

The effect of fluid flow rate on observed mixing was also determined. As expected, the amount of mixing observed in the channels increased as the flow rate decreased (Figure 2.7).

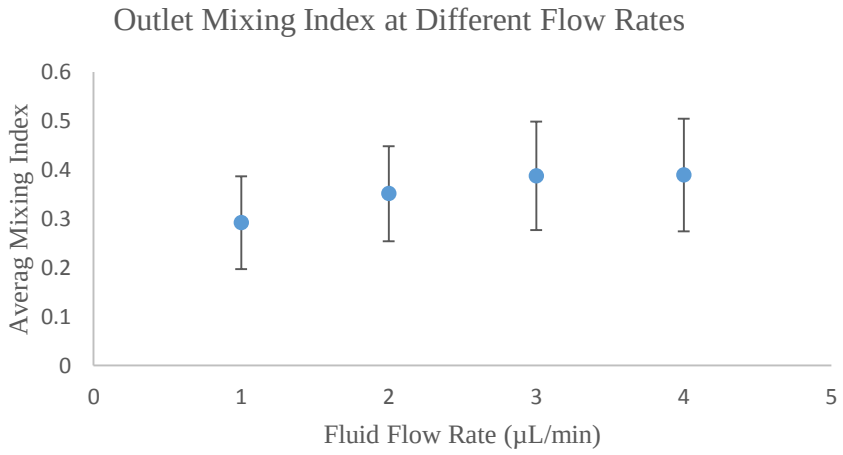

Figure 2.7 Outlet mixing index observed in 5 mm long two-layer mats at different flow rates. 3 channels were tested at each flow rate.

Multiple linear regression was used to determine if the mixing observed in the channels containing PVA nanofibers was statistically different than the diffusive mixing observed in empty control channels (Table 2.2). Statistical analysis showed that the increase in fluid mixing observed in all the PVA nanofiber mats was statistically significant ($p<0.05$), with the greatest increase in mixing observed with the two-layer mat morphologies as expected. The p value for mixing observed in the 3 mm 2 layer morphology is $2.35x10^{-10}$ with values below 0.05 generally considered to show statistically significant difference in data sets[109].

In order to better understand the influence of nanofiber mat height (number of layers) and length on the observed mixing, additional statistical analysis was performed. Based on the outlet mixing index values for the channels containing PVA nanofiber mats, the number of fiber mats and the flow rate appear to have an effect on the mixing produced in the microchannels, while the length of the nanofiber mat does not appear to play a role. Therefore, multiple linear regression was used to test these hypotheses with significance set as $p<0.05$ (Table 2.3). Overall, the hypothesis that the number of fiber mats affects the mixing index was highly significant ($p=5.5x10^{-8}$). On average, the two-layer mats reduced the mixing index by 0.14 relative to the one-layer mat. The flow rate was also found to play a statistically significant role in the observed mixing, with $p=0.0045$. On average, the mixing index increased by 0.03 for each 1 μL/min increase in flow rate. However, the effect of nanofiber mat length was not significant ($p=0.24$).

Table 2.2 Multiple linear regression variables and their outcome. The outlet mixing index values for each PVA mat morphology was compared to the outlet mixing index for empty control channels. It was determined that mixing was significantly increased in all of the fiber mats, with the greatest mixing increase seen with the two-layer mats.

Variable	Significant within Family of Comparisons?	Average Change to Mixing Value	p-value
3mm, 1 Layer	Yes	-0.182	1.7234e-05
3mm, 2 Layer	Yes	-0.285	2.3516e-10
5mm, 1 Layer	Yes	-0.209	3.5847e-07
5mm, 2 Layer	Yes	-0.344	4.4726e-12
10mm, 1 Layer	Yes	-0.136	2.3049e-3
10mm, 2 Layer	Yes	-0.340	6.6718e-12

Table 2.3: Multiple linear regression variables and their outcome for analyzing the effect of poly(vinyl alcohol) mat morphology. There were three families for comparison: (1) the different fiber mat lengths, (2) having two layers, and (3) the flow rate. Having two layers and flow rate were each considered to be significantly increased. However, the different fiber mat lengths did not appear to have an effect on mixing index.

Variable	Significant within Family of Comparisons?	Average Change to Mixing Index Value	p-value
3mm	No	-	Over all p=0.24
5mm	No	-	
10mm	No	-	
2 Layers	Yes	-0.142	5.15×10^{-8}
Flow Rate	Yes	0.03 per (μL/sec)	0.0045

Studying the effect of fiber diameter and shape on the mixing efficiency

In order to study the effects of fiber diameter and shape on fluid mixing within the channels, PS fibers of different diameters were incorporated into Y-shaped channels. The PS fibers were chosen for this study since they afforded a much larger diameter (2-7 times lager) than the positively charged PVA nanofibers used in the previous parts of this work. Several labs have successfully used micropillars with diameters in the 10 μm range to encourage fluid mixing within microfluidic systems[110,111]. Therefore, investigation of mixing within the PS mats would determine if fibers with micrometer diameters could similarly be used as obstacles to enhance

fluid mixing. Fibers with diameters larger than 2.7μm were not investigated as they could not be successfully bonded into the microfluidic channels. Additionally, the PS fibers have a beads-on-a-string morphology when spun at lower polymer concentrations and a smooth, cylindrical morphology at high concentrations. Therefore, PS fibers were also used to determine which fiber shape (beaded or smooth) produces more mixing within the channels. In the end, three different PS fiber types were used in this study. Fibers spun from a 12.5% w/v PS solution had a beads-on-a-string morphology and a diameter of 0.84±0.14 μm (Figure 2.3). Fibers spun from a 15% w/v PS solution have few beads and a smooth cylindrical morphology with a diameter of 1.5±0.2 μm (Figure 2.2). Finally, fibers spun from a 17.5% w/v PS solution have no beads and a cylindrical morphology with a diameter of 2.7 ± 0.5 μm (Figure 2.2).

Based on the previous results, which indicated that mat length does not play a significant role in mixing, the nanofiber mats were always 10 mm long and stacked in one or two layers within the channels. The 10 mm mat length was chosen as PS fibers are difficult to cut into smaller mats and the most reproducible mats could be made at this length as shorter mats were prone to tearing and curling while being cut. SRB and water were pumped through the channels at flow rates between 1 μL/min and 5 μL/min (Figure 2.8). Similar flow profiles at the inlet (Figure 2.9) and outlet (Figure 2.10) of the channels were observed for the PS systems as described above for the PVA nanofiber mats.

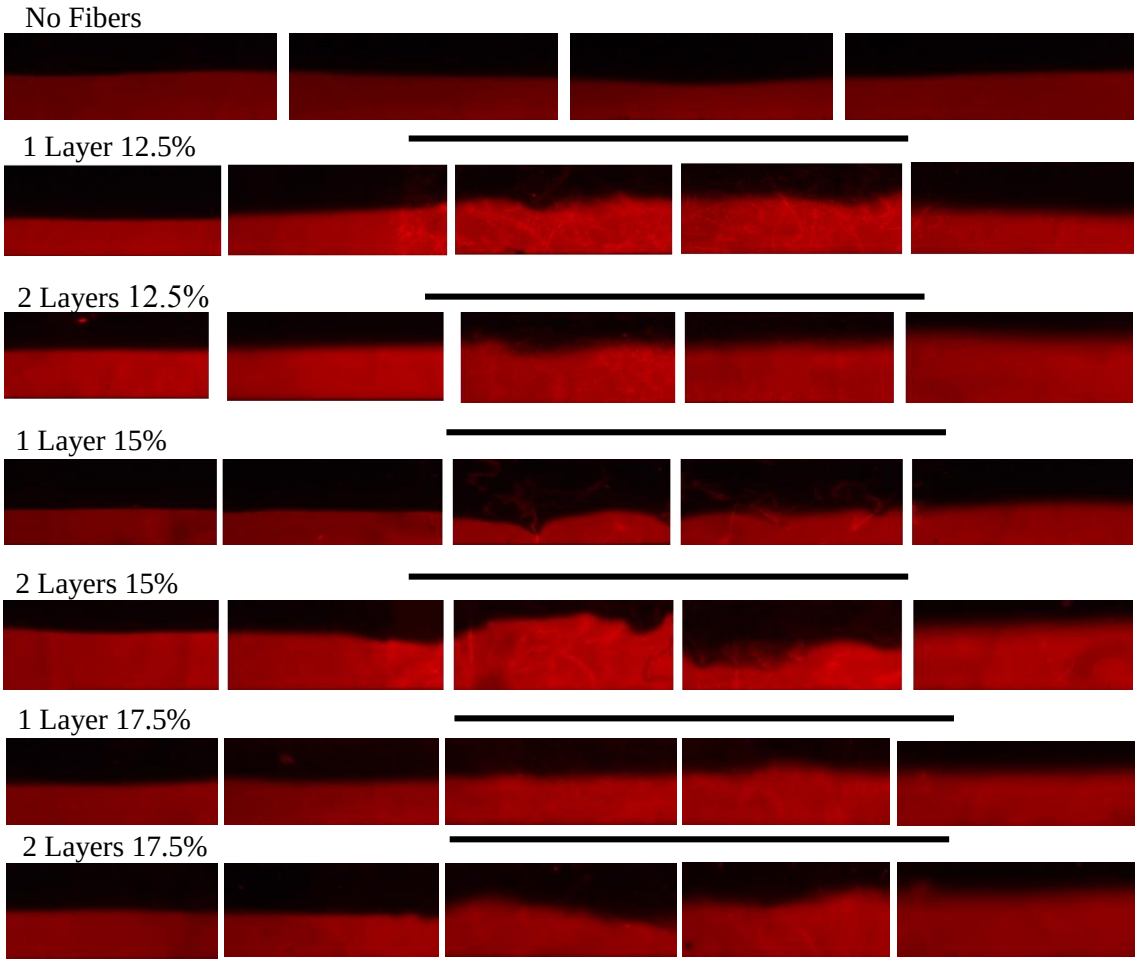

Figure 2.8 Flow profiles observed in channels containing PS fiber mats. Flow at 1 µL/min. Black lines indicate location of nanofiber mats within the channels. Leica Fluorescent Microscope. 5x objective.

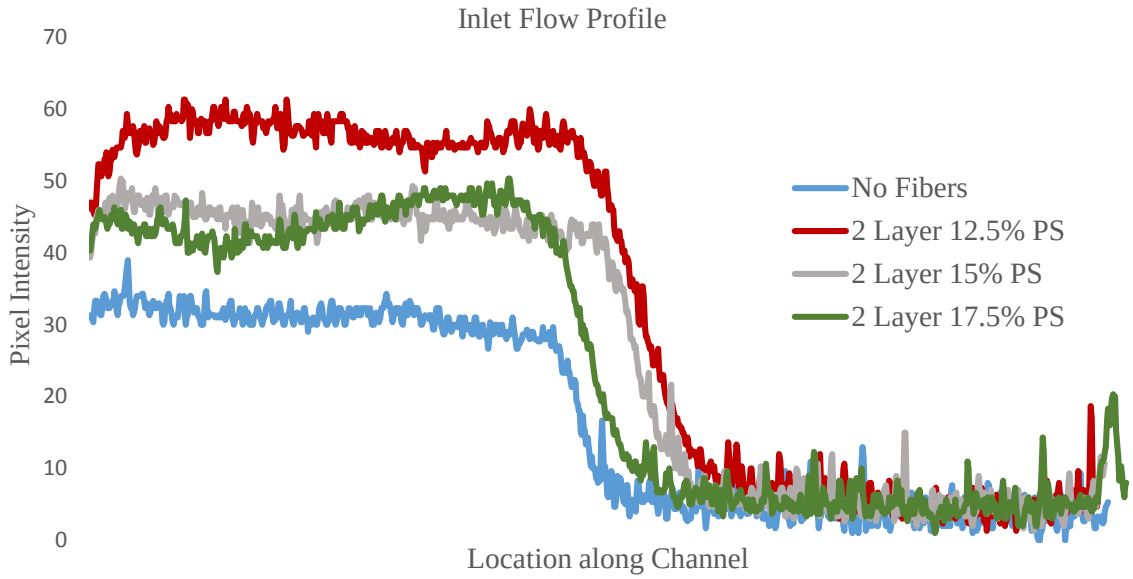

Figure 2.9 Flow profiles at inlets of channels containing different PS fiber morphologies. Flow rate was 1 µL/min.

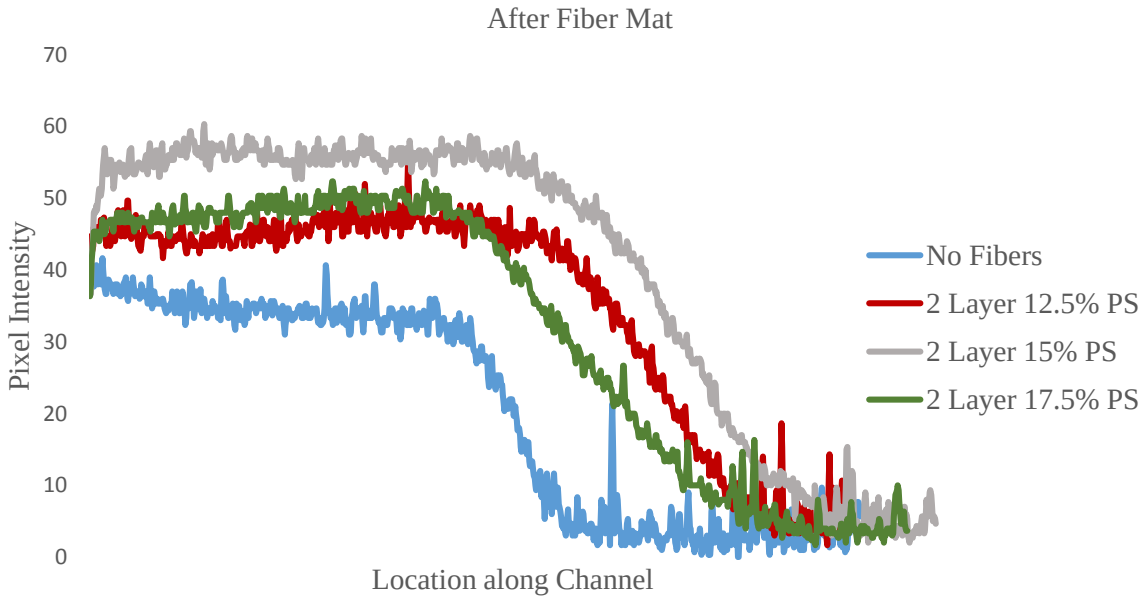

Figure 2.10 Flow profiles at outlets of channels containing different PS fiber morphologies. Flow rate was 1 µL/min.

The average mixing index values at the inlets and outlets of the different channels were calculated using image J as previously described (Table 2.4). The difference in outlet mixing index for the nanofiber channels and the control channels was used as a metric of how the various PS fiber morphologies affected mixing within the channels (Table 2.4). The mixing in the PS fibers exhibited many of the same trends as the mixing in the PVA nanofiber mats, though the average mixing indexes were higher for the PS fibers (indicating less mixing). As with the PVA nanofibers, the two-layer PS fiber morphologies produced a larger change in outlet mixing index than the one-layer morphologies (Table 2.4). Additionally, the two-layer morphologies had smaller standard deviations in their outlet mixing index values, indicating that their mixing is more reproducible than the one-layer mats. Finally, the inlet mixing index values for the two-layer mats were also smaller than the inlet mixing index of the control channels, indicating that the increase in mixing observed in two-layer fiber mats is due both to an increase of diffusive mixing in the inlet region of the channel and mixing from fluid flow through the fiber mat itself.

Table 2.4 Average mixing index in channels containing different PS fiber mats. Calculated for channels with a flow rate of 1 μL/min. Each mixing index is calculated as the average mixing index of at least three channels.

Mat Morphology	Mixing Index (Inlet)	Stdev	Mixing Index (Outlet)	Stdev	Difference from Control Outlet Mixing Index	Stdev
No fibers	0.80	0.17	0.71	0.12	-	-
1 layer 12.5%	0.84	0.12	0.64	0.17	0.07	0.21
2 layer 12.5%	0.77	0.05	0.56	0.09	0.15	0.15
1 layer 15%	0.87	0.02	0.78	0.05	-0.07	0.13
2 layer15%	0.67	0.05	0.49	0.03	0.22	0.12
1 layer 17.5%	0.71	0.28	0.56	0.19	0.15	0.22
2 layer 17.5%	0.72	0.23	0.57	0.18	0.14	0.22

The PS fibers produced a smaller change in outlet mixing index than the PVA nanofibers, indicating that it is more effective to use nanoscale fibers than microfibers to induce mixing in microfluidic channels. In order to determine if the mixing in the different PS mats was statistically significant (when compared to empty control channels), multiple linear regression was used. Multiple comparisons within the mat type group were made using the Holm test with the overall p-value set as $p<0.05$. The different fiber weight percentages and layer combinations were represented as individual variables and compared for significance relative to their respective control of no fiber mat (Table 2.5). There were three PS nanofiber morphologies that produced a statistically significant increase in mixing when compared to empty control channels: 1 layer 17.5% w/v PS, 2 layer 15% w/v PS, and 2 layer 17.5% w/v PS. Therefore, though overall mixing was highest with PVA nanofiber mats (which have the smallest diameters of all the fibers used in this study), within the PS microfibers mixing increased with increased diameter. This

suggests that the mixing observed in the microfibers may be caused by a different mechanism than the mixing observed in the nanofiber mats. Multiple linear regression analysis was performed once more to determine the effect of fiber mat thickness (number of layers) and morphology (12.5%, 15%, or 17.5% w/v PS) on the mixing observed in the PS mats (Table 2.6). Once again, the fiber mat thickness had a very significant effect on fluid mixing, though the magnitude of this effect was decreased for the PS fibers (-0.084 change to the outlet mixing index) when compared to using two layers of PVA fibers (-0.142 change to the outlet mixing index). Additionally, increasing the diameter of PS fibers also increased the mixing observed in the channels. Finally, flow rate once again affected the mixing observed, with decreasing mixing with increasing flow rate.

Table 2.5 Multiple linear regression variables and their outcome. The different fiber mat types were considered as one family for comparison, and the flow rate another. 1 Layer 17.5%, 2 Layer 15%, and 2 Layer 17.5%, along with flow rate, were all considered to be significantly increased.

Variable	Significant within Family of Comparisons?	Average Change to Mixing Index Value	p-value
1 Layer, 12.5%	No	-	-
1 Layer, 15%	No	-	-
1 Layer, 17.5%	Yes	-0.128	0.0018
2 Layer, 12.5%	No	-	-
2 Layer, 15%	Yes	-0.146	0.00046
2 Layer, 17.5%	Yes	-0.127	0.0021

Table 2.6 Multiple linear regression variables and their outcomes for analyzing effects of polystyrene mat morphology on mixing index. The effect of fiber diameter, fiber mat height, and flow rate on outlet mixing index was determined using multiple linear regression. The mixing increased with increasing fiber diameter, fiber mat height, and decreased with increasing flow rate.

Variable	Compared To	Significant within Family of Comparisons?	Average Change to Mixing Value	p-value
15%	12.5%	No	-	0.956
17.5%	12.5%	Yes	-0.078	0.0077
17.5%	15%	Yes	-0.077	0.0090
2 Layers	1 Layer	Yes	-0.084	5.17×10^{-4}
Flow Rate	-	Yes	0.017 per (μL/min)	0.0481

Conclusion

The incorporation of electrospun nanofibers into simple Y-shaped microfluidic channels was shown to significantly increase fluid mixing within the channels. The amount of fluid mixing observed was highest in the PVA nanofiber mats, which had a much smaller diameter (450-550 nm) than the PS microfibers (0.84μm, 1.5 μm, and 2.7μm). However, within the PS nanofiber mats, mixing increased with increasing fiber diameter, indicating that the mechanism of mixing within the PS and PVA fibers is different.

We assume that the largest PS microfibers can cause some flow manipulation through the volumetric presence of the microfiber, similar to using micropillar obstacles within the channel. However, the microfibers used within this study are still much smaller than the 10-100 μm diameter obstacles frequently used within micromixers, resulting in less mixing than reported in other obstacle-based micromixers (Table 2.7). In contrast, for the PVA nanofiber mat, it is the porous, inhomogeneous 3D shape of the mat itself that likely causes the increased dispersive mixing. It has been reported that micromixers that utilize an asymmetric arrangement of obstacles yield significantly more mixing than a symmetric obstacle arrangement[93,107]. An

asymmetrical obstacle distribution within the channel results in different resistances to flow in the lateral direction of the channel, causing the fluids to find paths of least resistance through the obstacles[93]. The fluid flow is then repeatedly distorted and redirected as it flows through the obstacles, which in turn increases dispersive mixing[93]. The inhomogeneous pore size, pore density, and fiber distribution of the PVA nanofiber mats would similarly force the fluid to find paths of least resistance as it enters and travels through the fiber mat, producing the increase in mixing reported in this work. The PS microfiber mats used in this study have a much more homogeneous pore size and distribution within the channels and thus produce less mixing within the channels. For all the fibers studied, mixing increased with mat height, while mixing decreased with increasing flow rate. Additionally, the nanofiber mat length did not have a significant impact on the final mixing observed, which leads to the conclusion that, for mixing in the PVA fiber mats, most of the observed mixing effects are from the fluid entering and exiting the nanofiber mats. Finally, the mixing index within the channels containing two layers of PS or PVA fiber mat was lower than the control mixing index at both the inlet and outlet of the channels, suggesting that the observed mixing was also caused by increased back pressure in the channels containing nanofiber mats.

Table 2.7 Comparison of passive micromixers.

Mixer	**Setting**	**Mixing Index**	**Reference**
Split and Recombine	Re=0.1	0.9	Anson et al. 2010
	Re=60	0.7	Anson et al. 2010
Diamond Obstacles	Asymmetric Distribution	0.23	Bhagat et al. 2007
Zigzag		0.1	Jean et al. 2009
Circular Baffles		0.3	Jean et al. 2009

To date, passive fluid mixing in microfluidic channels is accomplished through patterning of microstructures into polymer channels or by creating complex channel geometries that alter the flow pattern [6,92]. While these passive mixers can be very effective, they often utilize multi-step lithography or require aligned assembly of multilayered channel geometries [107]. Therefore, electrospun nanofibers, which can be fabricated without the use of a cleanroom, are an attractive alternative to conventional micromixers. Though expertise in electrospinning is required to spin and functionalize the fibers, a basic electrospinning system consists only of a syringe pump, a high voltage source, and a grounded collector plate and is thus much simpler than most microfluidic fabrication methods. Additionally, fibers produced by electrospinning can be spun out of many different polymers and with many different functionalities [25,32,112,113]. Further, the two-layer PVA micromixers described in this work produced an average outlet mixing index of between 0.29 and 0.36, corresponding to 71%-64% fluid mixing. This mixing index is comparable to or better than several previously reported passive micromixers, such as circular baffle, diamond obstacle, and split and recombine mixers, though it is less than the 90% mixing observed using zigzag mixing channels (Table 2.7). However, unlike these other micromixers, electrospun nanofiber mats can easily be further functionalized to allow for coupling of fluid mixing directly with analyte detection or sample preparation as demonstrated in our research group[9,10,17]. Therefore, electrospun nanofiber mats are a promising alternative for reproducible and rapid microfluidic mixing.

CHAPTER 3

Functionalized Electrospun Poly(vinyl alcohol) Nanofibers for On-Chip Concentration of *E. coli* Cells

Abstract

Positively and negatively charged electrospun poly(vinyl alcohol) (PVA) nanofibers were incorporated into poly(methyl methacrylate) (PMMA) microchannels in order to facilitate on-chip concentration of *E. coli* K12 cells. The effects of fiber distribution and fiber mat height on analyte retention were investigated. The 3D morphology of the mats was optimized to prevent mechanical retention of the *E. coli* while also providing a large enough surface area for analyte concentration. Positively charged nanofibers produced an 87% retention and over 80 fold concentration of the bacterial cells by mere electrostatic interaction, while negatively charged nanofibers reduced nonspecific analyte retention when compared to an empty microfluidic channel. In order to take advantage of this reduction in nonspecific retention, these negatively charged nanofibers were then modified with anti- *E. coli* antibodies. An on-chip antibody immobilization protocol was developed. Antibody-functionalized negatively charged nanofiber mats were capable of specific capture of 72% of the *E. coli* cells while also significantly reducing nonspecific analyte retention within the channel as expected. The ease of fabrication and immense surface area of the functionalized electrospun nanofibers make them a promising alternative for on-chip concentration of analytes. The pore size and fiber mat morphology, as well as surface functionality of the fibers, can be tailored to allow for specific capture and concentration of a wide range of analytes.

Introduction

Microfluidic biosensors that incorporate both sample preparation and analyte detection, called lab-on-a-chip (LOC) devices or microTotal Analysis systems (μTAS), offer several advantages over their conventional biosensing counterparts. First, because of their small size, microfluidic biosensors can analyze smaller sample volumes, which in turn requires smaller reagent volumes and allows for faster analyte detection than conventional sensors[1,90]. Additionally, LOC devices often require minimal or no external equipment, are portable, and are frequently less expensive to run than larger biosensors, making them ideal for use in point-of-care, rural, and developing world applications[91,114]. However, several key challenges face the development of true LOC devices. First, because miniaturized devices utilize very small sample volumes (nL-μL range), it is necessary to perform significant sample concentration[4]. This is particularly critical for analytes which are already present in low concentrations in the original sample, such as *E. coli* in food and water samples[115,116], *Cryptosporidium parvum* in water samples[117], and Human Immunodeficiency Virus (HIV) in clinical samples[118]. Further, the small feature sizes of microfluidic devices make them very sensitive to sample impurities, necessitating that sample purification be performed prior to analyte detection.

Several groups have developed sample concentrators that can be used for on-chip sample prepration[115,119–123]. Dielectrophoresis[115,119], fluid flow manipulation[122], and solid phase extraction (SPE)[124,125] have been used to allow for concentration of bacterial cells. During dielectrophoresis, a non-uniform electric field is used to separate and concentrate particles based on their dielectric properties[115]. Lagally et al. report a 160 fold concentration of *E. coli* cells using dielectrophoresis in a polydimethylsiloxane (PDMS) microchannel[115]. Additionally, dielectrophoresis has been used to separate and concentrate gram negative and gram positive

bacteria within a glass microchannel containing insulating posts[119]. However, despite the efficacy of these techniques, dielectrophoresis requires the incorporation of microelectrodes into the microfluidic device and the use of significant external instrumentation to generate the electric field, which significantly complicates the design and portability of the microfluidic device[115].

Several different fluidic techniques have also been utilized to concentrate analytes either by establishing concentration gradients within the flow[126] or by decreasing the total fluid volume within the device[122,123]. The meniscus dragging effect has been used to concentrate *E. coli* cells from liquid samples using a PDMS sample flow layer and a metal airflow layer sandwiching a porous polytetrafluoroethylene (PTFE) membrane[122]. Evaporation has also been used to concentrate liquid samples by creating an air/liquid interface within the channel[123]. Finally, passive-pump induced fluid flow has been used to create concentration gradients within microfluidic devices, which allow for the separation and concentration of small volumes of analyte[126]. While the evaporation and meniscus dragging techniques offer significant sample concentration and require minimal external equipment and relatively simple channel designs, they are most appropriate for use with samples that do not contain species that may interfere with analyte detection as the concentration is not specific to the analyte of interest.

Solid phase extraction (SPE) utilizes the physical and chemical characteristics of the analyte to concentrate the sample using a stationary phase such as microbeads[127,128], micropillars[120,129] and microfilters[120,121,130]. Superparamagnetic beads have been used to separate and concentrate *E. coli* DNA[125], while silica particles have been used for concentration of nucleic acids from both gram-negative and gram-positive bacteria from whole blood samples[124]. Despite the successful use of SPE for on-chip sample concentration, immobilization of the stationary phase into the microfluidic channel remains a key challenge[121,128]. Additionally, the surface-area-

to-volume ratio of the stationary phase has a direct impact on the efficiency of SPE, necessitating that devices be designed with the highest possible surface-area-to-volume ratio[127]. Electrospun nanofibers, which can be easily incorporated into microfluidic channels using UV-ozone-assisted thermal bonding[9,10], are characterized by extremely large surface-area-to-volume ratios and can be produced with a wide range of surface chemisitries[8,131]. In this work, positively and negatively charged poly(vinyl alcohol) (PVA) nanofibers were incorporated into poly(methyl methacrylate) (PMMA) microchannels in order to serve as high surface area sample concentrators for *E. coli* cells. The negatively charged PVA fibers were further functionalized through the immobilization of antibodies on the fiber surfaces.

Patented in 1934 by Formhals[132], electrospinning is a fiber formation process in which a high-voltage electric field is used to produce ultrathin fibers from a polymer spinning solution[8,38,133]. Basic electrospinning apparatuses are composed of three main components: a high voltage power source, a spinneret (typically a syringe and metal needle), and a grounded collector plate (Figure 3.1)[8]. Typically, a syringe pump is also used to feed a viscous polymer solution through the tip of the spinneret at a constant rate. During electrospinning, the high voltage source is connected to the spinneret, conferring a constant voltage to the polymer spinning solution as it is slowly pumped out of the spinneret. The polymer spinning dope is therefore subjected to two different electrostatic forces: the electrostatic repulsion of the surface charges of the spinning solution and the Coulombic forces exerted by the external electric field[8]. Once the applied voltage passes a threshold value, the polymer solution at the tip of the spinneret will change form from spherical droplets to a conical shape called the Taylor cone. Then, once the attraction between the grounded collector pate and the charged spinning solution overcomes the surface tension at the tip of the spinneret, thin polymer jets will be ejected from the tip of the

Taylor cone[38]. As the polymer jets travel through the air, the solvent evaporates and the polymer undergoes whipping and stretching, resulting in the formation of a solid fiber that collects as a nonwoven mat on the grounded collector plate. These fiber mats are characterized by extremely large surface-area-to-volume ratios, high porosities, and small pore sizes. Additionally, the nanofibers can be functionalized either through incorporation of additives (such as conductive materials[134,135], proteins[25,136], nucleic acids[137], and fluorescent materials[138]) directly into the spinning dope or through post-spinning modifications[38,131,139].

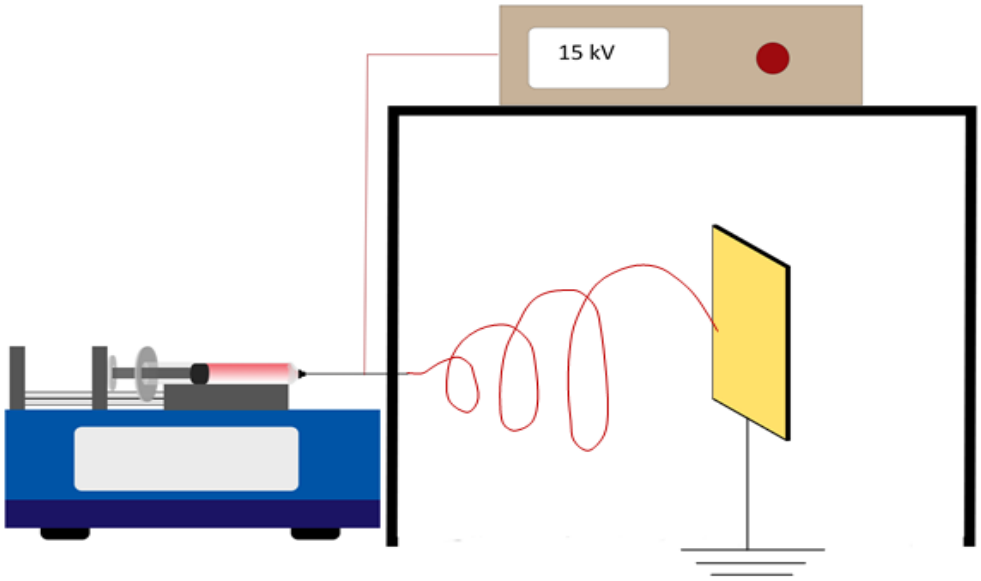

Figure 3.1 A standard electrospinning apparatus, consisting of a high voltage power source, a syringe pump, a grounded collector plate, and a spinneret containing a viscous polymer spinning dope.

Previously, we demonstrated that positively charged PVA nanofibers functionalized with hexadimethrine bromide (polybrene) could be used to concentrate negatively charged fluorescent liposomes within microfluidic channels[9,10]. Additionally, negatively charged PVA fibers spun with poly(methyl vinyl ether-alt-maleic anhydride) [poly(MVE/MA)] were shown to repel the

negatively charged analyte, limiting nonspecific retention of liposomes within the channels. In this work, we utilize these charged PVA nanofibers to perform concentration of *E. coli* K12 cells, which have a negative surface charge at pH of 3-9[140,141], within a simple microfluidic device. Because *E. coli* cells are much larger than fluorescent liposomes, the pore size and nanofiber mat height had to be optimized to eliminate nonspecific, mechanical retention of the analyte while also providing sufficient surface area for significant analyte concentration. Then, the carboxylated surface chemistry of the negatively charged PVA-poly(MVE/MA) fibers were used to allow for immobilization of anti-*E. coli* capture antibodies. An on-chip antibody immobilization procedure was developed in which nanofiber mats were functionalized after being bonded into microfluidic channels.

Materials and Methods

Materials

Nanofibers were spun using a highly hydrolyzed (99.7%) PVA with a molecular weight of 78,000 (Polysciences Inc., PA). Hexadimethrine bromide (polybrene), poly(methyl vinyl ether-alt-maleic anhydride) (poly(MVE/MA)), and Triton X-100 were purchased from Sigma Aldrich. Poly(methyl methacrylate) (PMMA) was purchased from Ridout Plastics (CA) and was 0.06" thick. Tygon tubing with a 0.02" inner diameter and 0.06" outer diameter (Cole-Parmer) was blocked using a 1% solution of Bovine Serum Albumin (BSA) (Invitrogen). *E. coli* K12 cells were grown using Miller LB Broth and agar plates (Sigma Aldrich). The surfaces of negatively charged nanofibers were functionalized using 1-ethyl-3-(3-dimethylaminopropyl) carbodiimide hydrochloride (EDC) and N-hydroxysulfosuccinimide (Suflo-NHS) (Thermo Fischer) in a 0.05M MES buffer (pH 5.0) (Sigma-Aldrich). A rabbit polyclonal anti-*E. coli* capture antibody (ab137967) was used for specific *E. coli* capture (abcam).

Electrospinning

Positively and negatively charged electrospun PVA nanofibers were fabricated as previously described[9,10]. Briefly, positively and negatively charged nanofibers were produced through the incorporation of polybrene and poly(MVE/MA), respectively, into a 10% w/v PVA spinning dope. The PVA spinning dope was prepared by dissolving PVA in deionized (DI) water at 95˚C for four hours. Polybrene was first dissolved in DI water at room temperature for 10 minutes and was then added to the 10% w/v PVA solution to yield the final 90/10 w/w PVA/polybrene spinning dope. Poly(MVE/MA) was dissolved in DI water at 95˚C for 20 minutes before being added to the PVA solution to make a 90/10 w/w PVA/poly(MVE/MA) spinning dope. In order to improve the spinnability of the PVA solutions, the nonionic surfactant Triton X-100 was added at a 99.5/0.5 w/w DI water/Triton X-100 ratio. The resulting spinning dopes were mixed for 2 minutes on a vortex at its highest setting.

Electrospinning was performed using a homemade electrospinning apparatus. First, the spinning dope was loaded into a 5 mL BD plastic syringe with an 18 gauge needle with a blunt tip. A syringe pump was used to pump the spinning dope out of the syringe at a rate of 0.01 mL/min. A high voltage power supply set at 15 kV was used to confer a constant positive charge to the syringe needle (Gamma High Voltage Research Inc., FL). A piece of copper was used as a grounded collector plate and was placed 15 cm from the syringe tip.

After spinning, the fiber mats were manually peeled of the grounded collector plate and placed on pieces of PMMA that had undergone UV-ozone (UVO) treatment for 15 minutes. During UVO treatment, the UVO oven had an oxygen flow rate of 0.5 L/min and an average lamp power of 28-32 mW/cm^2 at 253.7 nm (Jelite, CA). After transfer to the PMMA surfaces,

nanofiber mats were cut into 15 mm wide strips using a razor blade. Unwanted fibers were removed from the PMMA using double-sided tape. This method allows for incorporation of the PVA nanofibers into microfluidic channels without using the gold microelectrodes previously used by our lab[9,10], resulting in a simpler fabrication process.

It is well-understood that nanofibers do not evenly distribute along the surface of the grounded collector plate, resulting in non-uniformity of fiber mat thickness along the length of the mat [11,142]. Additionally, it has been observed that this non-uniformity increases with increasing spinning time[11,108]. Therefore, nanofiber mats were spun into thin layers and stacked together to create multilayered mats with more homogeneous morphologies. This approach has been used in the field of particulate filtration to create high efficiency nanofibrous filters and results in improved filtration efficiency when compared with thicker fiber mats [11,108]. Nanofiber mats with one, two, or three layers of PVA fibers were tested to see which morphology produced the best *E. coli* retention within the positively charged nanofiber mats. Additionally, in order to determine the effect of nanofiber mat pore size on *E. coli* retention, two different types of nanofiber mat were spun. Mats with large pore sizes (referred to as "sparse" nanofiber mats) were spun by manually moving the collector plate horizontally across the electrospinning system at a rate of approximately 50mm/min, which prevented the fibers from densely collecting in one location. Mats with smaller pore sizes (referred to as "dense" nanofiber mats) were spun using a stationary collection plate. Confocal microscopy was used to measure the height of the nanofiber mats prior to incorporation in microfluidic channels as previously described[10]. Additionally, confocal microscopy was used to confirm whether a mat had a sparse or dense morphology (Figure 3.2). The average pore size for each mat was not calculated as such calculations are challenging due to the complex three-dimensional morphology of the mats. While liquid

extrusion with a capillary flow porometer or liquid intrusion with a mercury porometer can be used to analyze average pore size within nanofiber mats, these methods do not allow for the mat to be reused within a microfluidic device after pore size measurement, making them ill-suited for use in this study[143]. Therefore, mats were designated as sparse or dense based on their confocal microscopy z scans and the visible distribution of the fibers. Despite their different fiber distributions, the nanofiber mat height of the sparse and dense mats were very similar. Sparse mats had an average height of 11.4 $\pm$ 2.6 μm and dense mats had an average height of 11.3 $\pm$ 2.7 μm when measured using a Leica SP2 confocal microscope. The diameters of the PVA nanofibers produced in our lab were previously measured using SEM. The negatively charged PVA/poly(MVE/MA) nanofibers had diameters between 300-400nm, while the positively charged PVA/polybrene nanofibers had a diameter of 450-550 nm[9].

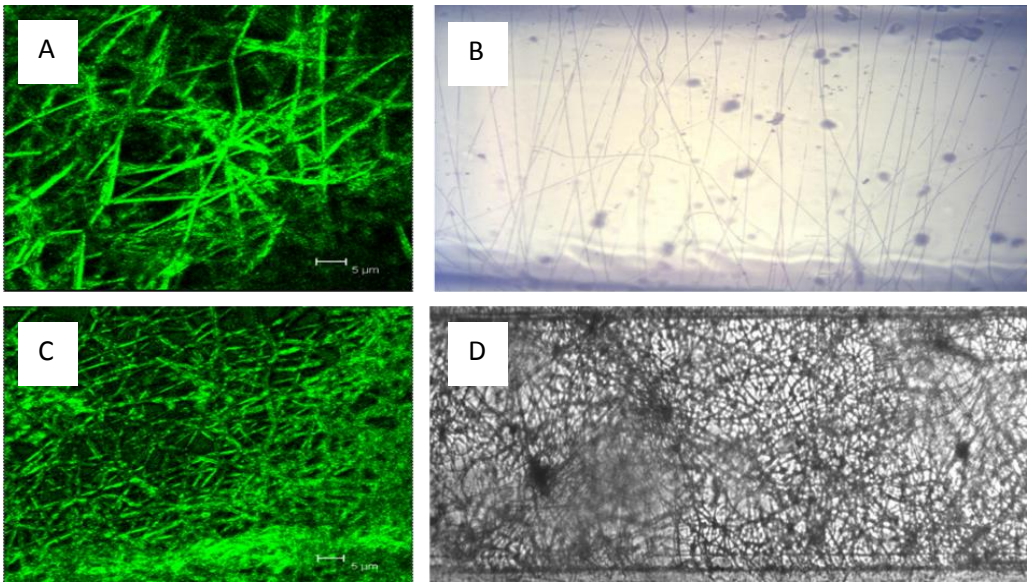

Figure 3.2 (a) Leica confocal image of sparse nanofiber mat. **(b)** Sparse nanofiber mat within a microfluidic channel. Leica fluorescent microscope. 10x objective. **(c)** Leica confocal image of a dense nanofiber mat. **(d)** Dense nanofiber mat within a microfluidic channel. Leica fluorescent microscope. 10x objective.

Hot Embossing and Bonding of Channels

Microfluidic channels were created on PMMA using hot embossing with a copper template[144]. The copper template was fabricated at the Cornell Nanoscale Facility (CNF) using photolithography and copper electroplating to produce raised copper channel structures on copper plates [101]. The copper template used in this work contained four parallel channels, each 42μm deep, 1 mm wide, and 20 mm long. The microfluidic channels were embossed into pieces of PMMA using a Carver Laminating Hot Press at 130˚C and 10,000 lbs (44,482 N) of force for 5 minutes (Carver, NJ). Inlet and outlet holes were drilled at each end of the channel with a 0.8 mm steel drill bit.

UVO-assisted thermal bonding was used to produce the microfluidic devices. First, the piece of PMMA embossed with microfluidic channels was UVO treated for 15 minutes. Then, the piece of PMMA with nanofiber mats was UVO treated for 4 minutes (longer UVO treatments changed the morphology of the PVA nanofiber mats). All UVO treatment was done using an oxygen flow rate of 0.5 L/min and an average lamp power of 28-32 mW/cm^2 at 253.7 nm. Then, the two pieces of PMMA were sandwiched together with the nanofibers facing the microchannels, and placed between two blank pieces of copper. This assembly was then pressed on the Carver hot press for 10 minutes at 95˚C and 5,000 lbs (22,241 N) of force. If air bubbles were still present in the channels after the first application of pressure, additional bonding cycles were repeated (using the same temperature and pressure) until all air bubbles were removed. Between each additional bonding cycle the chip was rotated 90˚. Once bonding was complete, polyvinyl chloride tubing with a 0.06” external diameter was glued into the inlet and outlet holes

of the channels with Quicktite instant adhesive gel (Loctite). The tubing was blocked with 1% BSA for 24 hours prior to gluing to limit nonspecific retention of *E. coli*.

E. coli Retention

In order to study the interaction of negatively charged *E. coli* K12 cells with the positively and negatively charged PVA nanofibers, channels containing fiber mats were used to perform *E. coli* retention experiments (Figure 3.3). First, *E. coli* K12 was grown overnight in a sterile 2.5% Luria Broth (LB) solution in a shaking incubator at 37˚C. Then, the overnight culture was serially diluted (2-5x depending on experiment) in sterile 1x phosphate buffered saline (PBS) (pH 7.0). Plastic 1 mL BD plastic syringes (which had been blocked with a 1% BSA solution for 24 hours prior to use) pumped the diluted *E. coli* solution through the microfluidic channels at a flow rate of 1 μL/min for 60 minutes. Then, 1x sterile PBS (pH 7.0) was used to wash unbound *E. coli* cells from the channels using two wash steps of 45 minutes each with a flow rate of 1 μL/min. The effluent from each flow step was collected and plated (10μL effluent/plate) on 2.5%LB and 2% Agar plates. The plates were grown overnight at 37˚C and colonies were counted to determine the retention of *E. coli* within the nanofiber mats. Control plates containing 10 μL of the diluted *E. coli* solution that had not passed through the microchannels were also plated. The percentage of *E. coli* cells retained in the nanofiber mats was calculated by comparing the number of colonies grown on the effluent plates to the number of colonies grown on control plates.

The effects of nanofiber mat height and distribution (sparse or dense) on analyte retention were tested. The goal was to find a nanofiber mat morphology that maximized the amount of *E. coli* K12 cells retained within positively charged nanofiber mats (through attraction between the

negatively charged cells and the positively charged fibers) while minimizing retention of the cells in negatively charged mats (which would occur via mechanical retention if mats were too dense). Thereofore, *E. coli* retention in the following nanofiber mat morphologies was tested: one-layer sparse, one-layer dense, two-layer sparse, two-layer dense, three-layer sparse, and three-layer dense.

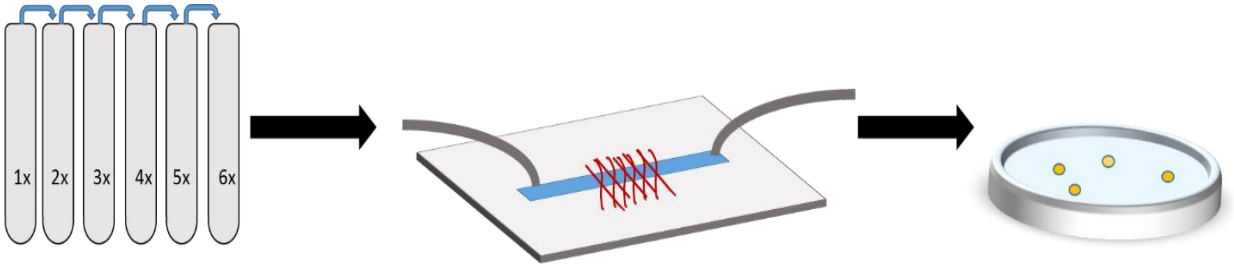

Figure 3.3 Schematic of *E. coli* retention experiments. Overnight cultures were serially diluted, pumped through microfluidic channels, and then plated on agar plates. The number of colonies on the plates was compared to the number of colonies on control plates that were produced from *E. coli* that had not been pumped through a channel.

Antibody Immobilization

Negatively charged PVA-poly(MVE/MA) nanofibers were used to immobilize anti-*E. coli* antibodies within the channels. The negatively charged mats were used because they repel the negatively charged *E. coli*, thus minimizing the amount of nonspecific retention observed within the channels. Therefore, *E. coli* retention seen in these experiments could be attributed to antibody capture of the cells. Additionally, the surface of the PVA/poly(MVE/MA) nanofibers is carboxylated[144], allowing for antibody immobilization using the EDC/sulfo-NHS coupling chemistry.

An on-chip antibody immobilization protocol was developed in order to functionalize the nanofibers after they had been bonded into microfluidic channels. This was necessary for two reasons. First, PVA nanofiber mats will curl up when exposed to liquid unless they are

physically held in place by the walls of microfluidic channels, making them difficult to functionalize prior to incorporation into microfluidic channels. Further, the bonding process requires UVO exposure, high temperatures, and high pressures, all of which could compromise the functionality of antibodies immobilized on nanofibers prior to bonding.

Antibody immobilization in the channel took place using a multistep procedure. First, channels were manually filled with 0.2M EDC 0.2M sulfo-NHS in MES buffer (pH 5.0) to completely saturate the nanofiber mats. A high flow rate was necessary to prevent the formation of air bubbles within the channels. The EDC/sulfo-NHS solution was allowed to sit in the channels for 60 minutes. Then, channels were rinsed with 1xPBS (pH 7.0) to remove unreacted EDC/sulfo-NHS. A 100 μg/mL antibody solution was pumped through the channels at 5 μL/min for 18 minutes and was then allowed to sit for 60 minutes with no flow. Any unreacted EDC/sulfo-NHS functional sites on the nanofiber mats were then blocked using a 1% BSA solution at a flow rate of 2 μL/min for 30 minutes, following by a channel rinse with 1xPBS (pH 7.0) at 2 μL/min for 30 minutes. Finally, *E. coli* retention experiments were performed in the antibody-functionalized channels as described above.

In order to control for variations in nanofiber mat morphology, each microfluidic chip (which contains four parallel microchannels bonded to the same nanofiber mat) had antibodies immobilized in two channels, while the other two channels were left unaltered. Therefore, retention in the antibody-modified channels could be compared directly to channels on the same chip containing the same nanofiber mat but without antibodies.

Results and Discussion

Positively charged PVA nanofiber mats have previously been used for the concentration of negatively charged fluorescent liposomes in microfluidic channels[113,144]. Because of their negative surface charge, *E. coli* cells are an ideal model analyte to determine whether electrospun nanofiber membranes can be used as sample concentrators for larger analytes. The average diameter of *E. coli* cells is approximately 1 μm, necessitating that the nanofiber mat morphology be optimized to prevent nonspecific mechanical retention of the analyte (due to pores that are too small) while providing enough surface area to provide significant capture of the cells. Additionally, to allow for specific capture of *E. coli* cells, an on-chip antibody immobilization protocol was developed.

E. coli Retention in Charged Nanofibers

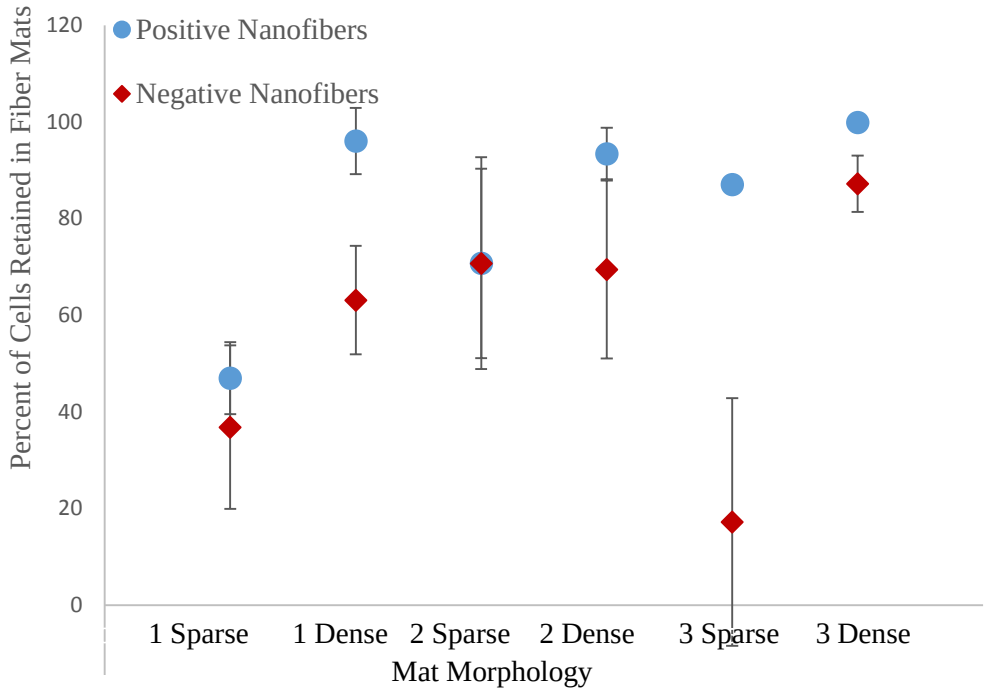

Figure 3.4 Percent of cells retained in positively and negatively charged nanofiber mats with different morphologies. Retention in negatively charged nanofiber mats had much larger standard deviations than retention in positively charged nanofiber mats.

Six different nanofiber mat morphologies were tested to determine which produced the most *E. coli* concentration within channels filled with positively charged nanofiber mats and the least nonspecific retention of *E. coli* cells within channels containing negatively charged mats (Figure 3.4). Based on the percentage of cells that were retained in the negatively charged nanofiber mats, it was found that using the dense nanofiber morphology results in significant nonspecific analyte retention. Therefore, in order to avoid the size-dependent retention of impurities or particulates that may be present in the sample, only sparse nanofiber mats should be used. However, dense nanofiber mats could be used to perform nonspecific sample purification or concentration via size exclusion filtration by allowing for the collection of large species within the channels while smaller species are allowed to pass through the mats. This could either be used to concentrate a relatively large analyte within the channel or to remove large sample impurities that could hinder detection of smaller analytes. For example, the positively charged three-layer dense nanofiber mats used in this work had an average *E. coli* retention of 99 $\pm$ 0.2% and could be coupled with a specific biorecognition element to allow for on-chip concentration and detection of the analyte. While these nanofiber mat structures produced minimal back pressure within the channel, further studies are needed using real-world samples in order to assess the risk for clogging and increases in back pressure that can occur with any size-exclusion filtration process.

In order to avoid unwanted mechanical retention of species within the nanofiber mats, only the sparse morphology nanofiber mats should be used. As expected, the three-layer sparse morphology was the morphology in which the negatively charged nanofibers retained the fewest *E. coli* cells (17%) while the positively charged nanofibers captured most of the cells (87%). This indicates that it is necessary for the fiber mats to fill as much of the channel height as

possible in order to maximize the likelihood of an analyte encountering the functionalized nanofiber surfaces. Not only did *E. coli* retention in the positively charged sparse nanofiber mats increase as the number of fiber mat layer increased, the standard deviation in retention decreased as well, indicating that more reproducible retention can be achieved by increasing the amount of functionalized surface area available within the channel (Table 3.1). Using the positively charged three-layer sparse morphology nanofibers resulted in an 82x concentration of the *E. coli* solution. A higher concentration factor would be possible through the use of dense nanofiber mats (which would also utilize mechanical retention of analytes in addition to electrostatic attraction) or increasing nanofiber mat size (longer mats would allow for more *E. coli* capture without substantially increasing the volume of sample retained in the channels).

Table 3.1 Average retention of *E. coli* cells within sparse morphology nanofiber mats.

Fiber Type	**1 layer +**	**2 layer +**	**3 layer +**	**1 layer -**	**2 layer -**	**3 layer -**
Average *E. coli* retention	47.0%	70.8%	87.1%	36.8%	70.7%	17.2%
Standard deviation	7.4%	22.0%	1.4%	17.0%	19.6%	25.6%

Negatively charged three-layer sparse nanofiber mats demonstrated less *E. coli* retention than empty unblocked PMMA channels (Figure A.3 in Appendix A), indicating that the negatively charged nanofibers could be used to limit nonspecific binding within channels much like conventional blocking agents. However, while *E. coli* retention within the positively charged three-layer nanofiber mats was very reproducible, the retention in negatively charged sparse nanofiber mats featured large standard deviations (Table 3.1). We assume that this is caused by slight variations in nanofiber mat morphology, which naturally occur when spinning is performed in systems that do not control ambient humidity and temperature. In particular, the

collection/filtration effect of negatively charged nanofiber mats is going to be very sensitive to slight variations in pore size, as *E. coli* cells will be mechanically retained if any pores within the mat are too small to allow the cells to pass. Therefore, even though the negatively charged fibers generally repel the bacterial cells and prevent their nonspecific retention within the channel, the pore sizes of the mats must be carefully controlled to ensure reproducible behavior. Thus, future work should investigate more precise means of controlling mat pore size, such as using porous collector plates that utilize air streams to prevent fiber collection across the pores of the plate[145] or utilizing a rotating wire mandrel collector to control the alignment of fiber deposition[146]. Additionally, variations in nanofiber mat morphology could be minimized through the use of a temperature- and humidity-controlled spinning apparatus.

Antibody Immobilization onto Negatively Charged Nanofibers

Negatively charged PVA-poly(MVE/MA) nanofibers have a carboxylated surface, making them ideal for antibody immobilization using the standard EDC/sulfo-NHS coupling chemistry[147]. Additionally, because they have a negative surface charge, the nanofiber mats significantly reduce nonspecific *E. coli* binding within microchannels when incorporated into the channels in the three-layer sparse morphology as discussed above. Therefore, negatively charged nanofiber mats were used for high surface area anti-*E. coli* antibody immobilization. An on-chip immobilization procedure was developed to prevent the antibodies from being harmed during the UVO-assisted thermal bonding process.

Initial antibody immobilization experiments demonstrated that the flow rate has a significant impact on antibody immobilization efficiency within the microchannels. Because microchannels containing nanofiber mats are prone to forming air bubbles when filled at slow flow rates (which would block access of fibers to immobilization reagents), it was determined that the best way to

eliminate air bubbles during initial filling of the channel was by manually pushing the EDC/sulfo-NHS solution through the channels until the entire mat was saturated. Using a slower flow rate of 1 μL/min resulted in 40% retention of *E. coli* in the antibody-functionalized nanofiber mats, which we assume is due to the visible air bubbles that formed within the channels and prevented homogeneous distribution of the EDC/sulfo-NHS solution. Filling the channels manually produced no air bubbles in the channel and resulted in 72% retention of the *E. coli* cells.

The ability of the immobilized antibodies to perform specific capture of the *E. coli* cells was measured using a range of *E. coli* concentrations (Table 3.2). While all of the nanofiber mats showed specific retention of *E. coli* cells, the best retention was observed in the lowest concentration (62 CFU per control plate). At this concentration, antibody immobilization on the fibers resulted in a 35% increase in *E. coli* concentration when compared to channels containing unmodified negatively charged nanofibers (Table 3.2). We assume the relatively low *E. coli* retention at higher *E. coli* concentrations is a function of the low antibody concentration chosen, which results in an antibody concentration of 0.6 μg of antibody per millimeter length of nanofiber mat (corresponding to 0.04 mm^3 of nanofiber mat). Such a low-density antibody distribution on the high surface area of the nanofiber mat was also most likely the reason for the large standard deviations observed. We predict that using a higher antibody concentration on the nanofiber surface will significantly improve the antibody distribution on the fibers and lead to higher specific *E. coli* retention and lower standard deviations. Therefore, future work will therefore focus on optimizing antibody concentration, buffer pH, and flow rates to allow for better on-chip antibody immobilization. Additionally, fibers should be spun using a humidity-

and temperature-controlled spinning apparatus to minimize batch-to-batch variations in morphology as observed in the studies using unmodified nanofibers (Figure 3.4).

Table 3.2 Average *E. coli* retention in antibody-modified negatively charged nanofibers with different inlet solution concentrations

Average number of colonies in inlet solution	62	148	738	1074
Average *E. coli* retention in unmodified negatively charged fibers	36.7% ±22.0%%	37.7% ± 26.6%	20.4% ± 22.8%	5.48% ± 25.5%
Average *E. coli* retention in antibody-functionalized fibers	71.9% ± 17.7%	40.0% ± 20.0%	45.5% ± 9.49%	40.7% ± 21.3%

Conclusion

Positively charged electrospun nanofibers were incorporated into polymer microfluidic channels in order to allow for on-chip sample concentration, while negatively charged nanofibers were used to limit nonspecific retention of *E. coli* cells. Multilayered nanofiber mats composed of one, two, or three nanofiber layers were used to create thicker nanofiber mats with more homogeneous fiber distribution. The morphology of the nanofiber mats was optimized to allow for maximum *E. coli* retention in positively charged nanofibers while eliminating mechanical retention of the bacteria in the negatively charged nanofiber mats. Positively charged nanofibers in the optimized nanofiber morphology produced a concentration factor of 82x. In addition to the electrostatic-based retention, specific retention was also investigated using the self-repelling, negatively charged nanofibers by immobilizing anti-*E. coli* antibodies. These antibody-functionalized negatively charged nanofibers yielded a 72% specific retention of the bacterial cells, compared with only 37% retention in unmodified negatively charged nanofibers. The studies described demonstrate the immense possibilities afforded by nanofibers for use as sample concentration matrices in microfluidic devices. The surface chemistries and fiber densities can

easily be adapted to suite the specific analytical challenge. However, the findings presented here also highlight the need for improvement in the reproducibility of both the electrospinning process and the antibody immobilization procedure.

One of the benefits of using multilayered nanofiber mats to perform sample purification and concentration within a microfluidic device is the possibility of creating heterogeneous nanofiber mats which alternate layers of fibers with different functionalities. This has already been investigated to some extent in the design of fibrous filters for air filtration[142]. By using a triple layer design composed of a layer of densely packed microfibers, a layer of nanofibers, and a layer of medium diameter fibers, Barhate et al. were able to improve filtration efficiency and mechanical stability of their fibrous filters[142]. A similar approach could be used to allow for size-selective concentration of different species within microfluidic biosensors. Additionally, nanofiber mats with a range of surface functionalities could be layered to allow for multiplexed analyte detection within the fiber mats. Alternatively, fiber mats with different surface chemistries could be arranged along the length of a microfluidic sensor to allow for selective capture of different analytes at specific locations within the microchannel geometry.

CONCLUSION AND FUTURE OUTLOOK

Nanoscale materials such as nanoparticles, nanowires, nanotubes, and nanofibers have all been incorporated into biosensors in order to improve the sensors' sensitivity by increasing the number of binding sites available without increasing the size of the sensor. Of these nanoscale materials, electrospun nanofiber mats stand out for their relatively ease-of-fabrication and their porous, nonwoven structure. Compared to other nanoscale materials, the surface area of electrospun nanofiber mats is immense. Additionally, electrospun nanofibers can be made from a variety of polymers and can be functionalized to allow for specific capture of a wide range of analytes.

To date, many labs have leveraged the large surface areas of nanofiber mats to create sensitive electrochemical sensors[30,148–150]. Often, the nanofibers are used to simply increase the surface area of the working electrode and are spun either from conductive polymers such as polyaniline and polypyrrole[30,151] or from easily spinnable polymers doped with conductive nanomaterials (such as carbon nanotubes)[152]. Additionally, electrospun nanofibers have been extensively used as enzyme-immobilization scaffolds within the sensors, resulting in improved sensitivity and lower limits of detection than conventional sensors.

Electrospun nanofibers have also been investigated as a means of providing stable on-chip storage of reagents within microfluidic biosensors[20,48]. Polyvinylpyrrolidone (PVP) nanofibers, which are water soluble, were shown to increase long term stability of horseradish peroxidase and allow for rapid and even enzyme distribution once the sample is injected into the microchannels. Due to the wide range of biological molecules and chemicals that can be encapsulated within nanofibers during the electrospinning process, this method has the potential to allow for the creation of self-contained microfluidic biosensors in which all necessary reagents

are stored in the chip until use. Storage of sensitive reagents within the microfluidic sensor would allow for the development of portable, user-friendly assays which require fewer steps to operate, thus making them ideal for use in point-of-care or developing world applications.

Novel nanofibers have also been developed to allow for enhanced analyte detection. Light-emitting nanofibers have been spun by doping optically inert polymers with fluorescent molecules and fluorescent quantum dots, creating fibers that can be used as a polarized light source for microfluidic sensors[153]. Additionally, fluorescent probes have also been immobilized onto the surfaces of cellulose acetate electrospun nanofibers to allow for the development of sensitive optical sensors[154].

In this work, we developed an on-chip sample concentrator by using positively charged poly(vinyl alcohol) (PVA) nanofibers to bind *E. coli* cells. Additionally, negatively charged PVA nanofiber mats were used to prevent nonspecific binding of analytes to poly(methyl methacrylate) microchannels. Finally, the negatively charged fibers were used to immobilize anti-*E. coli* antibodies to allow for selective binding of the bacterial cells. Retention of the *E. coli* cells in the positively charged nanofiber mats was highly reproducible, but the retention in antibody-functionalized nanofibers was marked by large standard deviations. These chip-to-chip variations may be caused by slight variations in fiber morphology, therefore future efforts should focus on better controlling the electrospinning process.

While there are several nanofiber-based biosensors reported in the literature, reproducibility remains a key challenge in the use of nanofibers in commercial sensors. Electrospinning is a well-understood process, however precisely controlling nanofiber mat morphology is difficult due to the processes' dependence on different parameters such as spinning solution viscosity and concentration, collector distance and shape, applied voltage, and ambient temperature and

humidity. Several groups have attempted to make electrospinning more reproducible through the use of humidity- and temperature-controlled spinning systems and specially designed collector plates. The gold microelectrodes our group has used to facilitate PVA incorporation into microfluidic devices also allows for control of nanofiber deposition based on the spacing of the microelectrode fingers[9]. Another group created a porous collector plate in order to control nanofiber mat pore size and overall porosity[145]. The collector plate used air-flow impedance to control the fiber deposition pattern on the collector plate, allowing for the production of nanofiber mats with specific structure. While these solutions can offer some control over nanofiber mat morphology, the electrospinning process must be fully optimized to allow for precise mat morphology before electrospun nanofibers can be used to their best effect in commercial biosensors.

Another challenge facing the use of electrospun nanofibers is the relative difficulty of quantifying nanofiber mat morphology. In general, nanofiber mats are characterized by nanofiber mat thickness, average fiber diameter, average mat pore size, average mat porosity, fiber wettability, and flux permeability within the mats. The thickness of a nanofiber mats influences flux through the mat and also partially determines the functional surface area of the mat[143]. Typically, measurement of mat thickness is done either by using a micrometer or through electron or confocal microscopy. However, none of these techniques is ideal. Micrometers are prone to compression of the mats and therefore tend to underestimate the nanofiber mat thickness. Microscopy can give a more accurate measurement of fiber mat thickness, however as thickness varies along the length of the nanofiber mats it is necessary to make several measurements per mat. For TEM and SEM analysis, this requires the fibers be cut with a surgical blade to view the cross-sectional thickness of the membrane. In order to maintain fiber

morphology during this process, it is often necessary to fix the nanofibers with paraffin wax or a mounting medium. Confocal measurement requires less sample preparation, but depends on the fiber mats producing a visible fluorescent signal and is a relatively imprecise measurement. Measurement of mat pore size and overall porosity is also difficult to measure. Mercury and capillary flow porometers and the particle challenge test can be used to determine average pore diameter and mat porosity. However, these tests can damage the fiber mats, making it difficult to quantify nanofiber mats prior to incorporation into biosensors. Therefore, it is necessary to develop better, more reliable methods for quantification of nanofiber mat morphology to allow mats to be characterized completely prior to use in biosensing devices.

Despite the challenges of reproducible electrospinning and nanofiber mat characterization, electrospun nanofibers are very promising for use in a wide range of bioanalytical systems due to their appealing surface functionalities and immense surface-area-to-volume ratios. In addition to incorporation in electrochemical sensors, lateral flow assays, and microfluidic biosensors, electrospun nanofibers are also frequently used as three-dimensional cell culture scaffolds due to their ability to physically mimic the structure of the extracellular matrix. Therefore, by coupling biorecognition elements onto cell culture scaffolds, it would be possible to allow for analysis of the cells as they grow. Such sensors would be of particular use in research settings and would allow researchers to collect detailed information about cellular responses to different growth conditions. Additionally, biocompatible nanofiber mats functionalized with antibacterial agents have been proposed as wound dressings both for use on external injuries and within the body following surgery[155–158]. Therefore, it would be possible to couple real-time monitoring of patient progress through incorporation of sensing moieties into the dressings.

Electrospun nanofiber mats have successfully been incorporated into several types of bioanalytical devices, including lateral flow[81,100] and microfluidic systems[20,48], resulting in improved mass transfer and sensitivity within the sensors. However, while a wide range of electrospun functionalities have been developed, nanofibers are most frequently used to enhance electrochemical detection. Therefore, a wider range of nanofiber chemistries should be investigated as a means of performing sensitive analyte detection and sample preparation in other assay formats. Additionally, future work should focus on optimizing the electrospinning process to allow for precise control of nanofiber mat morphology, allowing for more reproducible analyte concentration and detection within microfluidic devices. Methods of more simply and accurately measuring nanofiber mat thickness, pore size, and porosity are necessary to allow for proper characterization of mats prior to incorporation within biosensing devices. Finally, electrospun nanofiber mats are ideal for use as cell culture scaffolds due to their complex three-dimensional structure. The proven sensing capabilities of nanofibers should be leveraged to allow for real-time analysis of cell culture samples in a research environment.

APPENDIX A

Supplementary Information

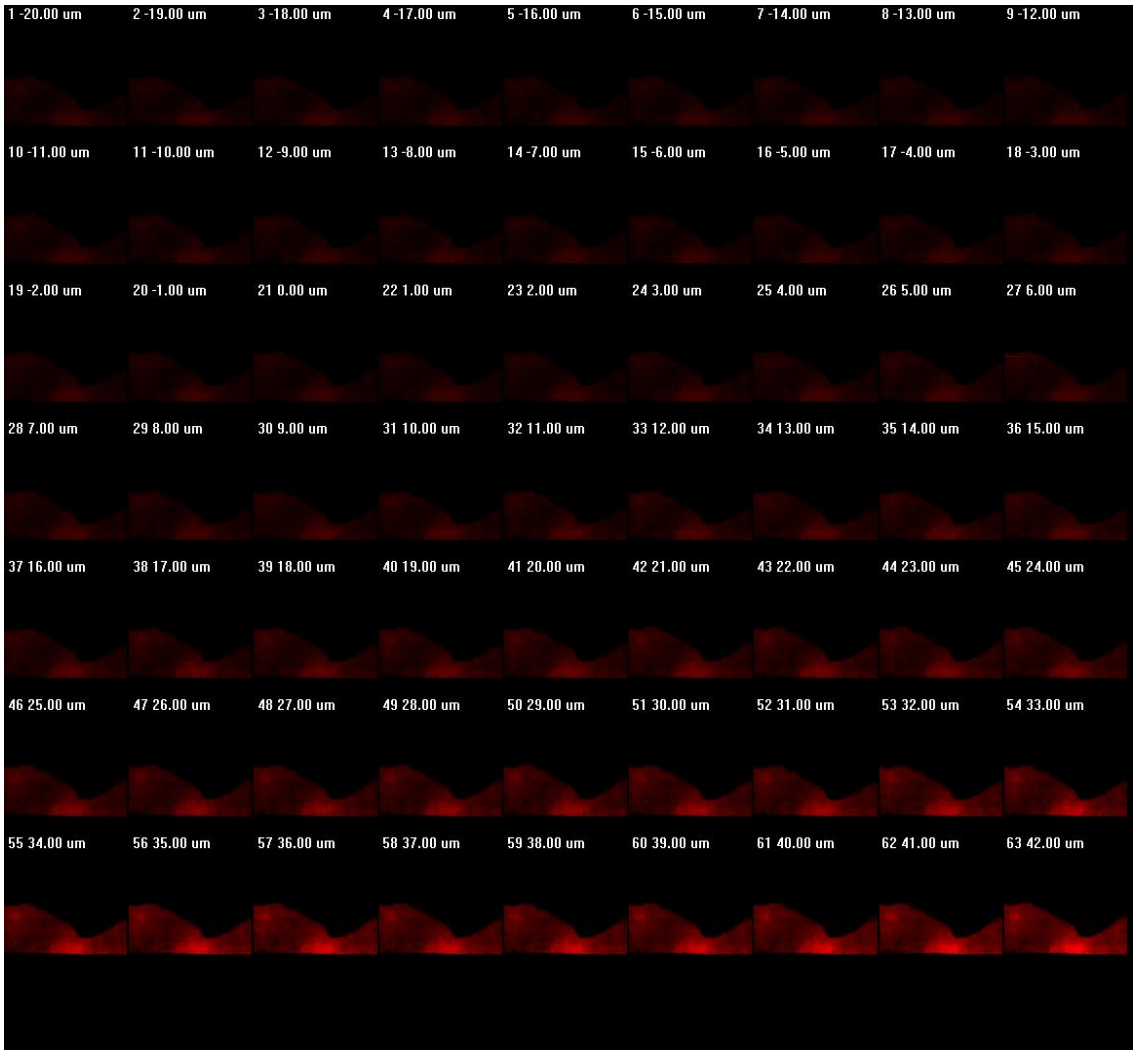

Figure A.1 A confocal Z scan of a microfluidic channel during fluid mixing experiments. The flow profile does not change as the focal point moves in the z direction, indicating that it is consistent throughout the height of the microchannel. Channel images shown were taken at 1 µm intervals.

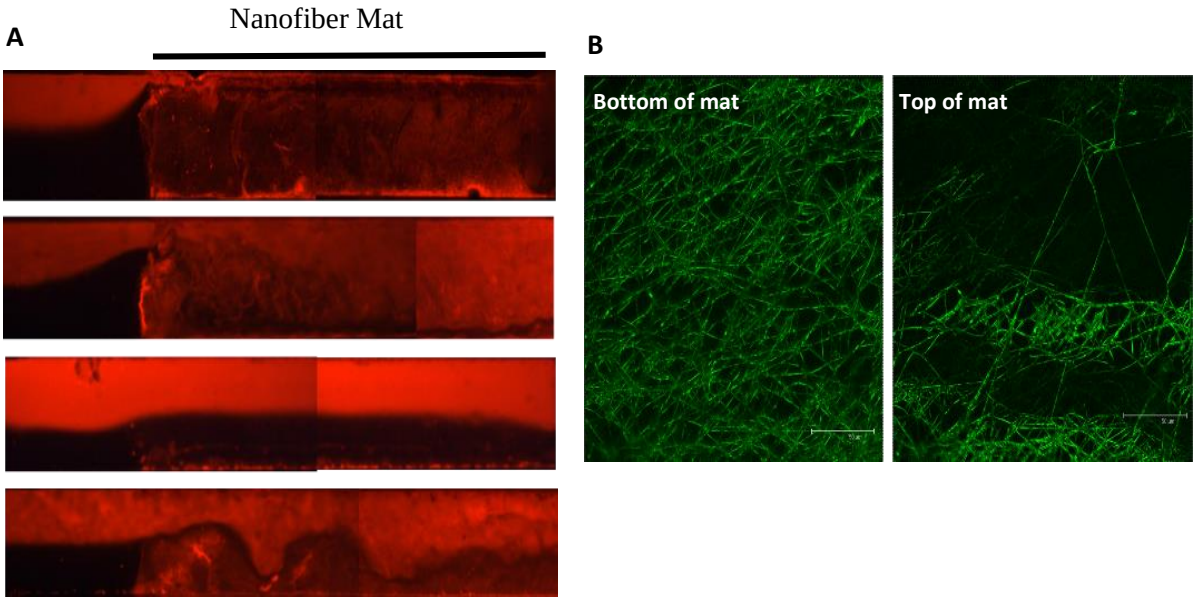

Figure A.2 (a) Examples of flow profiles observed in thick nanofiber mat samples. **(b)** Variation in nanofiber porosity and distribution along thickness of nanofiber mats. Confocal microscopy.

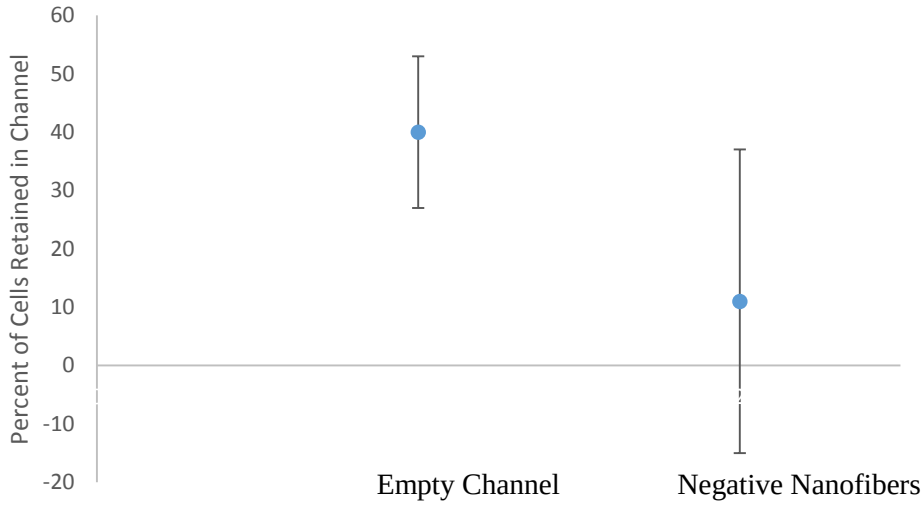

Figure A.3 Negatively charged nanofibers reduce nonspecific binding in unblocked PMMA microfluidic channels.

APPENDIX B

MATLOAB code for statistical analysis of fluid mixing.

PVA Analysis- Effect of length and number of fiber mat layers

```
%Multiple Regression on PVA Data Separated by Length and Layer
%Author: Lauren Colangelo and Nicholas Colangelo
%Last Edit: 03-23-2015

%As long as data input into the Table appropriately, everything should be taken care of between
data sets except for the following,
%which should be done for each new data set:
%To do:
%1) Make sure boxplots and other plots represent the data to be analyzed.
%2) Make sure labels for plots are appropriate.
%3) Make sure Holm Test is using the appropriate data from the SortData Table.

%Clear memory of variables that may be used here:
   clear
%Load the data:
   Data = readtable('C:\MatlabPVASep.xlsx');
   SortData = sortrows(Data,'Flow');
   SortData.Type = categorical(SortData.Type,'Ordinal',false);
   SortData.Length = categorical(SortData.Length,'Ordinal',false);
   SortData.Layer = categorical(SortData.Layer,'Ordinal',false);
   SortData.Channel = categorical(SortData.Channel,'Ordinal',false);

%Box Plot:
   figure(1)
   subplot(2,2,1)
   boxplot(SortData.Mixing,SortData.Length)
   xh = xlabel('Length');
   yh = ylabel('Mixing Value');
   set([xh,yh],'fontweight','bold');
   set(gca,'XTick', 1:3)
   set(gca,'XTickLabel',{'3mm', '5mm', '10mm'});

   subplot(2,2,2)
   boxplot(SortData.Mixing,SortData.Layer)
   xh = xlabel('Layer');
   yh = ylabel('Mixing Value');
```

```
    set([xh,yh],'fontweight','bold');

    subplot(2,2,3)
    boxplot(SortData.Mixing,SortData.Flow)
    xh = xlabel('Flow (\muL/sec)');
    yh = ylabel('Mixing Value');
    set([xh,yh],'fontweight','bold');
%Regression:
    modelspec = 'Mixing ~ Length + Layer + Flow';
    lm = fitlm(table2dataset(SortData),modelspec);
    disp(lm);
    %Table of ANOVA Results:
    disp(anova(lm));
    %Show Number of Outliers as Determined by Cook's Distance >= 3*MeanCooksDistance:
    Cook = sum(lm.Diagnostics.CooksDistance./mean(lm.Diagnostics.CooksDistance) >= 3);
    fprintf('Number of Values above Cook''s Distance %f', Cook)
%Obtain Parameters for Holm Test from the Regression
    %MSres
        MSres = double(lm.MSE);
    %Degrees of Freedom
        DF = double(lm.DFE);

%Length
    %Number of each length:
    for i = 1:max(double(SortData.Length)) %different types
        n(i) = sum(double(SortData.Length) == i);
    end %i
    %Input the number of types, less one (So it doesn't compare values against themselves)
    for i = 1:(max(double(SortData.Length)-1))
        %Input the total number of types, so it can make all the comparisons
        for j = (i+1):max(double(SortData.Length))
            %Comparison to Control
            if i  == 1
                t(i,j) = (lm.Coefficients.Estimate(j) - 0)/ sqrt(MSres*(1/n(j)+1/n(i)));
            %Between types comparison
            else
                t(i,j) = (lm.Coefficients.Estimate(j) - lm.Coefficients.Estimate(i))/
sqrt(MSres*(1/n(j)+1/n(i)));
            end %if i
        end %j
    end %i
        %Now we take the t values to p values
        p1 = 2*(1-tcdf(abs(t),DF));
        %Organize p-values
        Sorted1 = sort(reshape(p1,1,size(t,1)*size(t,2)));
        %Holm test p-value for comparison with uncorrected p-value of p=0.05:
```

```
        %Calculate number of comparisons:
        Comparisons = 0;
        i = 0;
        while i < max(double(SortData.Length))
           for i = 1:max(double(SortData.Length))
              Comparisons = Comparisons + (i-1);
           end %for i
        end %while i
        %Determine Significant Terms
        detect1 = 0;
        for i = 1:Comparisons
           pcomp = 0.05/(Comparisons-i+1);
           if Sorted1(i) <= pcomp
              Sig1(i) = 1;
              detect1 = 1;
           else
                 break
           end
     end %i
     %Display p values in p matrix that are significant
     if detect1 == 1
        fprintf('\np1 matrix is:\n')
        format short e
        disp(p1.*(p1<=Sorted1(length(Sig1))))
     else
        fprintf('\np1 matrix has no significant values.\n')
     end %if

%Layer
   %A lot of this code is unnecessary as there is only two layers to
   %compare.
   %Number of each Layer:
   for i = 1:max(double(SortData.Layer)) %different types
      n2(i) = sum(double(SortData.Layer) == i);
   end %i
      %Input the number of types, less one (So it doesn't compare values against themselves)
   for i = 1:(max(double(SortData.Layer)-1))
      %Input the total number of types, so it can make all the comparisons
      for j = (i+1):max(double(SortData.Layer))
         %Comparison to Control
         %Note: Accessing the coefficient array must account for Length variables
         if i  == 1
            t2(i,j) = (lm.Coefficients.Estimate(max(double(SortData.Length))-1+j) - 0)/
sqrt(MSres*(1/n2(j)+1/n2(i)));
         %Between types comparison
         else
```

```
            t2(i,j) = (lm.Coefficients.Estimate(max(double(SortData.Length))-1+j) -
lm.Coefficients.Estimate(i))/ sqrt(MSres*(1/n2(j)+1/n2(i)));
         end %if i
      end %j
   end %i
      %Now we take the t values to p values
      p2 = 2*(1-tcdf(abs(t2),DF));
      %Organize p-values
      Sorted2 = sort(reshape(p2,1,size(t2,1)*size(t2,2)));
      %Holm test p-value for comparison with uncorrected p-value of p=0.05:
         %Calculate number of comparisons:
         Comparisons2 = 0;
         i = 0;
         while i < max(double(SortData.Layer))
            for i = 1:max(double(SortData.Layer))
               Comparisons2 = Comparisons2 + (i-1);
            end %for i
         end %while i
         %Determine Significant Terms
         detect2 = 0;
         for i = 1:Comparisons2
            pcomp = 0.05/(Comparisons2-i+1);
            if Sorted2(i) <= pcomp
               Sig2(i) = 1;
               detect2 = 1;
            else
                  break
            end %p(i)
         end %i
      %Display p values in p matrix that are significant
      if detect2 == 1
         fprintf('\np2 matrix is:\n')
         format short e
         disp(p2.*(p2<=Sorted2(length(Sig2))))
      else
         fprintf('\np2 matrix has no significant values.\n')
      end %if

%Residuals
figure(2)
   gscatter(double(SortData.Type),lm.Residuals.Raw,SortData.Flow)
   yh = ylabel('Residuals');
   xh = xlabel('Types');
   legh = legend;
   htitle = get(legh,'Title');
   set(htitle,'String','Flow (\muL/sec)')
```

```
   set([xh,yh],'fontweight','bold');
   set(gca,'XTick', 1:6)
   set(gca,'XTickLabel',{'3mm 1 Layer', '3mm 2 Layer', '5mm 1 Layer', '5mm 2 Layer', '10mm 1
Layer', '10mm 2 Layer'})

%Test Normality
figure(3)
normplot(lm.Residuals.Standardized)
xh = xlabel('Standardized Residuals');
yh = ylabel('Normal Probability Scale');
set([xh,yh],'fontweight','bold');
```

PVA Analysis- Comparison of each PVA mat type

```
%Multiple Regression on PVA by Type
%Author: Lauren Colangelo and Nicholas Colangelo
%Last Edit: 03-23-2015
%As long as data input into the Table appropriately, everything should be taken care of between
data sets except for the following,
%which should be done for each new data set:
%To do:
%1) Make sure boxplots and other plots represent the data to be analyzed.
%2) Make sure labels for plots are appropriate.
%3) Make sure Holm Test is using the appropriate data from the SortData Table.

%Clear memory of variables that may be used here:
   clear
%Load the data:
   Data = readtable('C:\MatlabPVAType.xlsx');
   SortData = sortrows(Data,'Flow');
   SortData.Type = categorical(SortData.Type,'Ordinal',false);
   SortData.Channel = categorical(SortData.Channel,'Ordinal',false);
%Box Plot:
   figure(1)
   subplot(2,1,1)
   boxplot(SortData.Mixing,SortData.Type)
   xh = xlabel('Type');
   yh = ylabel('Mixing Value');
    set([xh,yh],'fontweight','bold');
   set(gca,'XTick', 1:7)
   set(gca,'XTickLabel',{'Control', '3mm 1 Layer', '3mm 2 Layer', '5mm 1 Layer', '5mm 2 Layer',
'10mm 1 Layer', '10mm 2 Layer'});
   subplot(2,1,2)
   boxplot(SortData.Mixing,SortData.Flow)
   xh = xlabel('Flow (\muL/min)');
   yh = ylabel('Mixing Value');
```

```
   set([xh,yh],'fontweight','bold');
%Regression:
   modelspec = 'Mixing ~ Type + Flow';
   lm = fitlm(table2dataset(SortData),modelspec);
   disp(lm);
   %Table of ANOVA Results:
   disp(anova(lm));
   %Show Number of Outliers as Determined by Cook's Distance >= 3*MeanCooksDistance:
   Cook = sum(lm.Diagnostics.CooksDistance./mean(lm.Diagnostics.CooksDistance) >= 3);
   fprintf('Number of Values above Cook''s Distance %f', Cook)
%Obtain Parameters for Holm Test from the Regression
   %TBL(3,3) = MSres
      MSres = double(lm.MSE);
   %TBL(3,2) = Degrees of Freedom
      DF = double(lm.DFE);
   %Number of each type:
   for i = 1:max(double(SortData.Type)) %different types
      n(i) = sum(double(SortData.Type) == i);
   end %i
%Holm Test
   %Input the number of types, less one (So it doesn't compare values against themselves)
   for i = 1:(max(double(SortData.Type)-1))
      %Input the total number of types, so it can make all the comparisons
      for j = (i+1):max(double(SortData.Type))
         %Comparison to Control
         if i  == 1
            t(i,j) = (lm.Coefficients.Estimate(j) - 0)/ sqrt(MSres*(1/n(j)+1/n(i)));
         %Between types comparison
         else
            t(i,j) = (lm.Coefficients.Estimate(j) - lm.Coefficients.Estimate(i))/
sqrt(MSres*(1/n(j)+1/n(i)));
         end %if i
      end %j
   end %i
   %Now we take the t values to p values
   p = 2*(1-tcdf(abs(t),DF));
   %Organize p-values
   Sorted = sort(reshape(p,1,size(t,1)*size(t,2)));
   %Holm test p-value for comparison with uncorrected p-value of p=0.05:
      %Calculate number of comparisons:
      Comparisons = 0;
      i = 0;
      while i < max(double(SortData.Type))
         for i = 1:max(double(SortData.Type))
            Comparisons = Comparisons + (i-1);
         end %for i
```

```
        end %while i
        %Determine Significant Terms
        detect = 0;
        for i = 1:Comparisons
            pcomp = 0.05/(Comparisons-i+1);
            if Sorted(i) <= pcomp
                Sig(i) = 1;
                detect = 1;
            else
                    break
            end %if Sorted
        end %if i
        %Display p values in p matrix that are significant
        if detect == 1
            fprintf('\np matrix is:\n')
            format short e
            disp(p.*(p<=Sorted(length(Sig))))
        else
            fprintf('\np1 matrix has no significant values.\n')
        end %if
%Residuals
figure(2)
    gscatter(double(SortData.Type),lm.Residuals.Raw,SortData.Flow)
    yh = ylabel('Residuals');
    xh = xlabel('Types');
    legh = legend;
    htitle = get(legh,'Title');
    set(htitle,'String','Flow (\muL/min)')
    set([xh,yh],'fontweight','bold');
    set(gca,'XTick', 1:7)
    set(gca,'XTickLabel',{'Control', '3mm 1 Layer', '3mm 2 Layer', '5mm 1 Layer', '5mm 2 Layer',
'10mm 1 Layer', '10mm 2 Layer'})

%Test Normality with a Normal Probability Plot
figure(3)
    normplot(lm.Residuals.Standardized)
    xh = xlabel('Standardized Residuals');
    yh = ylabel('Normal Probability Scale');
    set([xh,yh],'fontweight','bold');
```

PS Analysis- Effect of polymer weight percent and number of layers

```
%Multiple Regression on Polystyrene Data Separated by Weight and Layer

%Author: Lauren Colangelo and Nicholas Colangelo

%Last Edit: 03-23-2015
```

```
%As long as data input into the Table appropriately, everything should be taken care of between
data sets except for the following,

%which should be done for each new data set:

%To do:

%1) Make sure boxplots and other plots represent the data to be analyzed.

%2) Make sure labels for plots are appropriate.

%3) Make sure Holm Test is using the appropriate data from the SortData Table.


%Clear memory of variables that may be used here:

   clear

%Load the data:

   Data = readtable('C:\MatlabPolyStySep.xlsx');

   SortData = sortrows(Data,'Flow');

   SortData.Type = categorical(SortData.Type,'Ordinal',false);

   SortData.Weight = categorical(SortData.Weight,'Ordinal',false);

   SortData.Layer = categorical(SortData.Layer,'Ordinal',false);

   SortData.Channel = categorical(SortData.Channel,'Ordinal',false);


%Box Plot the data:

   figure(1)

      subplot(2,2,1)

      boxplot(SortData.Mixing,SortData.Weight)

      xh = xlabel('Weight');

      yh = ylabel('Mixing Value');

      set([xh,yh],'fontweight','bold');

      set(gca,'XTick', 1:3)

      set(gca,'XTickLabel',{'12.5%', '15%', '17.5%'});

      subplot(2,2,2)

      boxplot(SortData.Mixing,SortData.Layer)
```

```
    xh = xlabel('Layer');
    yh = ylabel('Mixing Value');
    set([xh,yh],'fontweight','bold');
    subplot(2,2,3)
    boxplot(SortData.Mixing,SortData.Flow)
    xh = xlabel('Flow (\muL/sec)');
    yh = ylabel('Mixing Value');
    set([xh,yh],'fontweight','bold');
%Regression:
  modelspec = 'Mixing ~ Weight + Layer + Flow';
  lm = fitlm(table2dataset(SortData),modelspec);
  disp(lm);
  %Table of ANOVA Results:
  disp(anova(lm));
  %Show Number of Outliers as Determined by Cook's Distance >= 3*MeanCooksDistance:
  Cook = sum(lm.Diagnostics.CooksDistance./mean(lm.Diagnostics.CooksDistance) >= 3);
  fprintf('Number of Values above Cook"s Distance %f', Cook)
%Obtain Parameters for Holm Test from the Regression
  %MSres
    MSres = double(lm.MSE);
  %Degrees of Freedom
    DF = double(lm.DFE);

%Weight Percentage
  %Number of each weight percentage:
  for i = 1:max(double(SortData.Weight)) %different types
    n(i) = sum(double(SortData.Weight) == i);
  end %i
  %Input the number of types, less one (So it doesn't compare values against themselves)
```

```
    for i = 1:(max(double(SortData.Weight)-1))
        %Input the total number of types, so it can make all the comparisons
        for j = (i+1):max(double(SortData.Weight))
            %Comparison to Control
            if i  == 1
                t(i,j) = (lm.Coefficients.Estimate(j) - 0)/ sqrt(MSres*(1/n(j)+1/n(i)));
            %Between types comparison
            else
                t(i,j) = (lm.Coefficients.Estimate(j) - lm.Coefficients.Estimate(i))/
sqrt(MSres*(1/n(j)+1/n(i)));
            end %if i
        end %j
    end %i
        %Now we take the t values to p values
        p1 = 2*(1-tcdf(abs(t),DF));
        %Organize p-values
        Sorted1 = sort(reshape(p1,1,size(t,1)*size(t,2)));
        %Holm test p-value for comparison with uncorrected p-value of p=0.05:
            %Calculate number of comparisons:
            Comparisons = 0;
            i = 0;
            while i < max(double(SortData.Weight))
                for i = 1:max(double(SortData.Weight))
                    Comparisons = Comparisons + (i-1);
                end %for i
            end %while i
            %Determine Significant Terms
            detect1 = 0;
            for i = 1:Comparisons
```

```
            pcomp = 0.05/(Comparisons-i+1);
            if Sorted1(i) <= pcomp
               Sig1(i) = 1;
               detect1 = 1;
            else
                  break
            end
         end %i
         %Display p values in p matrix that are significant
         if detect1 == 1
            fprintf('\np1 matrix is:\n')
            disp(p1.*(p1<=Sorted1(length(Sig1))))
            format short e
         else
            fprintf('\np1 matrix has no significant values.\n')
         end %if


%Layer
   %A lot of this code is unnecessary as there is only two layers to
   %compare.
   %Number of each Layer:
   for i = 1:max(double(SortData.Layer)) %different types
      n2(i) = sum(double(SortData.Layer) == i);
   end %i
      %Input the number of types, less one (So it doesn't compare values against themselves)
   for i = 1:(max(double(SortData.Layer)-1))
      %Input the total number of types, so it can make all the comparisons
      for j = (i+1):max(double(SortData.Layer))
         %Comparison to Control
```

```
        %Note: Accessing the coefficient array must account for weight variables
        if i  == 1
            t2(i,j) = (lm.Coefficients.Estimate(max(double(SortData.Weight))-1+j) - 0)/
sqrt(MSres*(1/n2(j)+1/n2(i)));
        %Between types comparison
        else
            t2(i,j) = (lm.Coefficients.Estimate(max(double(SortData.Weight))-1+j) -
lm.Coefficients.Estimate(i))/ sqrt(MSres*(1/n2(j)+1/n2(i)));
        end %if i
      end %j
   end %i
      %Now we take the t values to p values
      p2 = 2*(1-tcdf(abs(t2),DF));
      %Organize p-values
      Sorted2 = sort(reshape(p2,1,size(t2,1)*size(t2,2)));
      %Holm test p-value for comparison with uncorrected p-value of p=0.05:
        %Calculate number of comparisons:
        Comparisons2 = 0;
        i = 0;
        while i < max(double(SortData.Layer))
          for i = 1:max(double(SortData.Layer))
            Comparisons2 = Comparisons2 + (i-1);
          end %for i
        end %while i
        %Determine Significant Terms
        detect2 = 0;
        for i = 1:Comparisons2
          pcomp = 0.05/(Comparisons2-i+1);
          if Sorted2(i) <= pcomp
            Sig2(i) = 1;
```

```
            detect2 = 1;
        else
            break
        end %p(i)
    end %i
    %Display p values in p matrix that are significant
    if detect2 == 1
        fprintf('\np2 matrix is:\n')
        format short e
        disp(p2.*(p2<=Sorted2(length(Sig2))))
    else
        fprintf('\np2 matrix has no significant values.\n')
    end %if
%Residuals
figure(2)
    gscatter(double(SortData.Type),lm.Residuals.Raw,SortData.Flow)
    yh = ylabel('Residuals');
    xh = xlabel('Types');
    legh = legend;
    htitle = get(legh,'Title');
    set(htitle,'String','Flow (\muL/sec)')
    set([xh,yh],'fontweight','bold');
    set(gca,'XTick', 1:6)
    set(gca,'XTickLabel',{'3mm 1 Layer', '3mm 2 Layer', '5mm 1 Layer', '5mm 2 Layer', '10mm 1
Layer', '10mm 2 Layer'})


%Test Normality
figure(3)
    normplot(lm.Residuals.Standardized)
```

```
xh = xlabel('Standardized Residuals');
yh = ylabel('Normal Probability Scale');
set([xh,yh],'fontweight','bold');
```

PS Analysis- Comparison of each type of PS fiber mat

```
%Multiple Regression on Polystyrene Data by Type
%Author: Lauren Colangelo and Nicholas Colangelo
%Last Edit: 03-23-2015

%As long as data input into the Table appropriately, everything should be taken care of between data sets except for the following,
%which should be done for each new data set:
%To do:
%1) Make sure boxplots and other plots represent the data to be analyzed.
%2) Make sure labels for plots are appropriate.
%3) Make sure Holm Test is using the appropriate data from the SortData Table.

%Clear memory of variables that may be used here:
clear
%Load the data:
Data = readtable('C:\MatlabPolyStyType.xlsx');
SortData = sortrows(Data,'Flow');
SortData.Type = categorical(SortData.Type,'Ordinal',false);
SortData.Channel = categorical(SortData.Channel,'Ordinal',false);

%Box Plot:
figure(1)
subplot(2,1,1)
boxplot(SortData.Mixing,SortData.Type)
```

```
    xh = xlabel('Type');
    yh = ylabel('Mixing Value');
     set([xh,yh],'fontweight','bold');
    set(gca,'XTick', 1:7)
    set(gca,'XTickLabel',{'Control', '1 Layer 12.5%', '1 Layer 15%', '1 Layer 17.5%', '2 Layer
12.5%', '2 Layer 15%', '2 Layer 17.5%'});


    subplot(2,1,2)
    boxplot(SortData.Mixing,SortData.Flow)
    xh = xlabel('Flow (\muL/min)');
    yh = ylabel('Mixing Value');
    set([xh,yh],'fontweight','bold');



%Regression:
    modelspec = 'Mixing ~ Type + Flow';
    lm = fitlm(table2dataset(SortData),modelspec);
    disp(lm);
    %Table of ANOVA Results:
    disp(anova(lm));
    %Show Number of Outliers as Determined by Cook's Distance >= 3*MeanCooksDistance:
    Cook = sum(lm.Diagnostics.CooksDistance./mean(lm.Diagnostics.CooksDistance) >= 3);
    fprintf('Number of Values above Cook''s Distance %f', Cook)
%Obtain Parameters for Holm Test from the Regression
    %TBL(3,3) = MSres
        MSres = double(lm.MSE);
    %TBL(3,2) = Degrees of Freedom
        DF = double(lm.DFE);
    %Number of each type:
```

```
    for i = 1:max(double(SortData.Type)) %different types
        n(i) = sum(double(SortData.Type) == i);
    end %i
%Holm Test
    %Input the number of types, less one (So it doesn't compare values against themselves)
    for i = 1:(max(double(SortData.Type)-1))
        %Input the total number of types, so it can make all the comparisons
        for j = (i+1):max(double(SortData.Type))
            %Comparison to Control
            if i  == 1
                t(i,j) = (lm.Coefficients.Estimate(j) - 0)/ sqrt(MSres*(1/n(j)+1/n(i)));
            %Between types comparison
            else
                t(i,j) = (lm.Coefficients.Estimate(j) - lm.Coefficients.Estimate(i))/
sqrt(MSres*(1/n(j)+1/n(i)));
            end %if i
        end %j
    end %i
    %Now we take the t values to p values
    p = 2*(1-tcdf(abs(t),DF));
    %Organize p-values
    Sorted = sort(reshape(p,1,size(t,1)*size(t,2)));
    %Holm test p-value for comparison with uncorrected p-value of p=0.05:
        %Calculate number of comparisons:
        Comparisons = 0;
        i = 0;
        while i < max(double(SortData.Type))
            for i = 1:max(double(SortData.Type))
                Comparisons = Comparisons + (i-1);
```

```
        end %for i
    end %while i
    %Determine Significant Terms
    detect = 0;
    for i = 1:Comparisons
        pcomp = 0.05/(Comparisons-i+1);
        if Sorted(i) <= pcomp
            Sig(i) = 1;
            detect = 1;
        else
                break
        end %if Sorted
    end %if i
    %Display p values in p matrix that are significant
    if detect == 1
        fprintf('\np matrix is:\n')
        format short e
        disp(p.*(p<=Sorted(length(Sig))))
    else
        fprintf('\np1 matrix has no significant values.\n')
    end %if

%Residuals
figure(2)
    gscatter(double(SortData.Type),lm.Residuals.Raw,SortData.Flow)
    yh = ylabel('Residuals');
    xh = xlabel('Types');
    legh = legend;
```

```
    htitle = get(legh,'Title');
    set(htitle,'String','Flow (\muL/min)')
    set([xh,yh],'fontweight','bold');
    set(gca,'XTick', 1:7)
    set(gca,'XTickLabel',{'Control', '1 Layer 12.5%', '1 Layer 15%', '1 Layer 17.5%', '2 Layer 12.5%', '2 Layer 15%', '2 Layer 17.5%'})


%Test Normality with a Normal Probability Plot
figure(3)
    normplot(lm.Residuals.Standardized)
    xh = xlabel('Standardized Residuals');
    yh = ylabel('Normal Probability Scale');
    set([xh,yh],'fontweight','bold');
```

REFERENCES

1. Ahn, C. H. *et al.* Disposable smart lab on a chip for point-of-care clinical diagnostics. *Proc. IEEE* **92,** 154–173 (2004).
2. Srinivasan, V., Pamula, V. K. & Fair, R. B. An integrated digital microfluidic lab-on-a-chip for clinical diagnostics on human physiological fluids. *Lab. Chip* **4,** 310–315 (2004).
3. Christodoulides, N. *et al.* Lab-on-a-Chip Methods for Point-of-Care Measurements of Salivary Biomarkers of Periodontitis. *Ann. N. Y. Acad. Sci.* **1098,** 411–428 (2007).
4. Nugen, S. R. & Baeumner, A. J. Trends and opportunities in food pathogen detection. *Anal. Bioanal. Chem.* **391,** 451–454 (2008).
5. Nguyen, N.-T. & Wu, Z. Micromixers—a review. *J. Micromechanics Microengineering* **15,** R1 (2005).
6. Hessel, V., Löwe, H. & Schönfeld, F. Micromixers—a review on passive and active mixing principles. *Chem. Eng. Sci.* **60,** 2479–2501 (2005).
7. Li, J. *Computational Analysis of Nanofluid Flow in Microchannels with Applications to Micro-heat Sinks and Bio-MEMS.* (ProQuest, 2008).
8. Li, D. & Xia, Y. Electrospinning of Nanofibers: Reinventing the Wheel? *Adv. Mater.* **16,** 1151–1170 (2004).
9. Cho, D. *et al.* Electrospun nanofibers for microfluidic analytical systems. *Polymer* **52,** 3413–3421 (2011).
10. Matlock-Colangelo, L., Cho, D., Pitner, C. L., Frey, M. W. & Baeumner, A. J. Functionalized electrospun nanofibers as bioseparators in microfluidic systems. *Lab. Chip* **12,** 1696–1701 (2012).
11. Zhang, Q. *et al.* Improvement in nanofiber filtration by multiple thin layers of nanofiber mats. *J. Aerosol Sci.* **41,** 230–236 (2010).

12. Przekop, R. & Gradon, L. Deposition and Filtration of Nanoparticles in the Composites of Nano- and Microsized Fibers. *Aerosol Sci. Technol.* **42,** 483–493 (2008).
13. Wang, J. Nanomaterial-based electrochemical biosensors. *Analyst* **130,** 421–426 (2005).
14. Yun, Y. *et al.* in *Applications of Nanomaterials in Sensors and Diagnostics* (ed. Tuantranont, A.) 43–58 (Springer Berlin Heidelberg, 2012). at <http://link.springer.com/chapter/10.1007/5346_2012_43>
15. Lee, S. H., Sung, J. H. & Park, T. H. Nanomaterial-based biosensor as an emerging tool for biomedical applications. *Ann. Biomed. Eng.* **40,** 1384–1397 (2012).
16. Matlock-Colangelo, L. & Baeumner, A. J. Recent progress in the design of nanofiber-based biosensing devices. *Lab. Chip* **12,** 2612–2620 (2012).
17. Li, D., Frey, M. W. & Baeumner, A. J. Electrospun polylactic acid nanofiber membranes as substrates for biosensor assemblies. *J. Membr. Sci.* **279,** 354–363 (2006).
18. Wang, D., Sun, G., Xiang, B. & Chiou, B.-S. Controllable biotinylated poly(ethylene-co-glycidyl methacrylate) (PE-co-GMA) nanofibers to bind streptavidin–horseradish peroxidase (HRP) for potential biosensor applications. *Eur. Polym. J.* **44,** 2032–2039 (2008).
19. Huang, Z.-M., Zhang, Y.-Z., Kotaki, M. & Ramakrishna, S. A review on polymer nanofibers by electrospinning and their applications in nanocomposites. *Compos. Sci. Technol.* **63,** 2223–2253 (2003).
20. Jin, S., Dai, M., Ye, B. & Nugen, S. R. Development of a capillary flow microfluidic Escherichia coli biosensor with on-chip reagent delivery using water-soluble nanofibers. *Microsyst. Technol.* **19,** 2011–2015 (2013).

21. Kowalczyk, T., Nowicka, A., Elbaum, D. & Kowalewski, T. A. Electrospinning of bovine serum albumin. Optimization and the use for production of biosensors. *Biomacromolecules* **9,** 2087–2090 (2008).
22. Lee, I., Luo, X., Huang, J., Cui, X. T. & Yun, M. Detection of Cardiac Biomarkers Using Single Polyaniline Nanowire-Based Conductometric. *Biosensors* **2,** 205–220 (2012).
23. Wang, J. Electrochemical biosensors: Towards point-of-care cancer diagnostics. *Biosens. Bioelectron.* **21,** 1887–1892 (2006).
24. Herricks, T. E. *et al.* Direct fabrication of enzyme-carrying polymer nanofibers by electrospinning. *J. Mater. Chem.* **15,** 3241–3245 (2005).
25. Xie, J. & Hsieh, Y.-L. Ultra-high surface fibrous membranes from electrospinning of natural proteins: casein and lipase enzyme. *J. Mater. Sci.* **38,** 2125–2133 (2003).
26. Zhang, Y. Z. *et al.* Coaxial electrospinning of (fluorescein isothiocyanate-conjugated bovine serum albumin)-encapsulated poly(epsilon-caprolactone) nanofibers for sustained release. *Biomacromolecules* **7,** 1049–1057 (2006).
27. Wimpenny, I., Hampson, K., Yang, Y., Ashammakhi, N. & Forsyth, N. R. One-step recovery of marrow stromal cells on nanofibers. *Tissue Eng. Part C Methods* **16,** 503–509 (2010).
28. Shin, M., Yoshimoto, H. & Vacanti, J. P. In Vivo Bone Tissue Engineering Using Mesenchymal Stem Cells on a Novel Electrospun Nanofibrous Scaffold. *Tissue Eng.* **10,** 33–41 (2004).
29. El-Aassar, M. R., Al-Deyab, S. S. & Kenawy, E.-R. Covalent immobilization of β-galactosidase onto electrospun nanofibers of poly (AN-co-MMA) copolymer. *J. Appl. Polym. Sci.* **127,** 1873–1884 (2013).

30. Shin, Y. J. & Kameoka, J. Amperometric cholesterol biosensor using layer-by-layer adsorption technique onto electrospun polyaniline nanofibers. *J. Ind. Eng. Chem.* **18,** 193–197 (2012).
31. Wu, J. & Yin, F. Sensitive enzymatic glucose biosensor fabricated by electrospinning composite nanofibers and electrodepositing Prussian blue film. *J. Electroanal. Chem.* **694,** 1–5 (2013).
32. Zhang, M. *et al.* Immobilization of anti-CD31 antibody on electrospun poly(ε-caprolactone) scaffolds through hydrophobins for specific adhesion of endothelial cells. *Colloids Surf. B Biointerfaces* **85,** 32–39 (2011).
33. Xie, J., Ma, B., Michael, P. L. & Shuler, F. D. Fabrication of Nanofiber Scaffolds With Gradations in Fiber Organization and Their Potential Applications. *Macromol. Biosci.* **12,** 1336–1341 (2012).
34. Ramakrishna, S. *et al.* Electrospun nanofibers: solving global issues. *Mater. Today* **9,** 40–50 (2006).
35. Min, B.-M. *et al.* Electrospinning of silk fibroin nanofibers and its effect on the adhesion and spreading of normal human keratinocytes and fibroblasts in vitro. *Biomaterials* **25,** 1289–1297 (2004).
36. Wang, S., Zhang, Y., Wang, H., Yin, G. & Dong, Z. Fabrication and Properties of the Electrospun Polylactide/Silk Fibroin-Gelatin Composite Tubular Scaffold. *Biomacromolecules* **10,** 2240–2244 (2009).
37. Huang, J., Virji, S., Weiller, B. H. & Kaner, R. B. Polyaniline Nanofibers: Facile Synthesis and Chemical Sensors. *J. Am. Chem. Soc.* **125,** 314–315 (2002).

38. Feng, C., Khulbe, K. C. & Matsuura, T. Recent progress in the preparation, characterization, and applications of nanofibers and nanofiber membranes via electrospinning/interfacial polymerization. *J. Appl. Polym. Sci.* **115,** 756–776 (2010).
39. Deitzel, J. M., Kleinmeyer, J., Harris, D. & Beck Tan, N. C. The effect of processing variables on the morphology of electrospun nanofibers and textiles. *Polymer* **42,** 261–272 (2001).
40. Li, D., Frey, M. W., Vynias, D. & Baeumner, A. J. Availability of biotin incorporated in electrospun PLA fibers for streptavidin binding. *Polymer* **48,** 6340–6347 (2007).
41. Dror, Y. *et al.* Nanofibers Made of Globular Proteins. *Biomacromolecules* **9,** 2749–2754 (2008).
42. Barnes, C. *et al.* Feasibility of Electrospinning the Globular Proteins Hemoglobin and Myoglobin. *J. Eng. Fibers Fabr.* **1,** 16–29 (2006).
43. Valmikinathan, C. M., Defroda, S. & Yu, X. Polycaprolactone and Bovine Serum Albumin Based Nanofibers for Controlled Release of Nerve Growth Factor. *Biomacromolecules* **10,** 1084–1089 (2009).
44. Ding, Y., Wang, Y., Li, B. & Lei, Y. Electrospun hemoglobin microbelts based biosensor for sensitive detection of hydrogen peroxide and nitrite. *Biosens. Bioelectron.* **25,** 2009–2015 (2010).
45. Liu, C.-Y. & Hu, J.-M. Hydrogen peroxide biosensor based on the direct electrochemistry of myoglobin immobilized on silver nanoparticles doped carbon nanotubes film. *Biosens. Bioelectron.* **24,** 2149–2154 (2009).
46. Shen, L., Huang, R. & Hu, N. Myoglobin in polyacrylamide hydrogel films: direct electrochemistry and electrochemical catalysis. *Talanta* **56,** 1131–1139 (2002).

47. Zhao, G.-C., Zhang, L., Wei, X.-W. & Yang, Z.-S. Myoglobin on multi-walled carbon nanotubes modified electrode: direct electrochemistry and electrocatalysis. *Electrochem. Commun.* **5,** 825–829 (2003).

48. Dai, M., Jin, S. & Nugen, S. R. Water-Soluble Electrospun Nanofibers as a Method for On-Chip Reagent Storage. *Biosensors* **2,** 388–395 (2012).

49. Wang, S.-G., Jiang, X., Chen, P.-C., Yu, A.-G. & Huang, X.-J. Preparation of Coaxial-Electrospun Poly[bis(p-methylphenoxy)]phosphazene Nanofiber Membrane for Enzyme Immobilization. *Int. J. Mol. Sci.* **13,** 14136–14148 (2012).

50. Hou, S. *et al.* Polymer Nanofiber-Embedded Microchips for Detection, Isolation, and Molecular Analysis of Single Circulating Melanoma Cells. *Angew. Chem. Int. Ed.* **52,** 3379–3383 (2013).

51. Senecal, A., Magnone, J., Marek, P. & Senecal, K. Development of functional nanofibrous membrane assemblies towards biological sensing. *React. Funct. Polym.* **68,** 1429–1434 (2008).

52. Awokoya, K. N. *et al.* Molecularly imprinted electrospun nanofibers for adsorption of nickel-5,10,15,20-tetraphenylporphine (NTPP) in organic media. *J. Polym. Res.* **20,** 1–9 (2013).

53. Chronakis, I. S., Jakob, A., Hagström, B. & Ye, L. Encapsulation and Selective Recognition of Molecularly Imprinted Theophylline and 17β-Estradiol Nanoparticles within Electrospun Polymer Nanofibers. *Langmuir* **22,** 8960–8965 (2006).

54. Spégel, P., Schweitz, L. & Nilsson, S. Molecularly imprinted polymers. *Anal. Bioanal. Chem.* **372,** 37–38 (2001).

55. Tonglairoum, P. *et al.* Development and Characterization of Propranolol Selective Molecular Imprinted Polymer Composite Electrospun Nanofiber Membrane. *AAPS PharmSciTech* **14,** 838–846 (2013).

56. Sueyoshi, Y., Utsunomiya, A., Yoshikawa, M., Robertson, G. P. & Guiver, M. D. Chiral separation with molecularly imprinted polysulfone-aldehyde derivatized nanofiber membranes☆. *J. Membr. Sci.* **401–402,** 89–96 (2012).

57. Mizushima, H., Yoshikawa, M., Li, N., Robertson, G. P. & Guiver, M. D. Electrospun nanofiber membranes from polysulfones with chiral selector aimed for optical resolution. *Eur. Polym. J.* **48,** 1717–1725 (2012).

58. Preparation of aptamer-linked gold nanoparticle purple aggregates for colorimetric sensing of analytes : Abstract : Nature Protocols. *Nat Protoc.* **1,** 246–252 (2006).

59. Zhao, Q., Li, X.-F. & Le, X. C. Aptamer-Modified Monolithic Capillary Chromatography for Protein Separation and Detection. *Anal. Chem.* **80,** 3915–3920 (2008).

60. Oktem, H. A., Bayramoglu, G., Ozalp, V. C. & Arica, M. Y. Single-Step Purification of Recombinant Thermus aquaticus DNA Polymerase Using DNA-Aptamer Immobilized Novel Affinity Magnetic Beads. *Biotechnol. Prog.* **23,** 146–154 (2007).

61. Kim, J. H., Hwang, E. T., Kang, K., Tatavarty, R. & Gu, M. B. Aptamers-on-nanofiber as a novel hybrid capturing moiety. *J. Mater. Chem.* **21,** 19203–19206 (2011).

62. Rodriguez, M. C., Kawde, A.-N. & Wang, J. Aptamer biosensor for label-free impedance spectroscopy detection of proteins based on recognition-induced switching of the surface charge. *Chem. Commun.* 4267–4269 (2005). doi:10.1039/B506571B

63. Lee, S. J., Tatavarty, R. & Gu, M. B. Electrospun polystyrene–poly(styrene-co-maleic anhydride) nanofiber as a new aptasensor platform. *Biosens. Bioelectron.* **38,** 302–307 (2012).

64. Wang, X. *et al.* Novel electrochemical biosensor based on functional composite nanofibers for sensitive detection of p53 tumor suppressor gene. *Anal. Chim. Acta* **765,** 63–69 (2013).

65. Lu, T. *et al.* The immobilization of proteins on biodegradable fibers via biotin–streptavidin bridges. *Acta Biomater.* **4,** 1770–1777 (2008).

66. Katti, D. S., Robinson, K. W., Ko, F. K. & Laurencin, C. T. Bioresorbable nanofiber-based systems for wound healing and drug delivery: Optimization of fabrication parameters. *J. Biomed. Mater. Res. B Appl. Biomater.* **70B,** 286–296 (2004).

67. Zeng, J. *et al.* Biodegradable electrospun fibers for drug delivery. *J. Controlled Release* **92,** 227–231 (2003).

68. Kim, K. *et al.* Incorporation and controlled release of a hydrophilic antibiotic using poly(lactide-co-glycolide)-based electrospun nanofibrous scaffolds. *J. Controlled Release* **98,** 47–56 (2004).

69. Hong, Y. *et al.* Generating Elastic, Biodegradable Polyurethane/Poly(lactide-co-glycolide) Fibrous Sheets with Controlled Antibiotic Release via Two-Stream Electrospinning. *Biomacromolecules* **9,** 1200–1207 (2008).

70. Taepaiboon, P., Rungsardthong, U. & Supaphol, P. Drug-loaded electrospun mats of poly(vinyl alcohol) fibres and their release characteristics of four model drugs. *Nanotechnology* **17,** 2317 (2006).

71. Choi, J. S., Lee, S. J., Christ, G. J., Atala, A. & Yoo, J. J. The influence of electrospun aligned poly(ε-caprolactone)/collagen nanofiber meshes on the formation of self-aligned skeletal muscle myotubes. *Biomaterials* **29,** 2899–2906 (2008).
72. Xu, C., Inai, R., Kotaki, M. & Ramakrishna, S. Electrospun Nanofiber Fabrication as Synthetic Extracellular Matrix and Its Potential for Vascular Tissue Engineering. *Tissue Eng.* **10,** 1160–1168 (2004).
73. Mo, X. M., Xu, C. Y., Kotaki, M. & Ramakrishna, S. Electrospun P(LLA-CL) nanofiber: a biomimetic extracellular matrix for smooth muscle cell and endothelial cell proliferation. *Biomaterials* **25,** 1883–1890 (2004).
74. Lee, S. J., Yoo, J. J., Lim, G. J., Atala, A. & Stitzel, J. In vitro evaluation of electrospun nanofiber scaffolds for vascular graft application. *J. Biomed. Mater. Res. A* **83A,** 999–1008 (2007).
75. Yoshimoto, H., Shin, Y. M., Terai, H. & Vacanti, J. P. A biodegradable nanofiber scaffold by electrospinning and its potential for bone tissue engineering. *Biomaterials* **24,** 2077–2082 (2003).
76. Wu, L. & Ding, J. In vitro degradation of three-dimensional porous poly(d,l-lactide-co-glycolide) scaffolds for tissue engineering. *Biomaterials* **25,** 5821–5830 (2004).
77. Choi, S.-W. *et al.* Alginate hydrogel embedding poly(D,L-lactide-co-glycolide) porous scaffold disks for cartilage tissue engineering. *Macromol. Res.* **20,** 447–452 (2012).
78. Inui, A. *et al.* Regeneration of Rotator Cuff Tear Using Electrospun Poly(d,l-Lactide-Co-Glycolide) Scaffolds in a Rabbit Model. *Arthrosc. J. Arthrosc. Relat. Surg.* **28,** 1790–1799 (2012).

79. Xin, X., Hussain, M. & Mao, J. J. Continuing differentiation of human mesenchymal stem cells and induced chondrogenic and osteogenic lineages in electrospun PLGA nanofiber scaffold. *Biomaterials* **28,** 316–325 (2007).

80. Ionescu, L. C., Lee, G. C., Sennett, B. J., Burdick, J. A. & Mauck, R. L. An anisotropic nanofiber/microsphere composite with controlled release of biomolecules for fibrous tissue engineering. *Biomaterials* **31,** 4113–4120 (2010).

81. Reinholt, S. J., Sonnenfeldt, A., Naik, A., Frey, M. W. & Baeumner, A. J. Developing new materials for paper-based diagnostics using electrospun nanofibers. *Anal. Bioanal. Chem.* **406,** 3297–3304 (2013).

82. Jeong, S. H., Lee, D. W., Kim, S., Kim, J. & Ku, B. A study of electrochemical biosensor for analysis of three-dimensional (3D) cell culture. *Biosens. Bioelectron.* **35,** 128–133 (2012).

83. Pasche, S. *et al.* Integrated optical biosensor for in-line monitoring of cell cultures. *Biosens. Bioelectron.* **26,** 1478–1485 (2010).

84. A. Schober, U. F. Applied nano bio systems with microfluidics and biosensors for three-dimensional cell culture. *Mater. Werkst.* **42,** 139 – 146 (2011).

85. Ziegler, C. Cell-based biosensors. *Fresenius J. Anal. Chem.* **366,** 552–559 (2000).

86. Wilson, G. S. & Hu, Y. Enzyme-based biosensors for in vivo measurements. *Chem. Rev.* **100,** 2693–2704 (2000).

87. Wilson, G. S. & Gifford, R. Biosensors for real-time in vivo measurements. *Biosens. Bioelectron.* **20,** 2388–2403 (2005).

88. Wilson, G. S. & Ammam, M. In vivo biosensors. *FEBS J.* **274,** 5452–5461 (2007).

89. Kirby, B. J. *Micro- and Nanoscale Fluid Mechanics: Transport in Microfluidic Devices*. (Cambridge University Press, 2010).

90. Khandurina, J. & Guttman, A. Bioanalysis in microfluidic devices. *J. Chromatogr. A* **943,** 159–183 (2002).

91. Yager, P., Domingo, G. J. & Gerdes, J. Point-of-Care Diagnostics for Global Health. *Annu. Rev. Biomed. Eng.* **10,** 107–144 (2008).

92. Marle, L. & Greenway, G. M. Microfluidic devices for environmental monitoring. *TrAC Trends Anal. Chem.* **24,** 795–802 (2005).

93. Wang, H., Iovenitti, P., Harvey, E. & Masood, S. Optimizing layout of obstacles for enhanced mixing in microchannels. *Smart Mater. Struct.* **11,** 662 (2002).

94. Yang, Z., Matsumoto, S., Goto, H., Matsumoto, M. & Maeda, R. Ultrasonic micromixer for microfluidic systems. *Sens. Actuators Phys.* **93,** 266–272 (2001).

95. Wong, S. H., Ward, M. C. L. & Wharton, C. W. Micro T-mixer as a rapid mixing micromixer. *Sens. Actuators B Chem.* **100,** 359–379 (2004).

96. Kim, D. S., Lee, S. W., Kwon, T. H. & Lee, S. S. A barrier embedded chaotic micromixer. *J. Micromechanics Microengineering* **14,** 798 (2004).

97. Doshi, J. & Reneker, D. H. Electrospinning process and applications of electrospun fibers. in , *Conference Record of the 1993 IEEE Industry Applications Society Annual Meeting, 1993* 1698–1703 vol.3 (1993). doi:10.1109/IAS.1993.299067

98. Ma, M., Mao, Y., Gupta, M., Gleason, K. K. & Rutledge, G. C. Superhydrophobic Fabrics Produced by Electrospinning and Chemical Vapor Deposition. *Macromolecules* **38,** 9742–9748 (2005).

99. Tamura, T. & Kawakami, H. Aligned Electrospun Nanofiber Composite Membranes for Fuel Cell Electrolytes. *Nano Lett.* **10,** 1324–1328 (2010).

100. Luo, Y. *et al.* Surface functionalization of electrospun nanofibers for detecting E. coli O157:H7 and BVDV cells in a direct-charge transfer biosensor. *Biosens. Bioelectron.* **26,** 1612–1617 (2010).

101. Nugen, S. R., Asiello, P. J. & Baeumner, A. J. Design and fabrication of a microfluidic device for near-single cell mRNA isolation using a copper hot embossing master. *Microsyst. Technol.* **15,** 477–483 (2008).

102. Lu, L.-H., Ryu, K. S. & Liu, C. A magnetic microstirrer and array for microfluidic mixing. *J. Microelectromechanical Syst.* **11,** 462–469 (2002).

103. Chang, S. T., Beaumont, E., Petsev, D. N. & Velev, O. D. Remotely powered distributed microfluidic pumps and mixers based on miniature diodes. *Lab. Chip* **8,** 117–124 (2007).

104. Holm, S. A Simple Sequentially Rejective Multiple Test Procedure. *Scand. J. Stat.* **6,** 65–70 (1979).

105. Glantz, S. & Slinker, B. *Primer of Applied Regression & Analysis of Variance*. (McGraw-Hill Education, 2000).

106. Johnson, T. J., Ross, D. & Locascio, L. E. Rapid Microfluidic Mixing. *Anal. Chem.* **74,** 45–51 (2002).

107. Bhagat, A. A. S., Peterson, E. T. K. & Papautsky, I. A passive planar micromixer with obstructions for mixing at low Reynolds numbers. *J. Micromechanics Microengineering* **17,** 1017 (2007).

108. Podgórski, A., Bałazy, A. & Gradoń, L. Application of nanofibers to improve the filtration efficiency of the most penetrating aerosol particles in fibrous filters. *Chem. Eng. Sci.* **61,** 6804–6815 (2006).

109. Bland, J. M. & Altman, D. G. Multiple significance tests: the Bonferroni method. *BMJ* **310,** 170 (1995).

110. Lin, Y., Gerfen, G. J., Rousseau, D. L. & Yeh, S.-R. Ultrafast Microfluidic Mixer and Freeze-Quenching Device. *Anal. Chem.* **75,** 5381–5386 (2003).

111. Evaluation of passive mixing behaviors in a pillar obstruction poly(dimethylsiloxane) microfluidic mixer using fluorescence microscopy - Springer. doi:10.1007/s10404-008-0386-1

112. Byung-Moo Min, S. W. L. Chitin and chitosan nanofibers: electrospinning of chitin and deacetylation of chitin nanofibers. *Polymer* 7137–7142 (2004). doi:10.1016/j.polymer.2004.08.048

113. Matlock-Colangelo, L., Cho, D., Pitner, C. L., Frey, M. W. & Baeumner, A. J. Functionalized electrospun nanofibers as bioseparators in microfluidic systems. *Lab. Chip* **12,** 1696 (2012).

114. Drain, P. K. *et al.* Diagnostic point-of-care tests in resource-limited settings. *Lancet Infect. Dis.* **14,** 239–249 (2014).

115. Lagally, E. T., Lee, S.-H. & Soh, H. T. Integrated microsystem for dielectrophoretic cell concentration and genetic detection. *Lab. Chip* **5,** 1053–1058 (2005).

116. Baeumner, A. J., Cohen, R. N., Miksic, V. & Min, J. RNA biosensor for the rapid detection of viable Escherichia coli in drinking water. *Biosens. Bioelectron.* **18,** 405–413 (2003).

117. Chappell, C. L., Okhuysen, P. C., Sterling, C. R. & DuPont, H. L. Cryptosporidium parvum: Intensity of Infection and Oocyst Excretion Patterns in Healthy Volunteers. *J. Infect. Dis.* **173,** 232–236 (1996).

118. Chen, G. D., Alberts, C. J., Rodriguez, W. & Toner, M. Concentration and Purification of Human Immunodeficiency Virus Type 1 Virions by Microfluidic Separation of Superparamagnetic Nanoparticles. *Anal. Chem.* **82,** 723–728 (2010).

119. Lapizco-Encinas, B. H., Simmons, B. A., Cummings, E. B. & Fintschenko, Y. Insulator-based dielectrophoresis for the selective concentration and separation of live bacteria in water. *ELECTROPHORESIS* **25,** 1695–1704 (2004).

120. Ji, H. M. *et al.* Silicon-based microfilters for whole blood cell separation. *Biomed. Microdevices* **10,** 251–7 (2008).

121. Long, Z., Shen, Z., Wu, D., Qin, J. & Lin, B. Integrated multilayer microfluidic device with a nanoporous membrane interconnect for online coupling of solid-phase extraction to microchip electrophoresis. *Lab. Chip* **7,** 1819–1824 (2007).

122. Zhang, J. Y., Do, J., Premasiri, W. R., Ziegler, L. D. & Klapperich, C. M. Rapid point-of-care concentration of bacteria in a disposable microfluidic device using meniscus dragging effect. *Lab. Chip* **10,** 3265–3270 (2010).

123. Walker, G. M. & Beebe, D. J. Evaporation-driven microfluidic sample concentration. in *Microtechnologies in Medicine amp; Biology 2nd Annual International IEEE-EMB Special Topic Conference on* 523–526 (2002). doi:10.1109/MMB.2002.1002397

124. Mahalanabis, M., Al-Muayad, H., Kulinski, M. D., Altman, D. & Klapperich, C. M. Cell lysis and DNA extraction of gram-positive and gram-negative bacteria from whole blood in a disposable microfluidic chip. *Lab. Chip* **9,** 2811–2817 (2009).

125. Karle, M. *et al.* Continuous microfluidic DNA extraction using phase-transfer magnetophoresis. *Lab. Chip* **10,** 3284–3290 (2010).

126. Du, Y. *et al.* Rapid generation of spatially and temporally controllable long-range concentration gradients in a microfluidic device. *Lab. Chip* **9,** 761–767 (2009).

127. Hwang, K.-Y. *et al.* Solid Phase DNA Extraction with a Flexible Bead-Packed Microfluidic Device to Detect Methicillin-Resistant Staphylococcus aureus in Nasal Swabs. *Anal. Chem.* **84,** 7912–7918 (2012).

128. Oleschuk, R. D., Shultz-Lockyear, L. L., Ning, Y. & Harrison, D. J. Trapping of Bead-Based Reagents within Microfluidic Systems: On-Chip Solid-Phase Extraction and Electrochromatography. *Anal. Chem.* **72,** 585–590 (2000).

129. Cady, N. C., Stelick, S. & Batt, C. A. Nucleic acid purification using microfabricated silicon structures. *Biosens. Bioelectron.* **19,** 59–66 (2003).

130. Lay, C. *et al.* Enhanced microfiltration devices configured with hydrodynamic trapping and a rain drop bypass filtering architecture for microbial cells detection. *Lab. Chip* **8,** 830–833 (2008).

131. Matlock-Colangelo, L. & Baeumner, A. J. Biologically Inspired Nanofibers for Use in Translational Bioanalytical Systems. *Annu. Rev. Anal. Chem.* **7,** 23–42 (2014).

132. Anton, F. Process and apparatus for preparing artificial threads. (1934). at <http://www.google.com/patents/US1975504>

133. Frenot, A. & Chronakis, I. S. Polymer nanofibers assembled by electrospinning. *Curr. Opin. Colloid Interface Sci.* **8,** 64–75 (2003).

134. Dror, Y. *et al.* Carbon Nanotubes Embedded in Oriented Polymer Nanofibers by Electrospinning. *Langmuir* **19,** 7012–7020 (2003).

135. Fu, J. *et al.* Laccase Biosensor Based on Electrospun Copper/Carbon Composite Nanofibers for Catechol Detection. *Sensors* **14,** 3543–3556 (2014).

136. Zeng, J. *et al.* Poly(vinyl alcohol) Nanofibers by Electrospinning as a Protein Delivery System and the Retardation of Enzyme Release by Additional Polymer Coatings. *Biomacromolecules* **6,** 1484–1488 (2005).

137. Ner, Y., Grote, J. G., Stuart, J. A. & Sotzing, G. A. White Luminescence from Multiple-Dye-Doped Electrospun DNA Nanofibers by Fluorescence Resonance Energy Transfer. *Angew. Chem. Int. Ed.* **48,** 5134–5138 (2009).

138. Li, M. *et al.* Electrospinning: A Facile Method to Disperse Fluorescent Quantum Dots in Nanofibers without Förster Resonance Energy Transfer. *Adv. Funct. Mater.* **17,** 3650–3656 (2007).

139. Wang, Z.-G., Wan, L.-S., Liu, Z.-M., Huang, X.-J. & Xu, Z.-K. Enzyme immobilization on electrospun polymer nanofibers: An overview. *J. Mol. Catal. B Enzym.* **56,** 189–195 (2009).

140. Sondi, I. & Salopek-Sondi, B. Silver nanoparticles as antimicrobial agent: a case study on E. coli as a model for Gram-negative bacteria. *J. Colloid Interface Sci.* **275,** 177–182 (2004).

141. Nadtochenko, V. A., Rincon, A. G., Stanca, S. E. & Kiwi, J. Dynamics of E. coli membrane cell peroxidation during TiO2 photocatalysis studied by ATR-FTIR spectroscopy and AFM microscopy. *J. Photochem. Photobiol. Chem.* **169,** 131–137 (2005).

142. Barhate, R. S. & Ramakrishna, S. Nanofibrous filtering media: Filtration problems and solutions from tiny materials. *J. Membr. Sci.* **296,** 1–8 (2007).

143. Kaur, S. *et al.* Review: the characterization of electrospun nanofibrous liquid filtration membranes. *J. Mater. Sci.* **49,** 6143–6159 (2014).

144. Cho, D. *et al.* Electrospun nanofibers for microfluidic analytical systems. *Polymer* **52,** 3413–3421 (2011).

145. McClure, M. J., Wolfe, P. S., Simpson, D. G., Sell, S. A. & Bowlin, G. L. The use of air-flow impedance to control fiber deposition patterns during electrospinning. *Biomaterials* **33,** 771–779 (2012).

146. Katta, P., Alessandro, M., Ramsier, R. D. & Chase, G. G. Continuous Electrospinning of Aligned Polymer Nanofibers onto a Wire Drum Collector. *Nano Lett.* **4,** 2215–2218 (2004).

147. Wongkaew, N., He, P., Kurth, V., Surareungchai, W. & Baeumner, A. J. Multi-channel PMMA microfluidic biosensor with integrated IDUAs for electrochemical detection. *Anal. Bioanal. Chem.* **405,** 5965–5974 (2013).

148. Ren, G. *et al.* Electrospun poly(vinyl alcohol)/glucose oxidase biocomposite membranes for biosensor applications. *React. Funct. Polym.* **66,** 1559–1564 (2006).

149. Marx, S., Jose, M. V., Andersen, J. D. & Russell, A. J. Electrospun gold nanofiber electrodes for biosensors. *Biosens. Bioelectron.* **26,** 2981–2986 (2011).

150. Huang, J., Liu, Y. & You, T. Carbon nanofiber based electrochemical biosensors: A review. *Anal. Methods* **2,** 202–211 (2010).

151. Ghanbari, K., Bathaie, S. Z. & Mousavi, M. F. Electrochemically fabricated polypyrrole nanofiber-modified electrode as a new electrochemical DNA biosensor. *Biosens. Bioelectron.* **23,** 1825–1831 (2008).

152. Wang, Z.-G., Wang, Y., Xu, H., Li, G. & Xu, Z.-K. Carbon Nanotube-Filled Nanofibrous Membranes Electrospun from Poly(acrylonitrile-co-acrylic acid) for Glucose Biosensor. *J. Phys. Chem. C* **113,** 2955–2960 (2009).

153. Camposeo, A., Persano, L. & Pisignano, D. Light-Emitting Electrospun Nanofibers for Nanophotonics and Optoelectronics. *Macromol. Mater. Eng.* **298,** 487–503 (2013).

154. Wang, X. *et al.* Electrostatic Assembly of Conjugated Polymer Thin Layers on Electrospun Nanofibrous Membranes for Biosensors. *Nano Lett.* **4,** 331–334 (2004).

155. Hong, K. H. Preparation and properties of electrospun poly(vinyl alcohol)/silver fiber web as wound dressings. *Polym. Eng. Sci.* **47,** 43–49 (2007).

156. Nair, L. S. & Laurencin, C. T. Nanofibers and Nanoparticles for Orthopaedic Surgery Applications. *J. Bone Jt. Surg.* **90,** 128–131 (2008).

157. Jayakumar, R., Prabaharan, M., Sudheesh Kumar, P. T., Nair, S. V. & Tamura, H. Biomaterials based on chitin and chitosan in wound dressing applications. *Biotechnol. Adv.* **29,** 322–337 (2011).

158. Rujitanaroj, P., Pimpha, N. & Supaphol, P. Wound-dressing materials with antibacterial activity from electrospun gelatin fiber mats containing silver nanoparticles. *Polymer* **49,** 4723–4732 (2008).